TECHNICAL MEMORANDUM 505-9S

SUPPLEMENT TO 505-9

Texas Transportation Institute
Texas A&M Research Foundation

EVALUATION OF CRASH CUSHIONS
CONSTRUCTION OF LIGHTWEIGHT CELLULAR CONCRETE

A Tentative Progress Memorandum on Contract No. CPR-11-5851

U.S. Department of Transportation
Federal Highway Administration

by

Don L. Ivey
Eugene Buth
T. J. Hirsch
Texas Transportation Institute

and

John G. Viner
Structures and Applied Mechanics Division
Federal Highway Administration

These crash tests and evaluations were conducted under the Office of Research and Development, Structures and Applied Mechanics Division's Research Program on Structural Systems in Support of Highway Safety (4S Program). The opinions, findings, and conclusions expressed in this report are those of the authors and not necessarily those of the Federal Highway Administration.

June 1971

INTRODUCTION

The feasibility of vehicle crash cushions constructed of lightweight cellular concrete was demonstrated by a series of three head-on vehicle impacts on prototype installations. These initial tests were reported in a previous Technical Memorandum[1*]. The concrete crash cushion is one of a group of first generation devices which include the Barrel Crash Cushion, the Fitch Inertia Barrier and the HI-DRO Cell Barrier. The evaluation sequence that has been followed on all of these systems was: (1) Feasibility testing, (2) full-scale head-on testing, and (3) side angle testing. Because of the excellent performance of the concrete cushion in the first three tests conducted, interest was expressed by several states in applying the concept to some of their potentially hazardous areas. A concrete cushion was designed for the State of Florida[2] incorporating the basic cushion which was tested under FHWA's 4S Program (Figure 1, Mod I) and side-fender panels which were previously tested as part of Barrel Crash Cushion designs[3]. The results of two side angle tests of the system which was constructed for Florida (Figure 1, Mod II) were reported to Florida in November 1970.

In consultation with the contract manager for FHWA it was decided that additional tests would be conducted to further evaluate the concrete cushion for both the side angle hit situation and for head-on impacts of small vehicles. Further modifications of the cushion were made prior to the final series of

*Superscript numerals refer to corresponding references at the end of this report.

tests which resulted in the design shown as Mod III in Figure 1. The chronological evolution of the Concrete Crash Cushion is illustrated by Figure 1. The most significant concrete cushion designs which have been tested are shown in Figures 2 through 4. This report describes in detail the three tests which were conducted on the Mod III Concrete Crash Cushion.

Appendix B presents the results of a limited scale-model study which was conducted to determine the effects of the dimensions and concrete strength on the static crush strength and energy absorption of the lightweight concrete model.

Appendix C presents the results of a limited study to evaluate the freeze-thaw durability of the vermiculite lightweight concrete used for construction of the crash cushion.

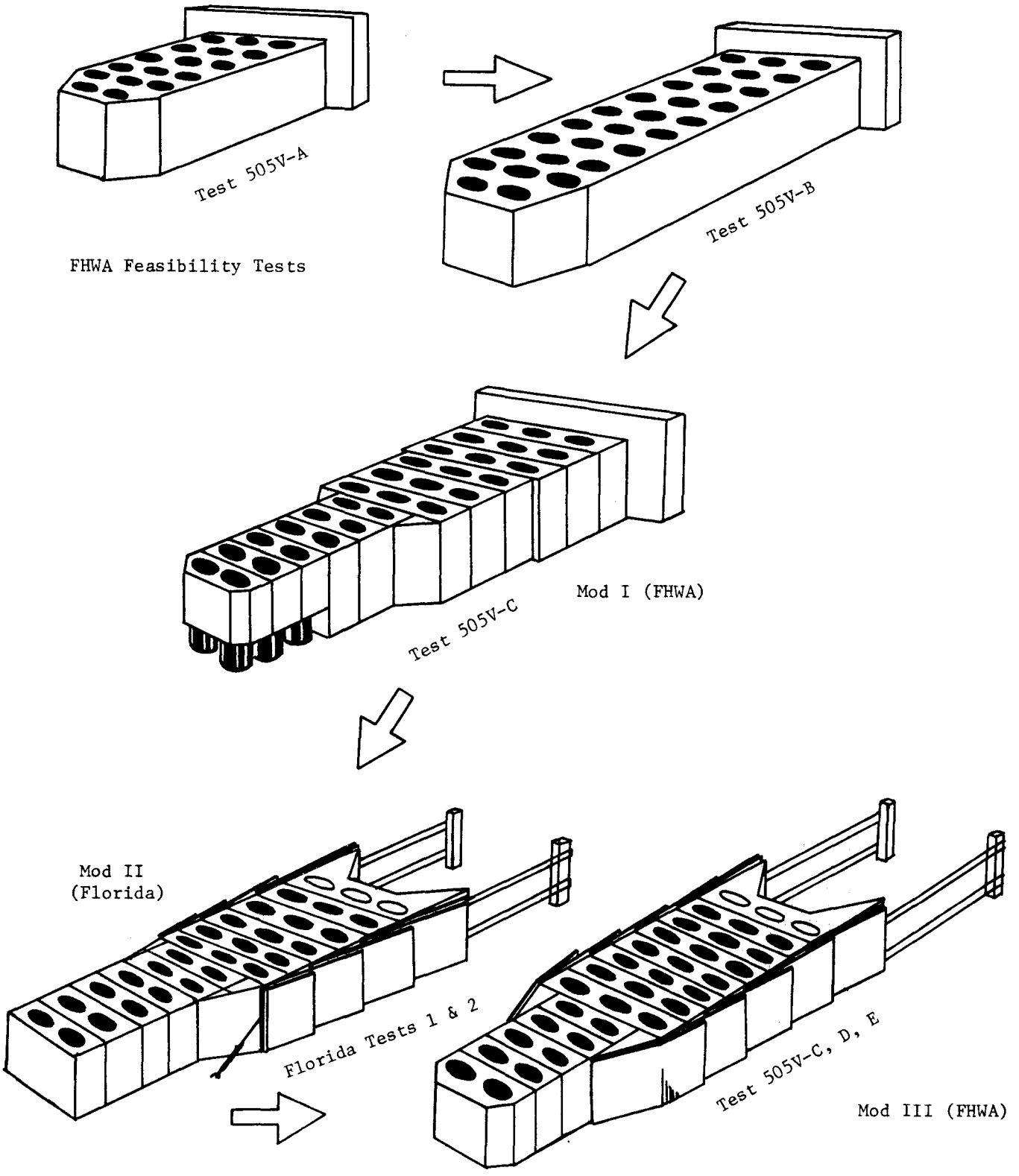

Figure 1, Evolution of Concrete Crash Cushion.

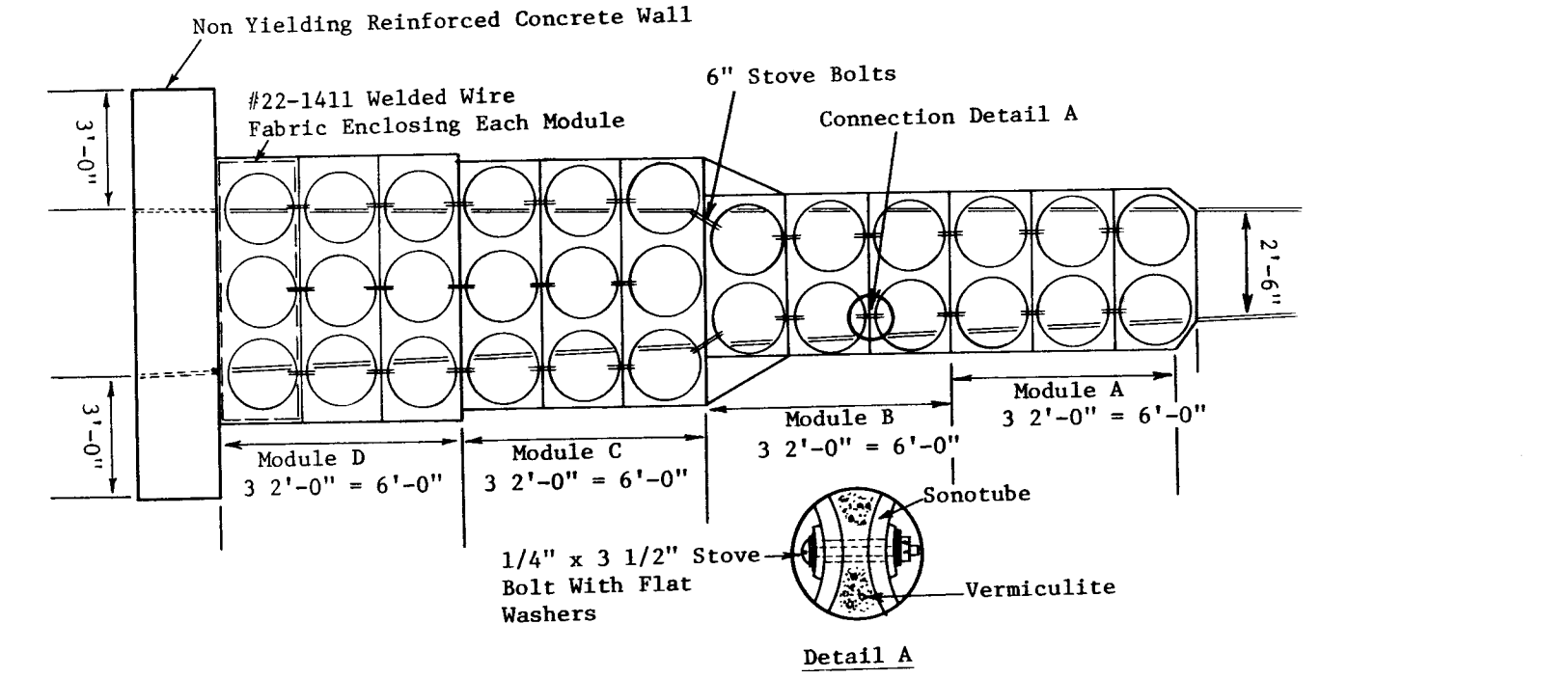

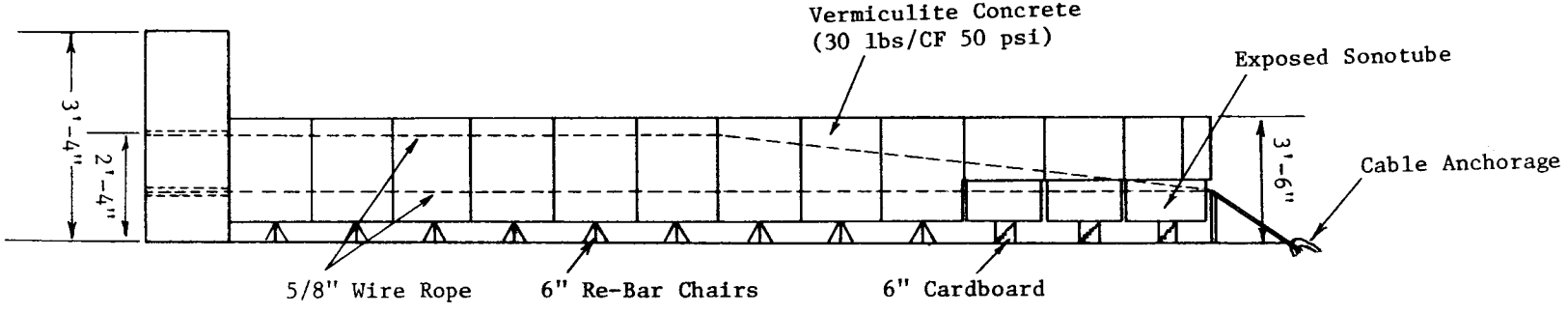

Figure 2, Details of Concrete Crash Cushion (Test 505V-C Mod I).

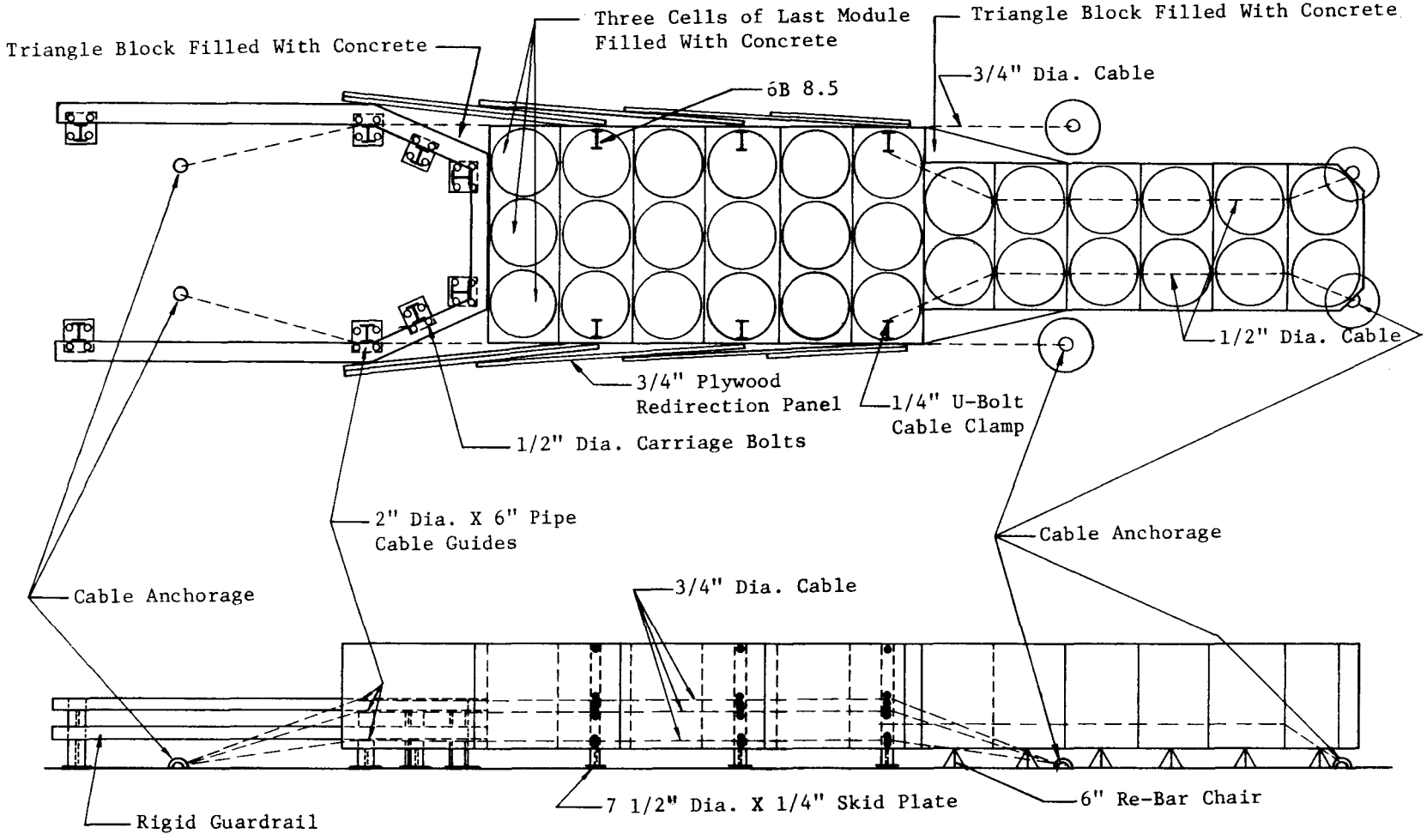

FIGURE 3, Details of Concrete Crash Cushion (Tests FLA-1 & FLA-2)(Mod II).

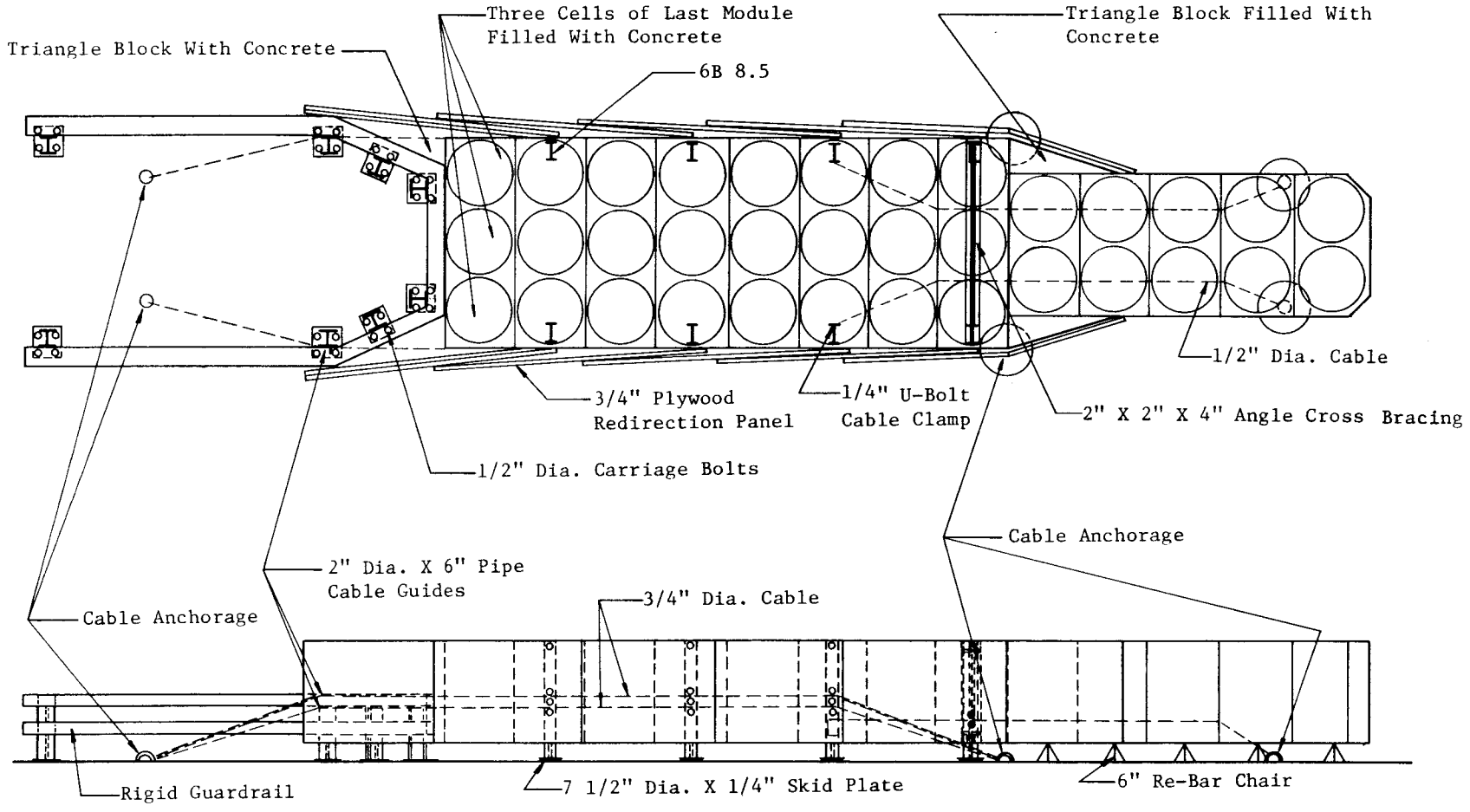

FIGURE 4, Details of Concrete Crash Cushion (505V-D, -E, and -F) (Mod III).

EXPERIMENTAL PROGRAM

General

Three full-scale vehicle crash tests of the Mod III Concrete Crash Cushion which is shown in Figure 4 were conducted in this final test series. These tests were designated 505V-D, -E, and -F respectively. The tests are summarized in Table 1. Properties of the concrete used in the various cushions tested are given in Table 2. Accelerometers and an Impact-O-Graph were used on each test to record vehicle decelerations. All accelerometers were Statham strain gage type and all electronic data was passed through an 80 HZ low-pass filter. High-speed cameras were also used to record the vehicle position and velocity throughout the test. Selected photographs of the vehicle before and after each test and sequential photographs of the test in progress are included.

Test 505V-D

A 1963 Chevrolet weighing 3790 lbs was used in this test. The impact angle was 10° from the longitudinal axis of the cushion and the contact point was 18 feet in advance of the rigid backup rail. The speed at contact was 57.2 mph and speed at loss of contact was 49.6 mph. The average longitudinal deceleration was 1.3 g's. The distance that the vehicle was in contact with the barrier was 20.4 feet over a period of approximately one-third of a second. The vehicle penetrated laterally a maximum distance of about two feet into the barrier and was smoothly redirected. Damage to the vehicle was relatively light as shown in Figure 5. Figure 6 shows that only five modules

TABLE 1

SUMMARY OF TESTS

Factor	Test		
	V-D	V-E	V-F
VEHICLE			
Year	1963	1962	1957
Make	Chevrolet	Chevrolet	Volvo
Weight, lb	3790	3820	2210
ANGLE OF IMPACT, deg	10	20	0
FILM DATA			
Initial Speed, V_1, fps	83.9	87.5	89.7
mph	57.2	59.7	61.2
Final Speed, V_2, fps	72.7	43.9	0
mph	49.6	29.3	0
*Average Deceleration, G_{avg}, g's	1.3	5.6	10.2
Stopping Distance or Contact Distance, S, ft	20.4	16.1	12.2
Time in Contact, sec	0.286	0.235	0.364
ACCELEROMETER DATA			
Longitudinal Deceleration			
Peak g's	6.2	14.7	19.0
Average g's	1.4	4.2	6.4
Time, sec	0.294	0.268	0.446
Transverse Deceleration			
Peak g's	9.8	12.7	--
Average g's	2.4	3.3	--
Time, sec	0.302	0.273	--

*$G_{avg} = (V_1^2 - V_2^2) / 2gS$

TABLE 2

PROPERTIES OF VERMICULITE CONCRETE

Test No.	Average Compressive Strength, psi	Average Unit Weight, pcf
505V-A	50	32
505V-B	71	32
505V-C	57	21
Fla.-1&2	64	22
505V-D,E & F	64	22

were significantly damaged and that the cushion could probably still sustain a head-on impact. The test was considered extremely successful both from the point of view of the safety of vehicle passengers and from the relatively light damage to the vehicle.

Test 505V-E

This test was a 20° side angle impact on the Mod III barrier using a 1962 Chevrolet weighing 3820 lbs. The point of contact was 16 ft in advance of the rigid backup wall. The impact speed was 59.7 mph and speed of the vehicle at loss of contact with the barrier was 29.3 mph. This represented an average deceleration of 5.6 g's in the longitudinal direction. The vehicle was in contact with the cushion for approximately 16 ft. Photographs of this test are shown in Figures 10 through 15. As the vehicle made contact and slid down the side of the cushion, a slight ramping tendency was observed. This interaction finally culminated in the generation of a high roll-initiating force as the vehicle reached the end of the cushion. The vehicle rolled in a counterclockwise direction, when viewed in the direction of vehicle travel; ramped on the rear end of the cushion near the end of the backup wall; traveled beyond the cushion installation, skidding on its left side; rolled clockwise to an upright position; and continued to roll over onto its top. It came to rest approximately 80 ft past the barrier. Although the decelerations which were imparted to the vehicle during its interaction with the cushion were within the range of human tolerance, the roll condition which occurred after the vehicle left the cushion is a very undesirable reaction and is unacceptable from a passenger safety viewpoint.

This is the only test conducted to date, in which an unacceptable reaction of the vehicle resulted. Recommendations are made in the discussion for modification of the barrier to preclude the recurrence of this situation.

Test 505V-F

A 1957 Volvo weighing 2210 lbs was used in this test. The vehicle impacted the cushion head-on at a speed of 61 mph. The average longitudinal deceleration was 10.2 g's, with a peak longitudinal deceleration of 19 g's. The interaction of the vehicle and cushion was considered acceptable and the damage resulting to the vehicle and cushion is shown in Figures 16, 17, and 18.

The decelerations which are imparted to a 2000 lb vehicle can be expected to be approximately twice the decelerations imparted to a 4000 lb vehicle. This is seen by comparing the values given above with the 6.4 average and 10.4 maximum decelerations observed in Test 505V-C[1].

Figure 5 , Vehicle After Test D.

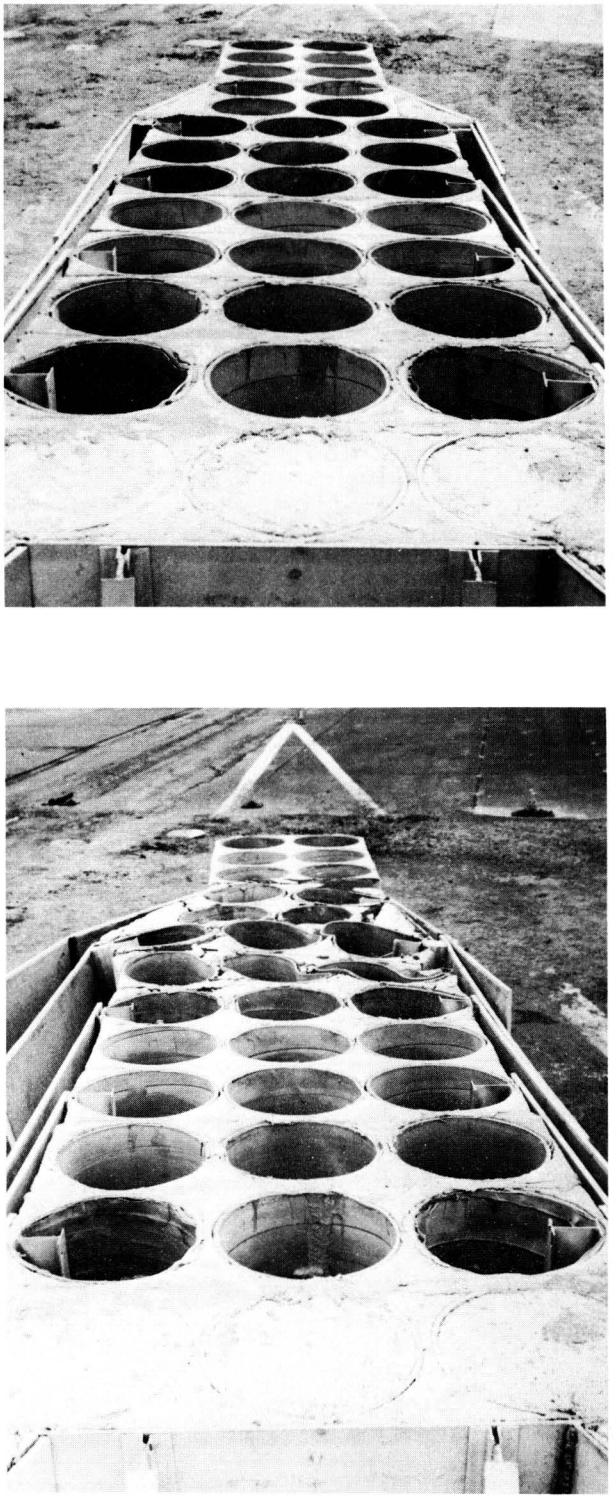

Figure 6, Barrier Before and After Test D (End View).

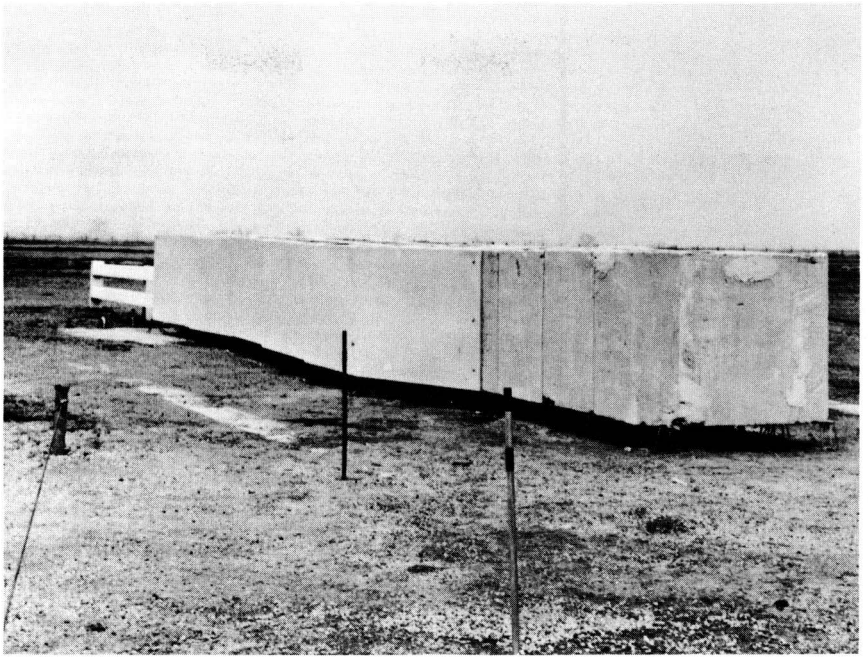

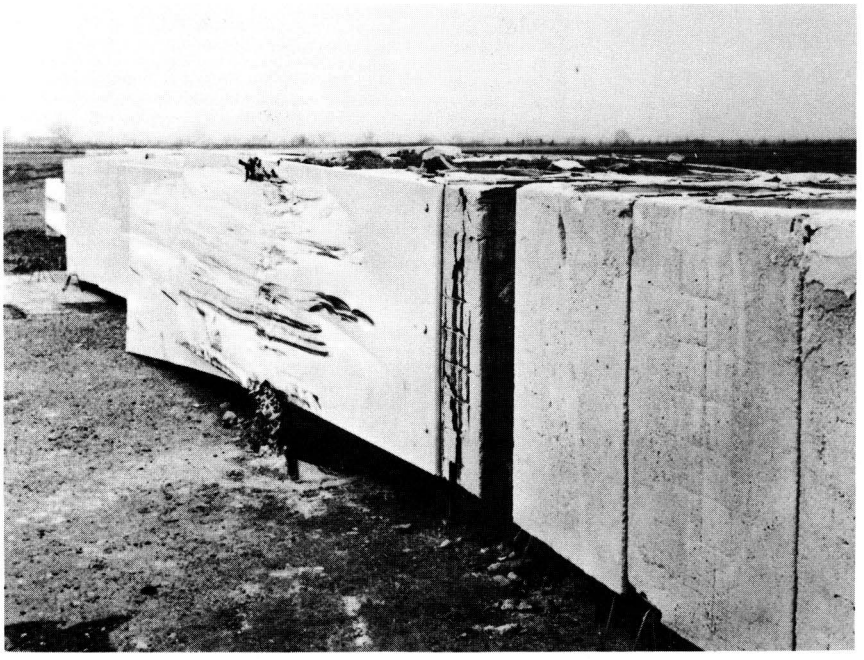

Figure 7, Barrier Before and After Test D (Oblique View).

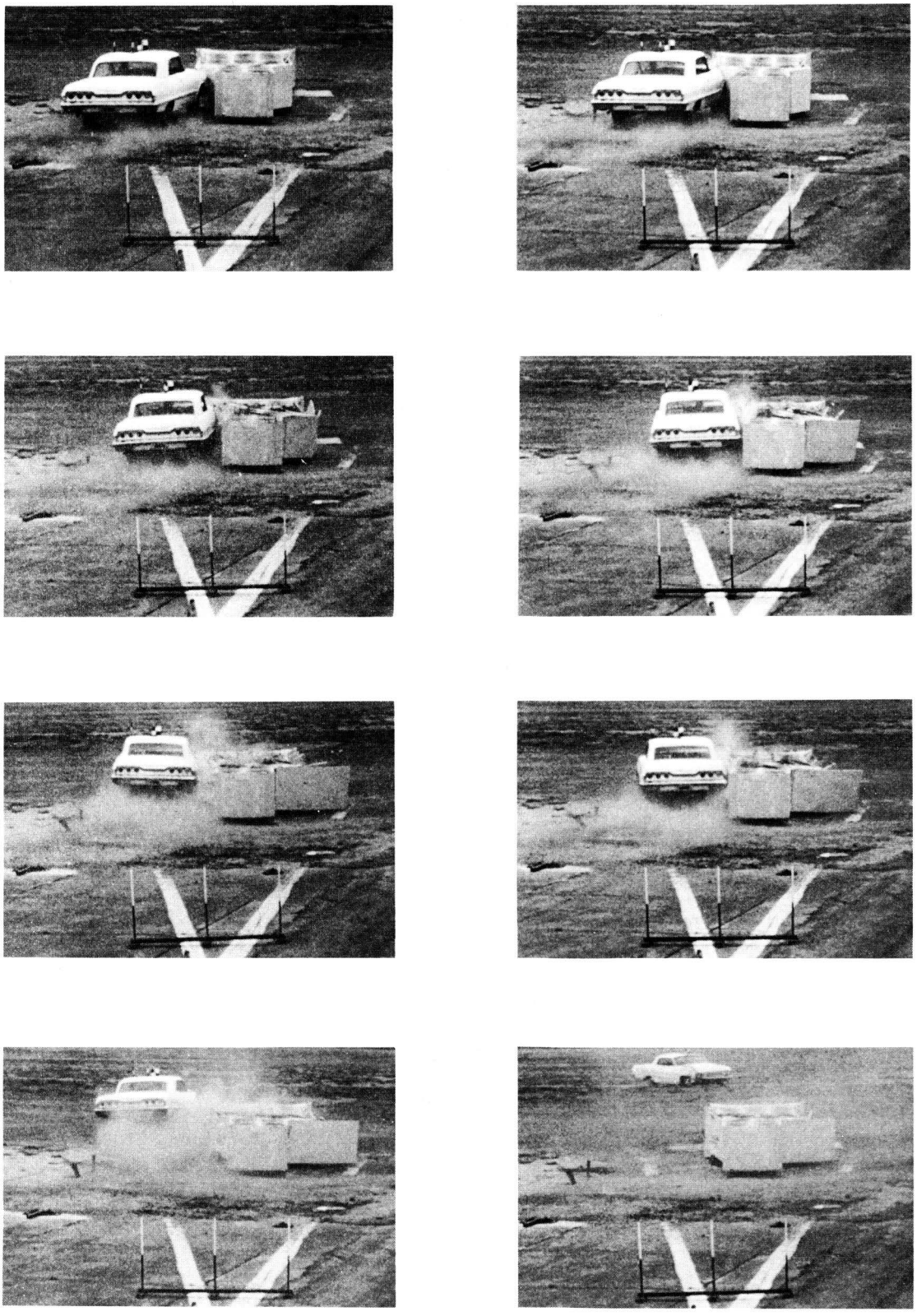

Figure 8, Test D Sequential Photographs
(View Parallel With Barrier).

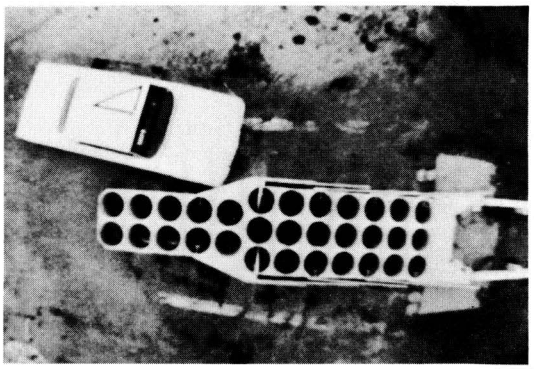

t = 0 sec

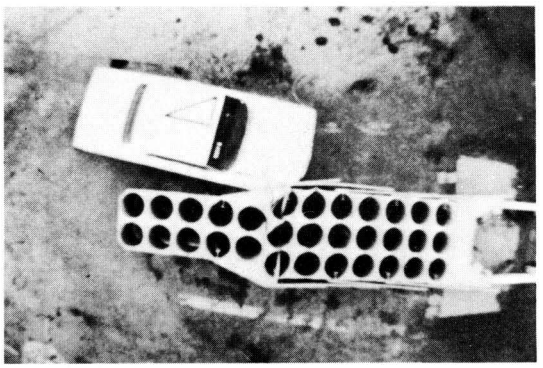

t = 0.046 sec

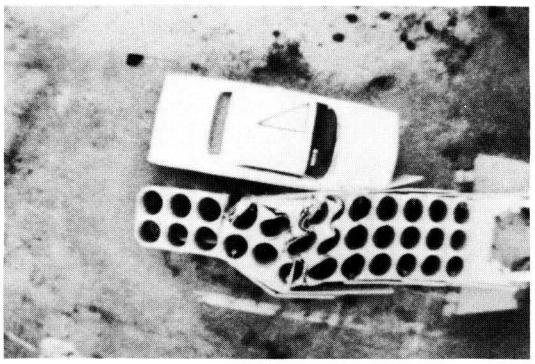

t = 0.112 sec

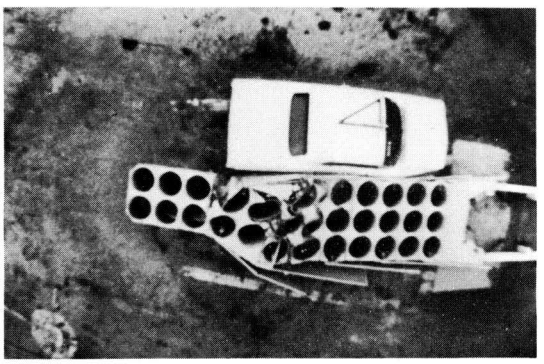

t = 0.199 sec

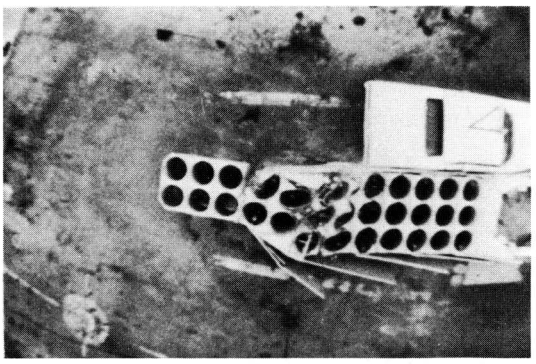

t = 0.306 sec

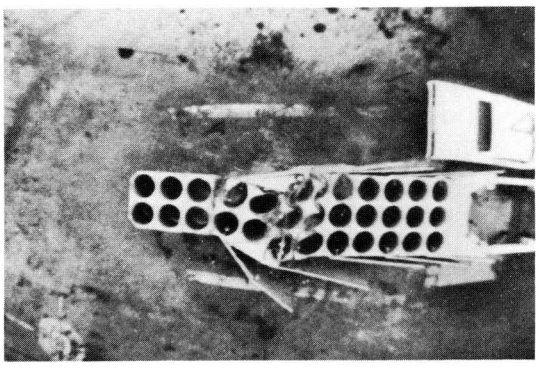

t = 0.429 sec

Figure 9, Test D Sequential Photographs (Overhead View).

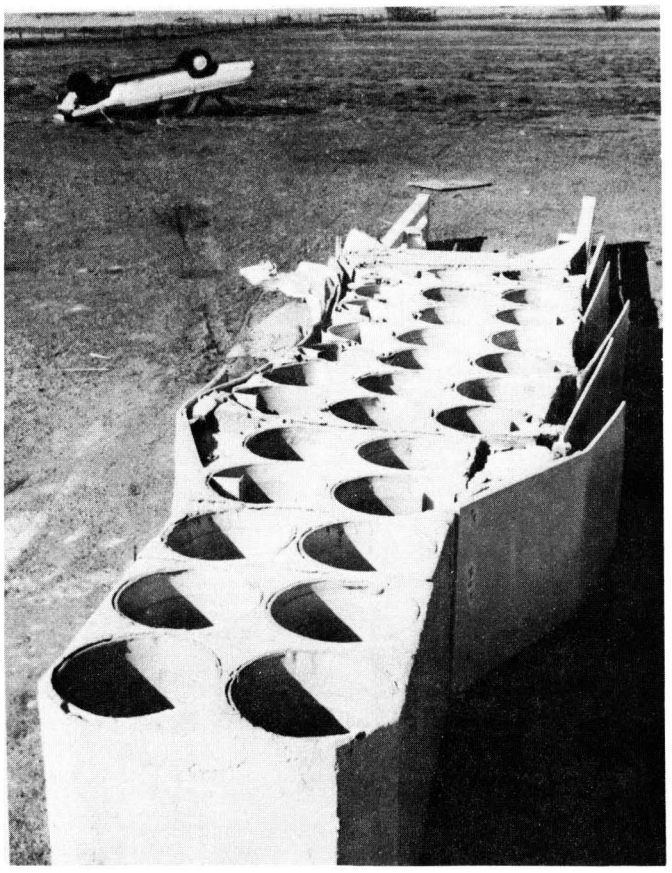

Figure 10, Vehicle Before Test E and in Final Position.

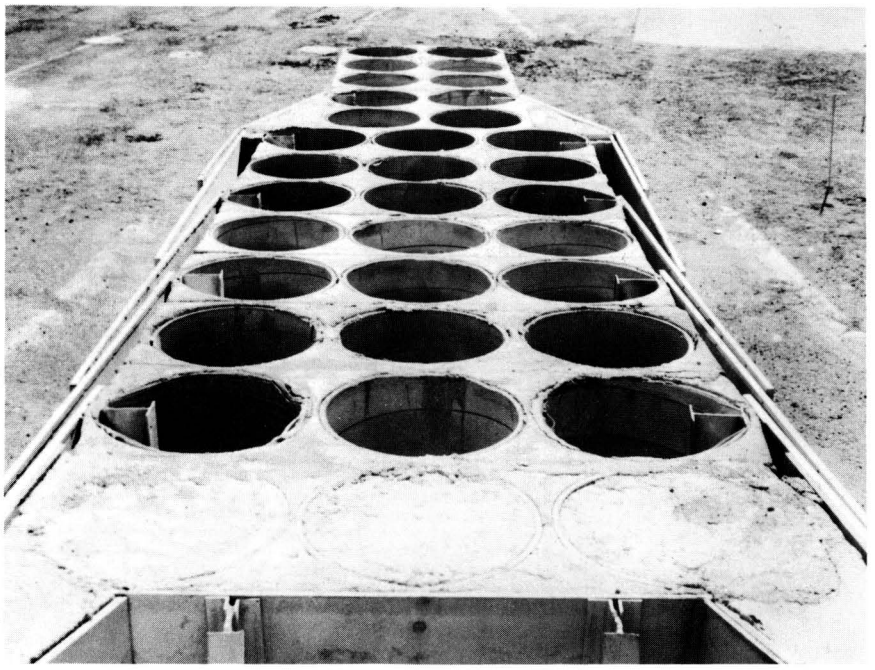

Figure 11, Barrier Before and After Test E.

Final Position

After Righting

Figure 12, Vehicle After Test E.

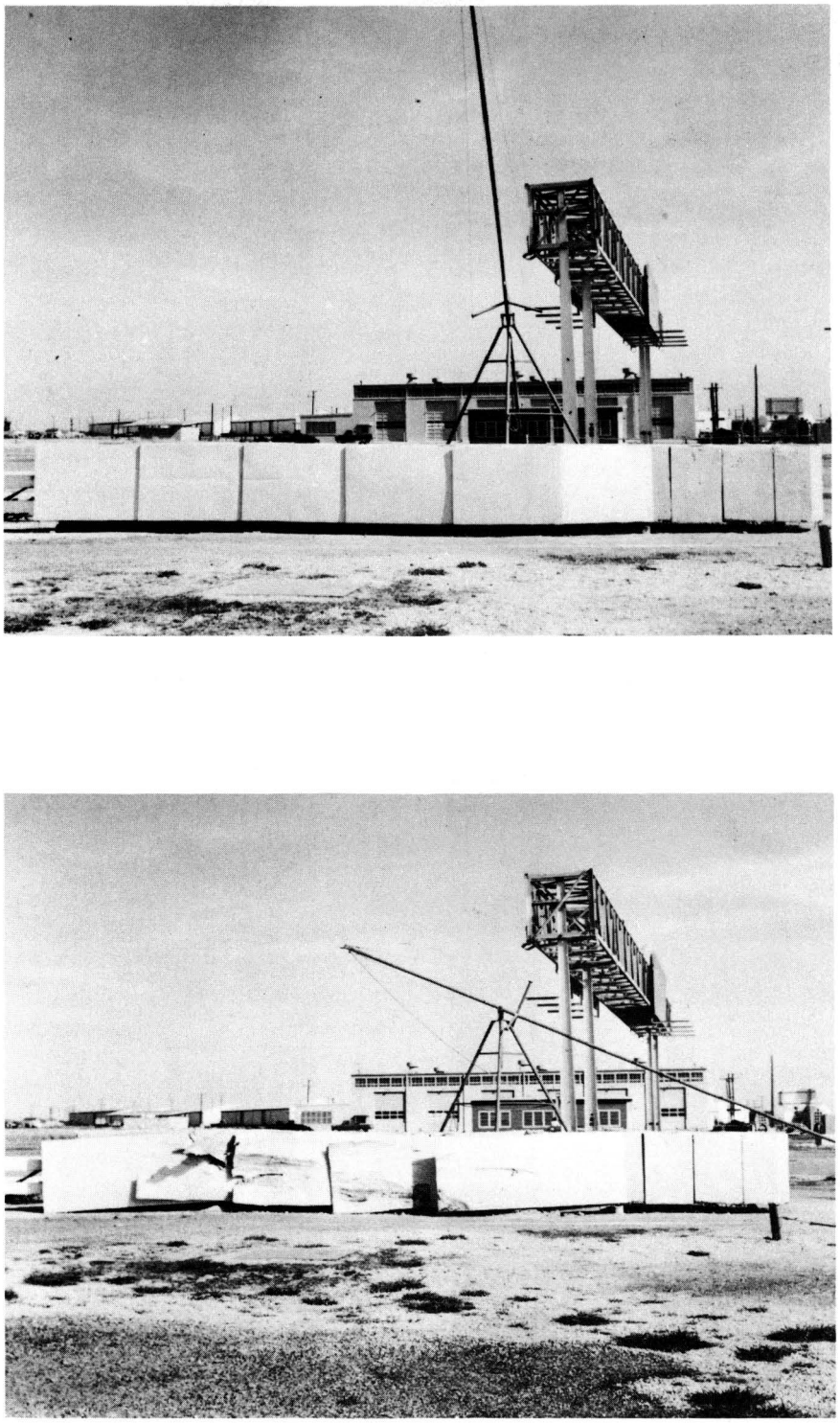

Figure 13. Barrier Before and After Test E
(View Perpendicular to Barrier).

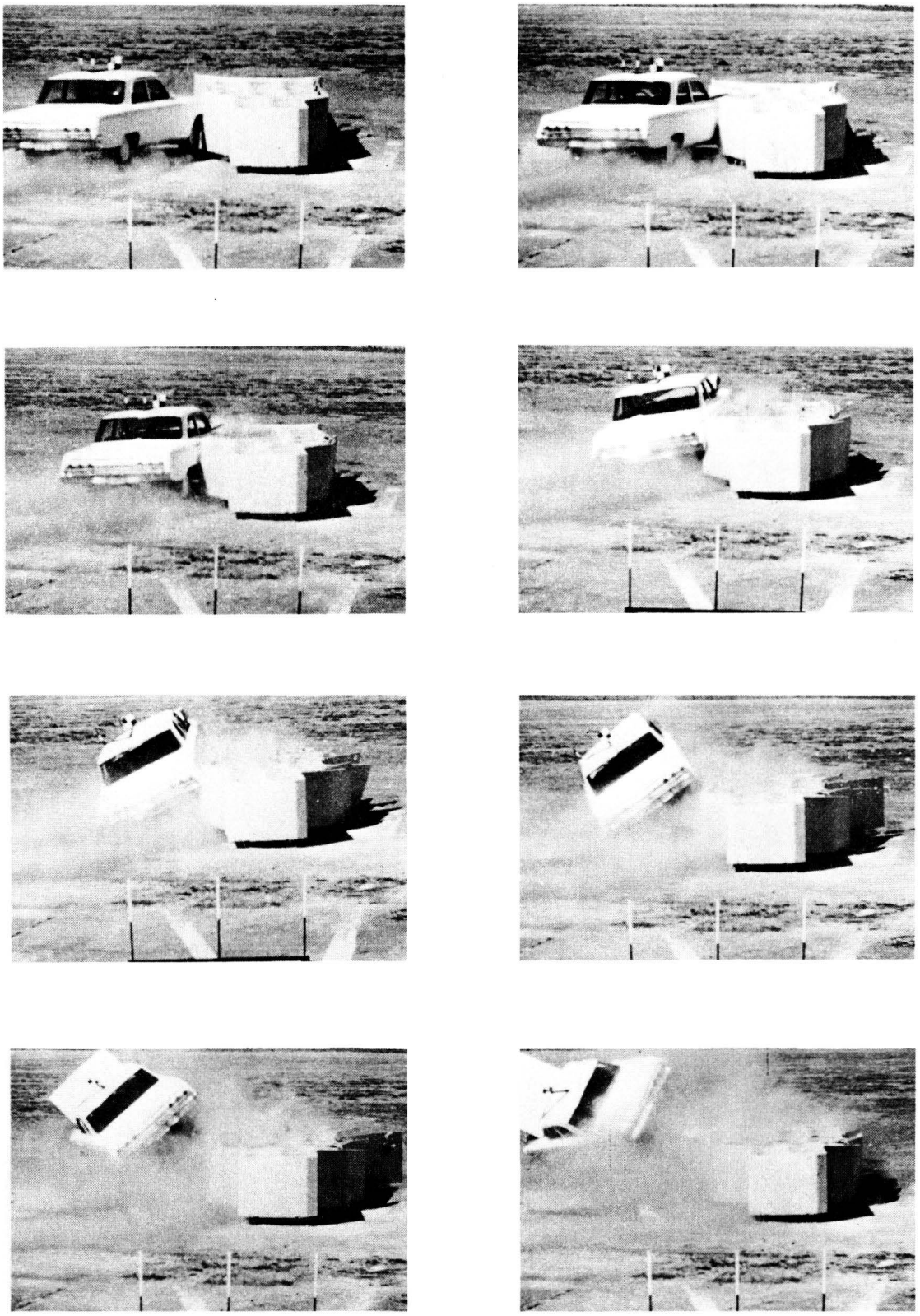

Figure 14, Test E Sequential Photographs
(View Parallel To Barrier).

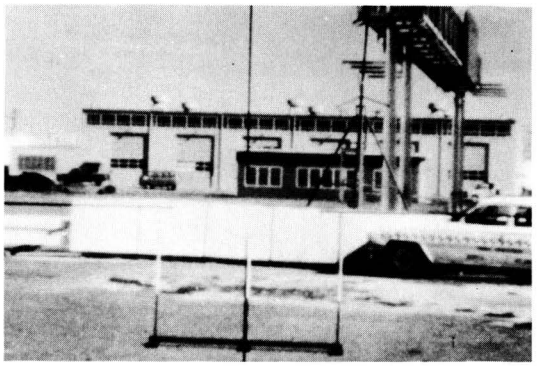

t = 0 sec

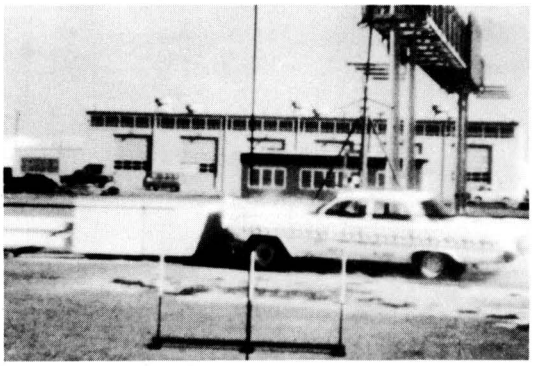

t = 0.104 sec

t = 0.153 sec

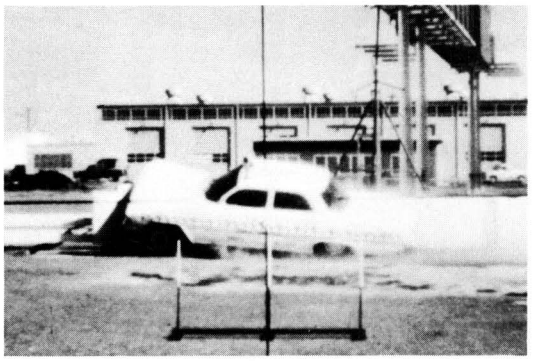

t = 0.213 sec

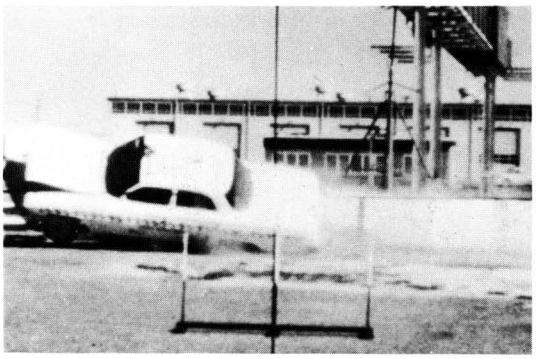

t = 0.351 sec

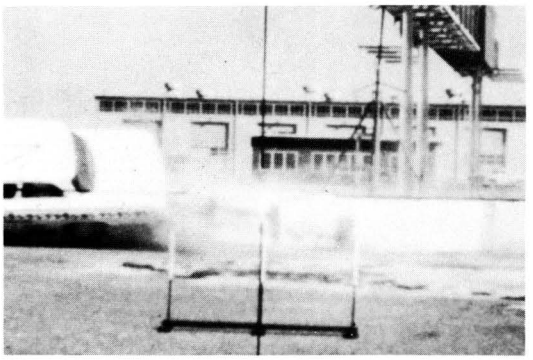

t = 0.536 sec

Figure 15, Test E Sequential Photographs (View Perpendicular To Barrier).

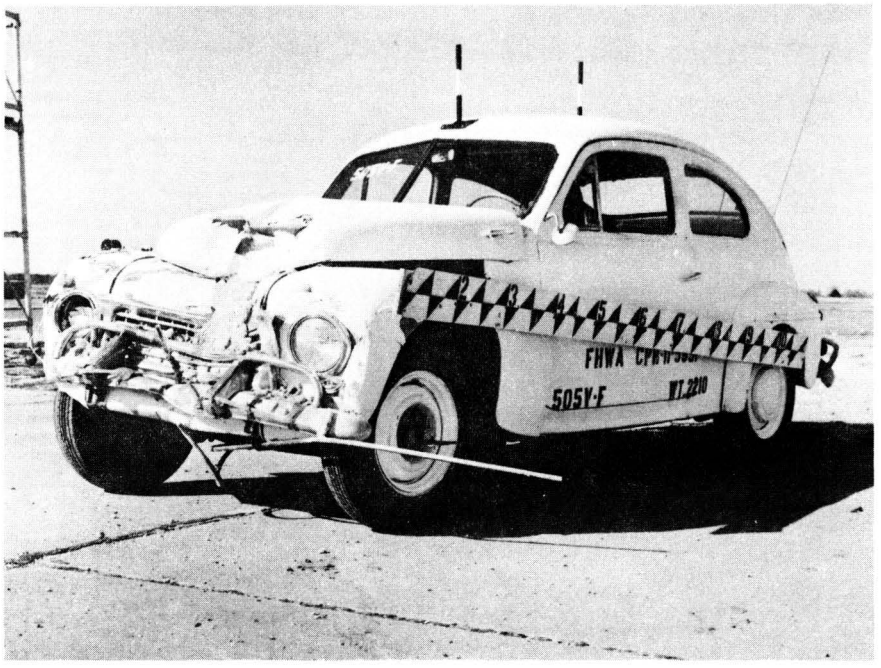

Figure 16, Vehicle Before and After Test F.

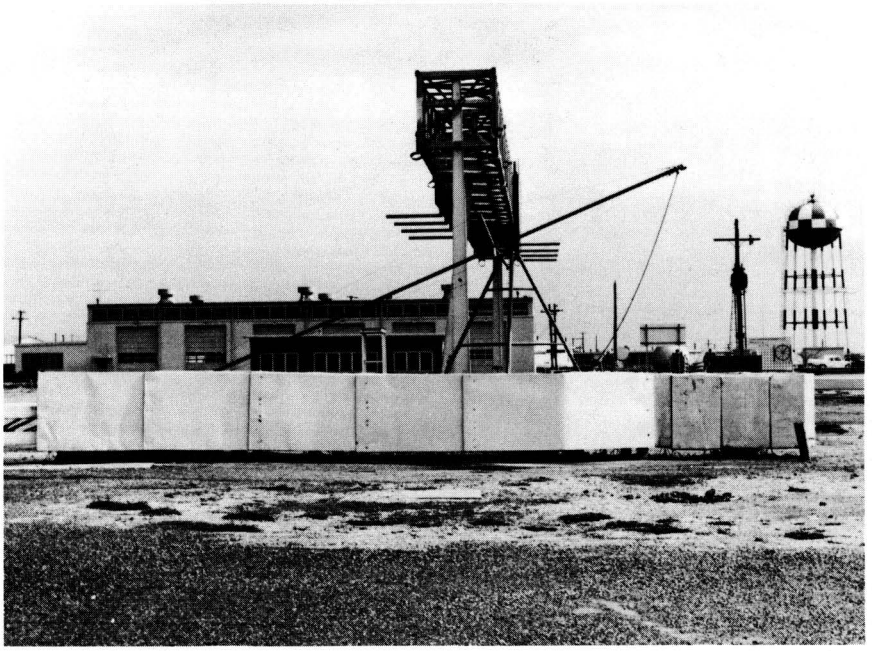

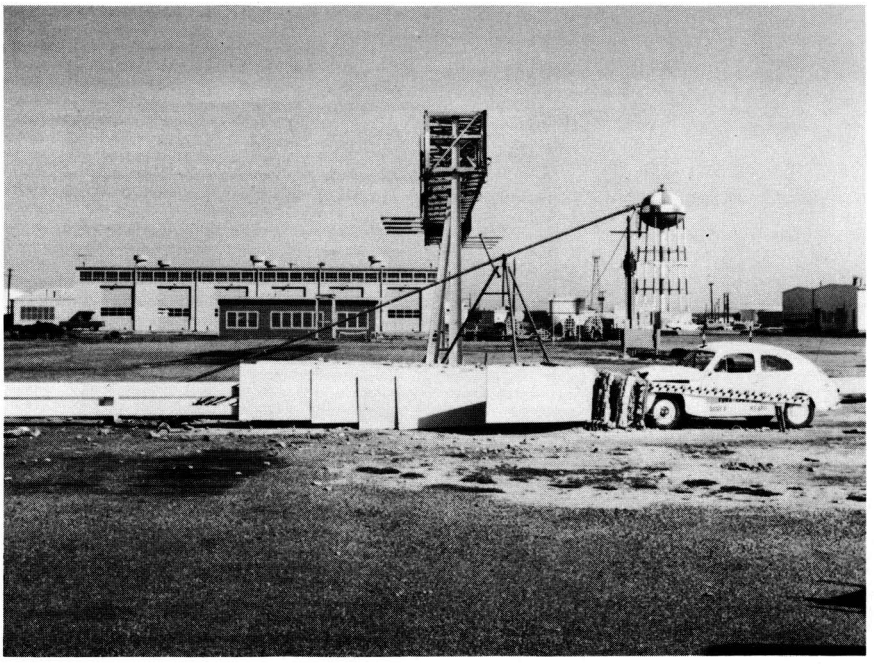

Figure 17, Barrier Before and After Test F
(View Perpendicular to Barrier).

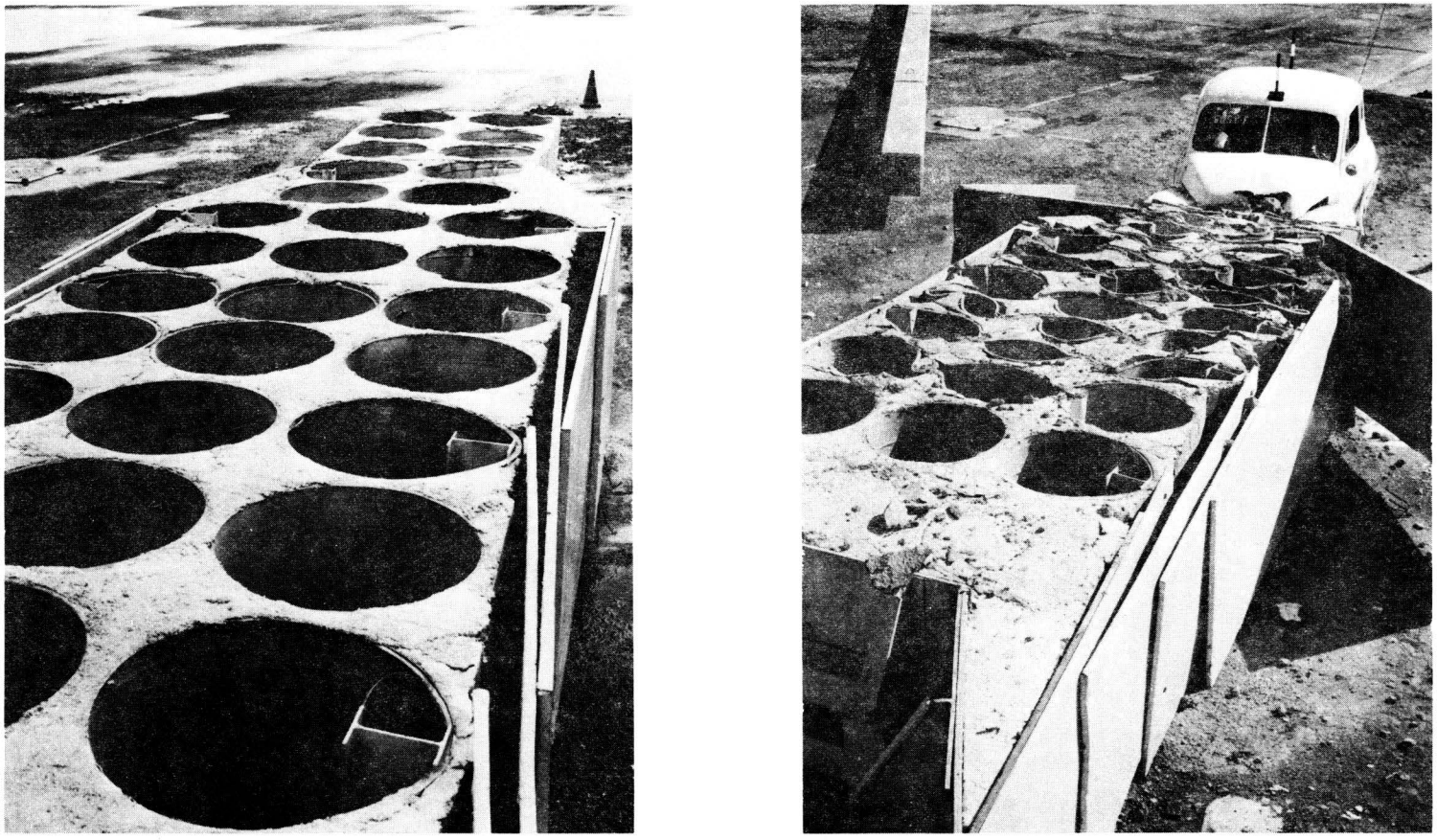

Figure 18, Barrier Before and After Test F (Oblique View).

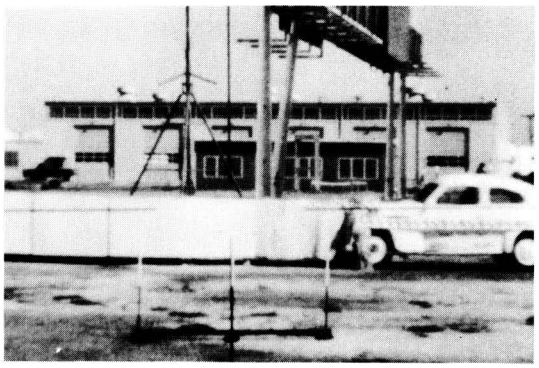

t = 0.023 sec

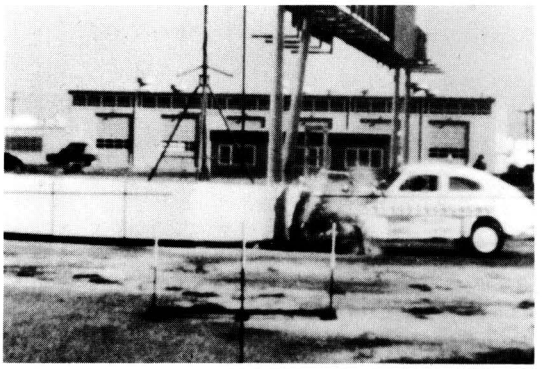

t = 0.054 sec

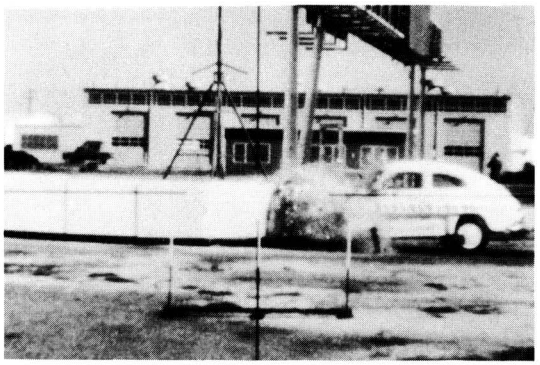

t = 0.085 sec

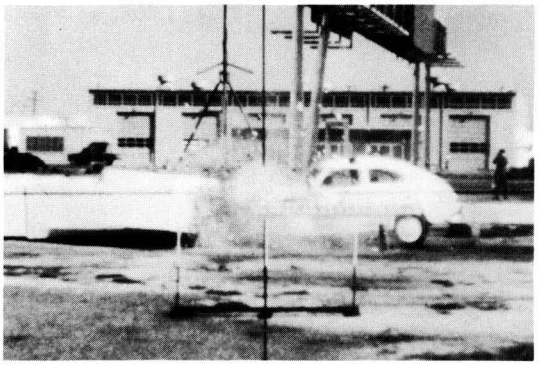

t = 0.208 sec

t = 0.309 sec

t = 1.712 sec

Figure 19. Test F Sequential Photographs (View Perpendicular To Barrier).

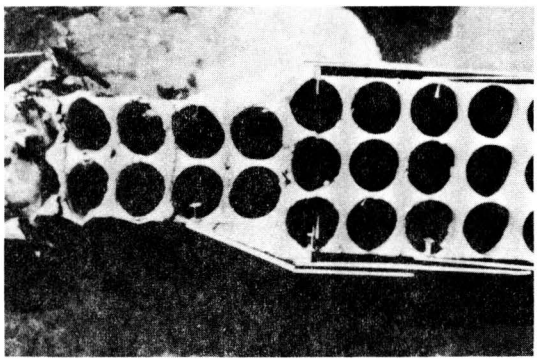

t = 0.031 sec

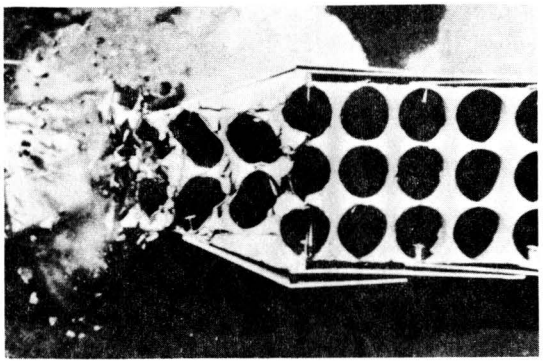

t = 0.064 sec

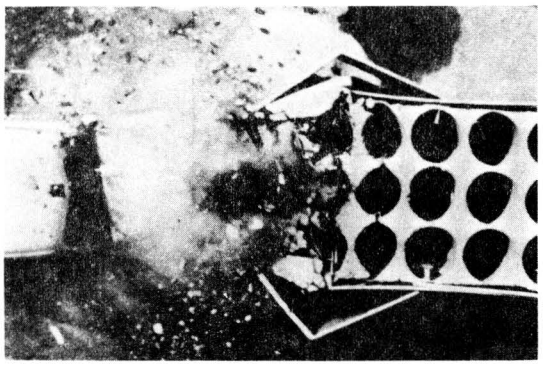

t = 0.130 sec

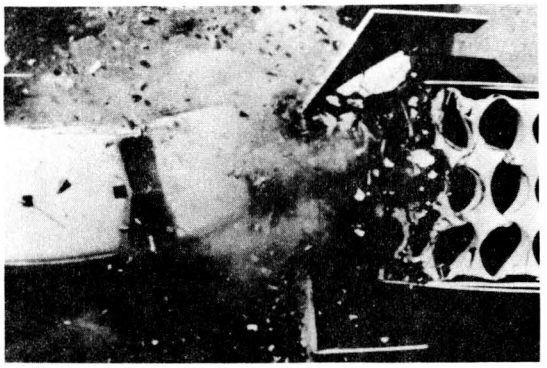

t = 0.199 sec

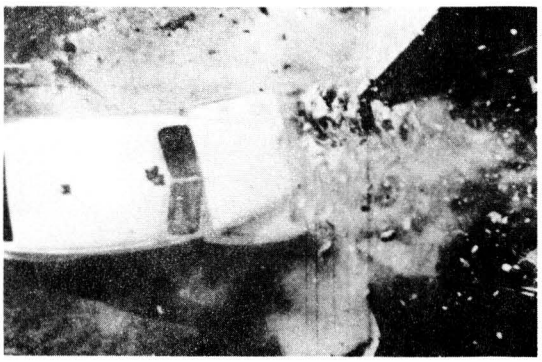

t = 0.380 sec

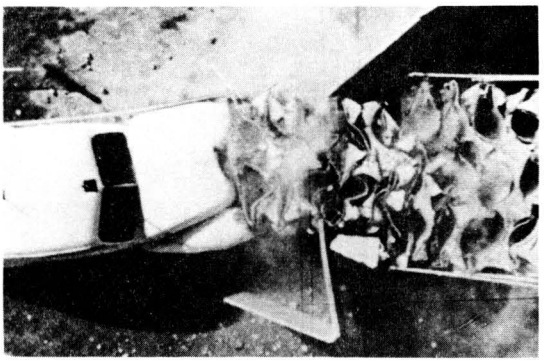

t = 1.480 sec

Figure 20, Test F Sequential Photographs (Overhead View).

DISCUSSION

Of the eight vehicle crash tests that have now been conducted on the concrete crash cushion, all but one have yielded results that appear very favorable from the passenger survivability point of view. The exception to this was the 20°, 59.7 mph, side angle impact of the Mod III cushion (Test 505V-E). In this test the vehicle was subjected to a large moment about the roll axis toward the end of the contact zone. This resulted in a hazardous roll after contact with the cushion was lost and the vehicle came to rest upside down. This tendency in side angle collisions has been noted in other crash tests, such as Test 505R-E[4] and USS Test 1*. In both of these tests, the vehicle contact-wheel appeared to ride up the side panels which resulted in the vehicle becoming airborne as contact with the barrier was lost. The phenomenon observed in Test 505V-E however, appears to be significantly different from that observed in previous tests. From observation of the high-speed test film, it appeared that the following events describe the phenomenon:

1. The vehicle contacts the cushion at the point shown by Figure 15, Photo No. 1, t=0. This point is approximately 16 ft. in advance of the rigid backup wall.
2. The vehicle begins to displace the barrier laterally and slide along the side panels as shown in photos for t=0.104, and t=0.153. There is a slight ramping tendency during this stage, with the

---

*The first test of a series of three tests conducted by United States Steel Corporation, U.S.S. Contract 6339, Texas A&M Research Foundation Project RF 719, March, 1970. No formal publication.

contact side of the vehicle rising approximately one ft as compared to its elevation at contact. This ramping is less severe than noted in the other tests which were referenced, 505R-E and USS Test 1.

3. At t=.213, Figure 15, the vehicle frame appears to be in a state of severe torsion as indicated by the sudden elevation of the right front quadrant of the vehicle. It is at this point, where contact with the last module of the cushion is made, that the severe upward thrust on the right front of the vehicle causes the counterclockwise roll motion. The last module of the Mod II and III cushions is solid vermiculite as compared to the other modules with sonotube openings. The comparative rigidity of this module necessitated one of the following events to occur:

   a) The contact area of the vehicle must be suddenly forced to the outside to pass the rigid module in a relatively violent redirection (barrier force causes a moment about the yaw axis of the vehicle). See Test 1 of the Florida test series[2]. Or,

   b) The contact area of the vehicle must be forced upward to pass over the rigid module resulting in a rolling motion (barrier forces cause a moment about the roll axis of the vehicle). In the slightly elevated position that the right front of the vehicle had achieved in Test 505V-E, the path of least resistance was over the final rigid module.

The question remaining to be answered is why this roll phonomenon occured in Test 505V-E but not in 505V-D or Test 1 of the Florida series. In V-D, the impact angle was only 10° and the vehicle had been almost completely redirected before reaching the solid module. Thus no traumatic force was necessary to get by the rigid portion of the cushion. In Florida Test 1, the impact angle was 20° as in V-E, but the contact point was only six feet in advance of the rigid module. In all other respects the final eight feet of the Florida Mod II cushion was identical to the final eight ft. of the FHWA Mod III cushion. It is hypothesized that the ramping which occured in test V-E was initiated when the vehicle struck the cushion at a point where the cables supporting the redirection panels was low; whereas in Florida Test 1 the cables at the impact point were almost fully elevated. It would therefore appear that the Mod III cushion has a weak point if struck at an angle of 20°, close to where the side panels start. No such weakness was demonstrated by tests on the Mod II cushion since the panels extend out only 11 ft from the rigid backup rail and angle hits in advance of the panels result in an acceptable "pocketing" interaction (see Florida Test 2)[2].

It is believed that this weakness in the Mod III cushion can be overcome by the following design changes: (a.) Replace the solid module at the rear of the Mod III cushion by a standard hollow module and (b.) elevate the side cables at the rear of the cushion 6 in. Item "a" results in reducing the forces imparted to the vehicle at this point

in the interaction and reduces the vehicle reaction necessary to get by the final module. Item "b" results in elevating the vertical position of maximum lateral resistance, and thus reduces the slight ramping tendency which has been noted.

CONCLUSION

The lightweight concrete crash cushion has now shown a capability to perform effectively in decelerating a vehicle for both the head-on and side angle crash conditions*. Seven of eight tests show deceleration levels within the tolerance of restrained humans. Concerning the single test of the Mod III cushion which resulted in an undesirable reaction of the vehicle during a cushion impact, modifications to prevent future reactions of this type are recommended. Since these proposed modifications have not been tested, full-scale tests should be performed before the Mod III barrier is considered for field installations.

The lightweight cellular concrete crash cushion can be installed by semi-skilled laborers using one of two methods. The formwork can be placed in the field, and a local vermiculite applicator can supply the necessary concrete; or the precast modular construction method can be used. The cost per installation compares favorably with that of the barrel crash cushion. Using the modular construction technique, considerable savings should be realized by mass production. Close quality control should be exercised on the geometry of the module and on the vermiculite concrete. Control of batch proportions and unit weight will give predictable crushing strengths. Replacement of segments of the crash cushion after a collision is feasible. For a cast-in-place cushion, the crushed material can be removed, that portion of the barrier reformed, and fresh vermiculite placed in the necessary areas. Fast setting cement will alleviate the problem of curing time. For the precast cushion, the

---

*Design method presented in Appendix B.

three-tube modules weigh approximately 250 lbs and could, therefore, be handled by two men. The modules which have been crushed during a collision can be unbolted, removed, and new modules slipped into place. This refurbishment could be accomplished during a low density traffic period.

The lightweight, low-strength concrete used in these crash cushions exhibits relatively poor durability when subjected to cycles of freezing and thawing if it is allowed to become saturated with water. Several waterproofing agents were tested with limited success as reported in Appendix C. The most certain method of achieving protection has been used by the State of Wisconsin. On two vermiculite cushion installations in Milwaukee, ruberized tarpaulin covers were used to protect the cushions against absorbing water and against the accumulation of ice and snow in the sonotube voids. There has been no durability problem in Wisconsin on the cushions covered in this way.

REFERENCES

1. Ivey, D. L., Buth, E., Hirsch, T. J., "Feasibility of Lightweight Concrete Vehicle Crash Cushions, Highway Research Record No. 306, 1970, pp. 50-57.

2. Ivey, D. L., Buth, E., "Side Angle Collisions with Concrete Vehicle Crash Cushions", Research Report 733, Florida State Department of Transportation, Texas Transportation Institute, November, 1970.

3. Hirsch, T. J., Hayes, G. G., Ivey, D. L., "The Modular Crash Cushion", Technical Memorandum 505-1S, Supplement To 505-1, Texas Transportation Institute, August, 1970.

4. Hayes, G. G., Ivey, D. L., Hirsch, T. J., "Performance of the HI-DRO Cushion Cell Barrier Vehicle-Impact Attenuator", Highway Research Record No. 343, 1971, pp. 93-99.

APPENDIX A

PHOTOGRAPHIC DATA

AND

ACCELEROMETER TRACES

TABLE A1

TEST 505 V-D

High-Speed Film Data

Time (msec)		Displacement (ft)	
-62		-5.2	V_1 = 83.9 fps
-52		-4.3	
-41		-3.4	
-31		-2.6	
-21		-1.7	
-10		-0.9	
0	Impact	0	
9		0.8	
19		1.5	
28		2.3	
38		3.0	
47		3.7	
56		4.4	
66		5.1	
75		5.8	
84		6.4	
94		7.1	
103		7.8	
113		8.4	
122		9.1	
131		9.7	
141		10.4	
150		11.0	
159		11.7	
169		12.3	
178		13.0	
188		13.6	

Time (msec)	Displacement (ft)	
(continued)		
197	14.3	
206	14.9	
216	15.5	
225	16.1	
234	16.7	
244	17.4	
253	18.1	
263	18.8	
272	19.4	
281	20.1	
290	20.8	V_2 = 72.7 fps
300	21.5	
310	22.2	
319	22.8	
329	23.5	
338	24.2	
347	24.9	
356	25.6	
366	26.3	
375	27.0	
385	27.6	
394	28.3	
403	29.0	
413	29.6	
422	30.2	
431	30.9	

TABLE A2

TEST 505 V-E

High-Speed Film Data

Time (msec)		Displacement (ft)	
-40		-3.5	V_1 = 87.5 fps
-30		-2.6	
-20		-1.8	
-10		-0.9	
0	Impact	0	
10		0.8	
20		1.7	
30		2.6	
40		3.5	
50		4.2	
60		5.0	
70		5.8	
80		6.6	
90		7.3	
100		8.1	
110		8.8	
120		9.5	
130		10.2	
140		10.8	
149		11.5	
159		12.1	

Time (msec)	Displacement (ft)	
(continued)		
169	12.7	
179	13.2	
189	13.8	
199	14.3	
209	14.8	
219	15.3	
229	15.8	
239	16.3	V_2 = 43.9 fps
249	16.7	
259	17.2	
269	17.6	
279	18.1	
289	18.5	
299	18.9	
309	19.4	
319	19.8	
339	20.6	
359	21.5	
379	22.3	
399	23.1	

TABLE A3

TEST 505 V-F

High-Speed Film Data

Time (msec)		Displacement (ft)	
-39		-3.5	V_1 = 89.7 fps
-30		-2.7	
-20		-1.8	
-10		-0.9	
0	Impact	0	
10		0.9	
20		1.8	
30		2.6	
39		3.4	
49		4.1	
59		4.8	
69		5.4	
79		6.1	
89		6.7	
98		7.2	
108		7.7	
118		8.2	
128		8.6	

Time (msec)	Displacement (ft)
(continued)	
138	9.0
148	9.4
167	10.0
187	10.5
207	10.9
227	11.2
246	11.5
266	11.8
286	11.9
305	12.1
325	12.2
345	12.2
364	12.2
561	11.6
808	10.8
1302	10.1

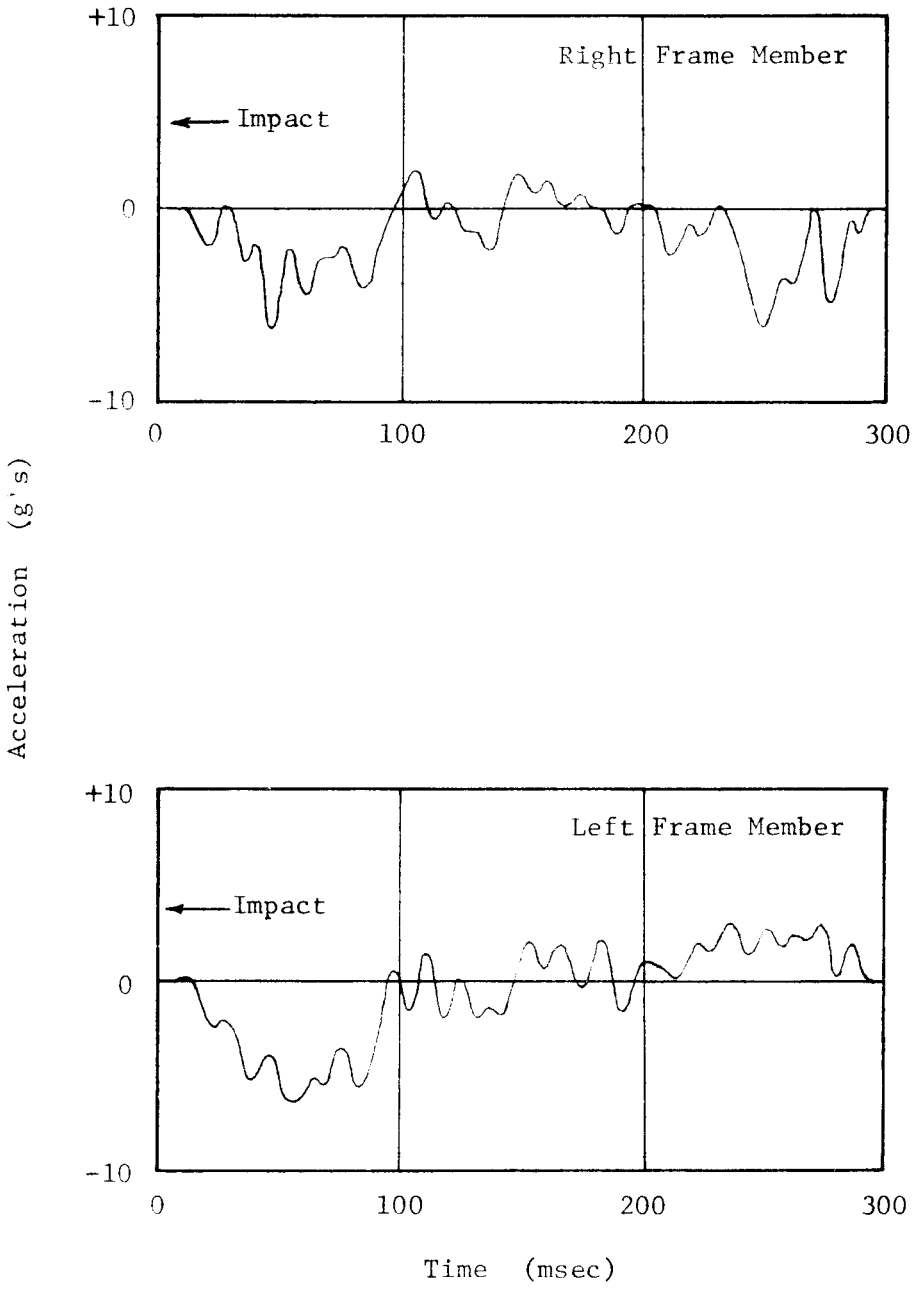

Figure A1, Longitudinal Accelerometer Data, Test D.

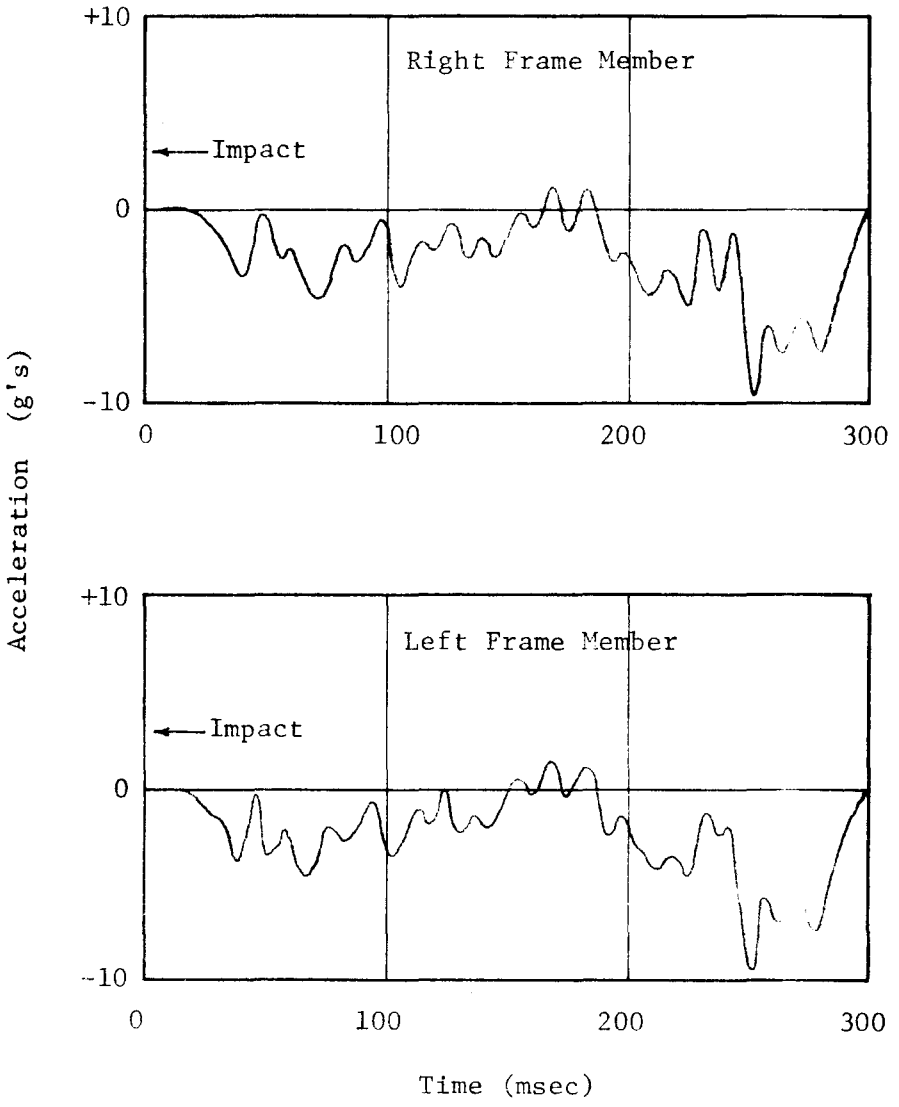

Figure A2, Transverse Accelerometer Data, Test P.

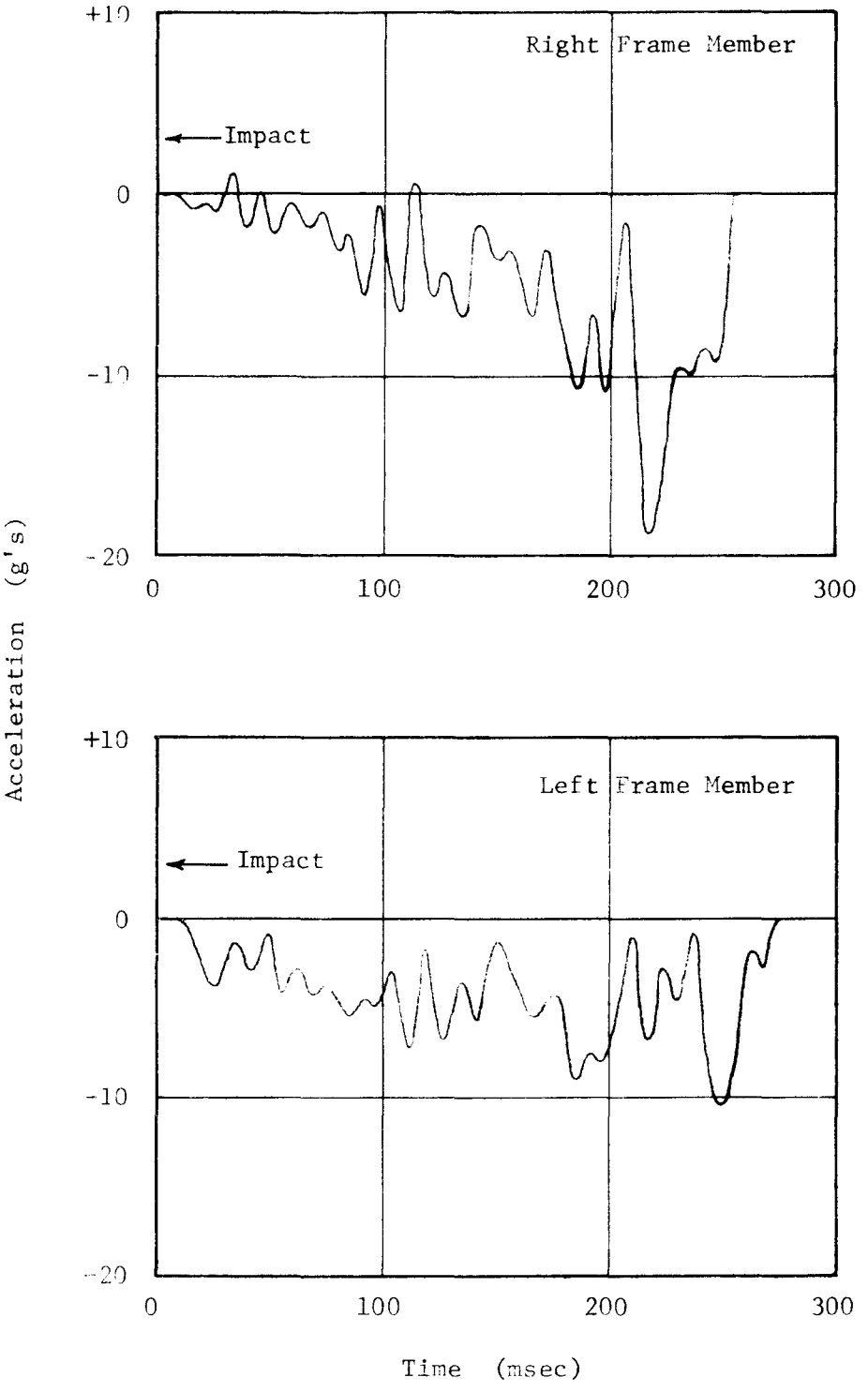

Figure A3, Longitudinal Accelerometer Data, Test E.

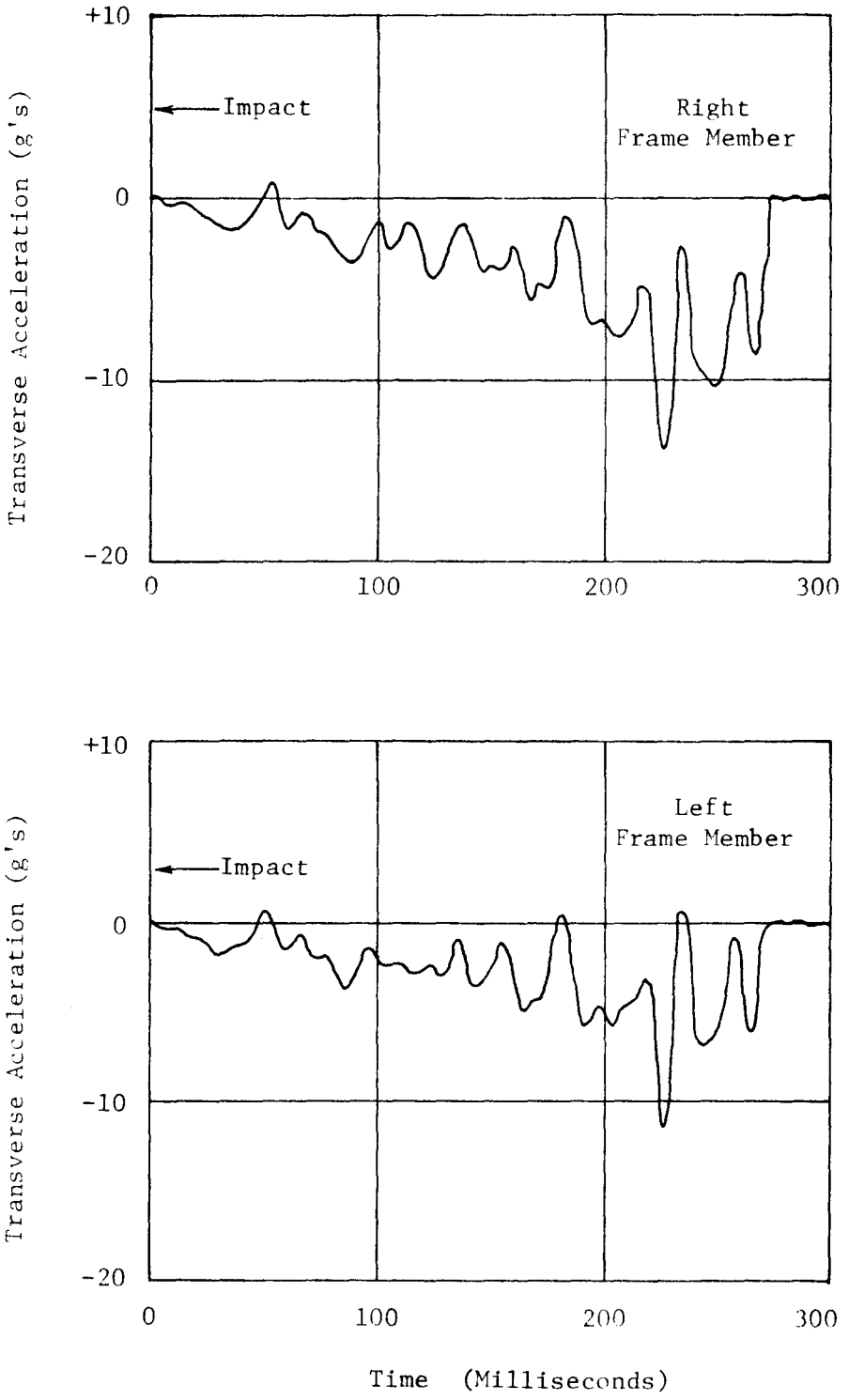

Figure A4 , Transverse Accelerometer Data, Test E

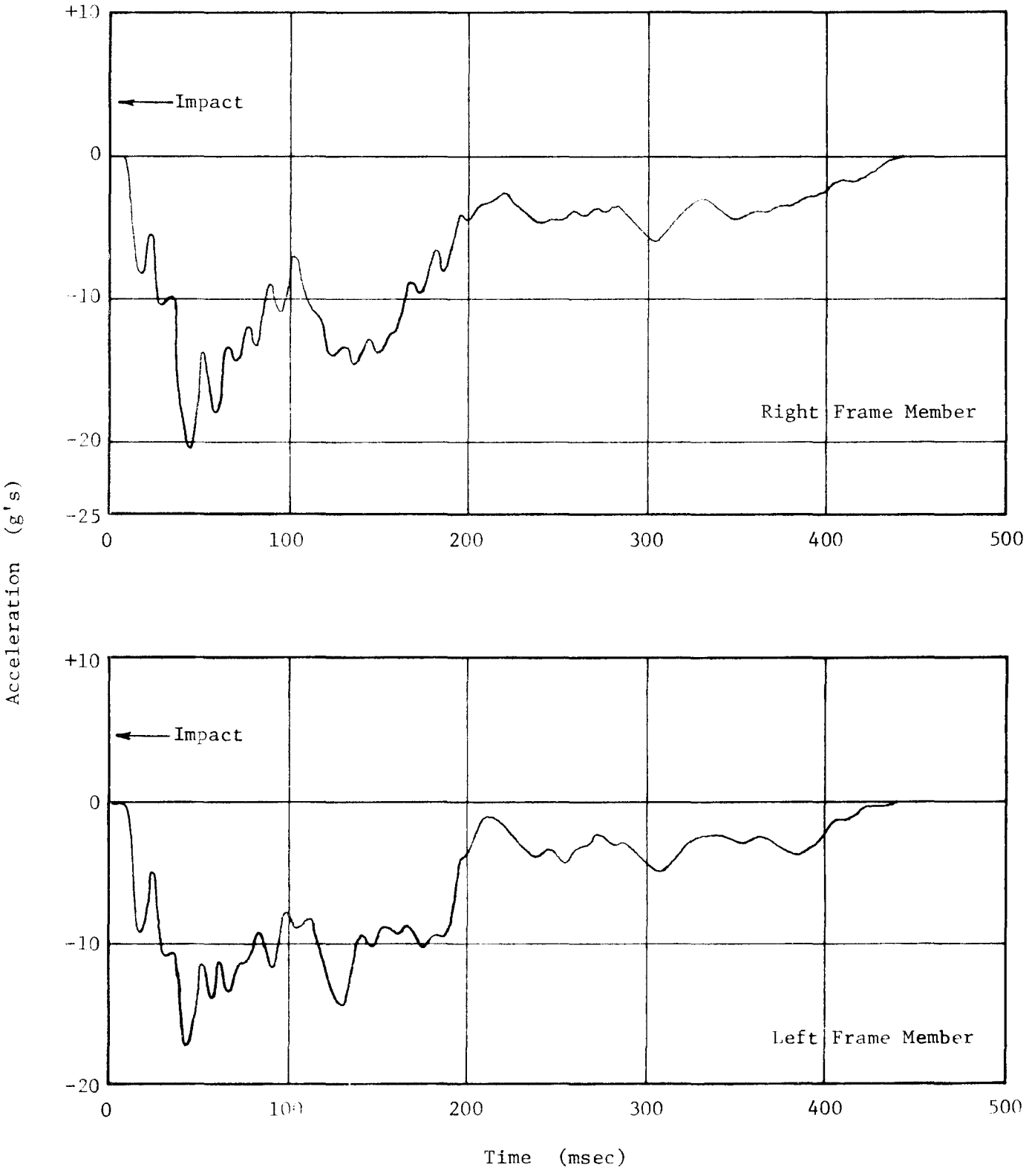

Figure A5, Longitudinal Accelerometer Data, Test F.

APPENDIX B

MODEL STUDY

MODEL ANALYSIS

The following model analysis describes the relationship between the static crushing energy of the full scale vermiculite concrete crash cushion and the static crushing energy of small scale modules.

In the judgment of the writers, the following geometric and material properties are the most important to the relationship between prototype and model. Other factors, which obviously are of some influence to static crushing energy are assumed to be of secondary importance.

Geometric Properties

1) a-(Refer to Figure B1)
2) b-(Refer to Figure B1)
3) h-(Refer to Figure B1)
4) B-(Refer to Figure B1)
5) D-(Refer to Figure B1)
6) t-(Refer to Figure B1)
7) A-Cross sectional area of reinforcement in a module cross section

Material Properties

8) f'_c -static crushing strength of the vermiculite concrete

Structural Property

9) E-static crushing energy of a particular module

In the following development the subscripts p and m refer to prototype and model respectively.

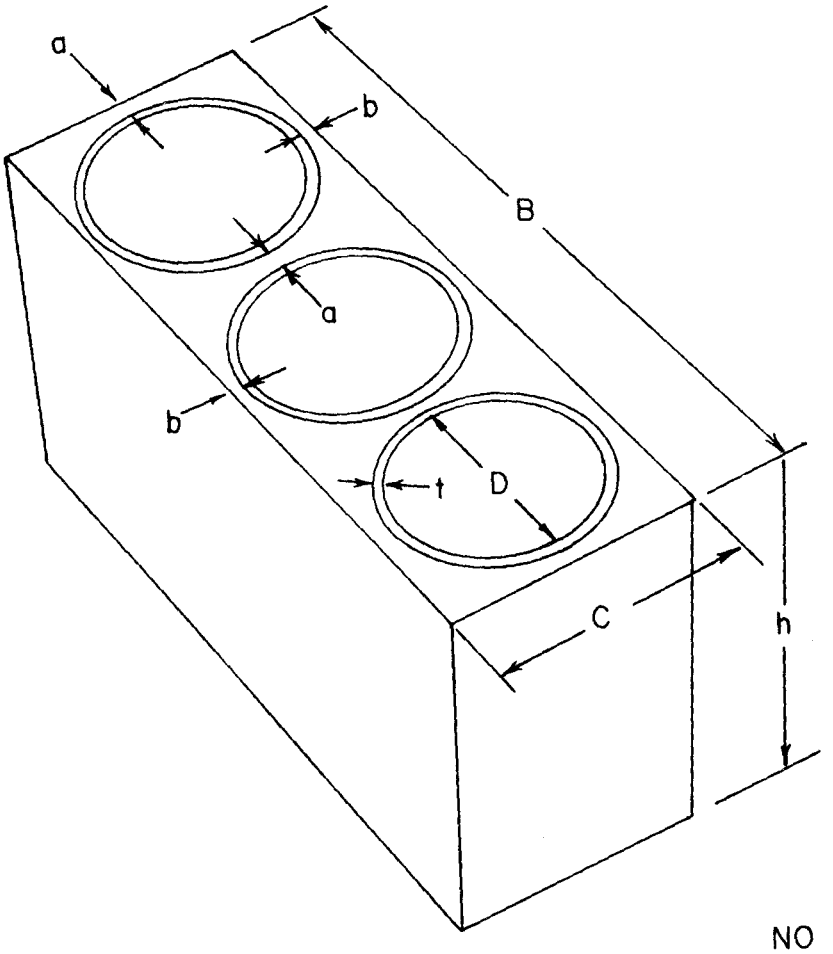

NO SCALE

FIGURE B1, MODULE DIMENSIONS

The interrelationship of static crushing strength and the geometric and material properties can be written as follows:

$$E = (\text{A function of}) \ (f'_c,\ a,\ b,\ h,\ t,\ B,\ D,\ A). \tag{1}$$

Since there are two dimensions involved (force and length) the number of Pi terms necessary to describe this relationship in dimensionless terms is two less than the total number of variables in Eq. 1.

i.e. 9 - 2 = 7 Pi terms

These terms can be chosen and the functional relationship written as:

$$\frac{E}{f'_c\ D^3} = (\text{A function of}) \left(\frac{a}{D},\ \frac{b}{D},\ \frac{h}{D},\ \frac{t}{D},\ \frac{B}{D},\ \&\ \frac{A}{D^2}\right). \tag{2}$$

For the model and the prototype this equation can be expressed as:

$$\frac{E_m}{f'_{c_m}\ D_m^3} = F\left(\frac{a_m}{D_m},\ \frac{b_m}{D_m},\ \frac{h_m}{D_m},\ \frac{t_m}{D_m},\ \frac{B_m}{D_m},\ \&\ \frac{A_m}{D_m^2}\right) \tag{3}$$

$$\frac{E_p}{f'_{c_p}\ D_p^3} = F\left(\frac{a_p}{D_p},\ \frac{b_p}{D_p},\ \frac{h_p}{D_p},\ \frac{t_p}{D_p},\ \frac{B_p}{D_p},\ \&\ \frac{A_p}{D_p^2}\right). \tag{4}$$

Then if the ratio of D_p to D_m is defined as the modeling factor, the following conditions must be maintained in order for the prediction equation to be valid:

$$a_p = n\ a_m \qquad B_p = n\ B_m$$

$$b_p = n\ b_m \qquad A_p = n^2\ A_m\ .$$

$$h_p = n\ h_m$$

$$t_p = n\ t_m$$

These equations are found by equating the corresponding Pi terms of Eqs. 3 and 4 and substituting n for the ratio D_p/D_m.

If these conditions are held, then the prediction equation is:

$$\frac{E_m}{f'_{c_m} D_m^3} = \frac{E_p}{f'_{c_p} D_p^3} .$$

Since F'_{c_m} can be made equal to f'_{c_p}, this equation reduces to:

$$E_p = n^3 E_m. \tag{5}$$

Thus if the static energy of a model module is determined by testing, the energy of a prototype would be predicted by Eq. 5.

EXPERIMENTAL PROGRAM

The design concrete mixtures and actual batch data are given in Tables B1 and B2. The schedule of model modules, including the parameters studied, are given in Table B3.

Cardboard molds for standard 6 x 12 in. concrete cylinders were used to simulate the "sonotubes" in the model modules. The forms for the modules (illustrated in Figure B2) were made of plywood. Half-inch hardware cloth with alternate wires removed to obtain the correct amount of cross-sectional area was used for reinforcement (Figure B3). The assembled form is shown in Figure B4, and a model module in Figure B5.

The model modules were tested in a hydraulic universal testing machine as shown in Figure B6. A scale on either end of the loading head was used to determine crushing distance. Figures B7 through B14 and B15 through B18 are sequential photographs of the two module tests.

Several limitations of the experimental design should be noted. First, no attempt was made to scale the strength of the cardboard sonotubes; and second, the loading technique used in the model study did not closely simulate the loading of a vehicle on a prototype.

Batches	Cement Type		Mix Properties		Expected f_c'
HE 1 (505V-A)	High Early		Cmt.	2.9 sk	50 psi
			Agg.	5 sk	
			Water	73 gal	
			Admix	1 pt/sk agg.	
			U. Wt.	37 pcf	
HE 2	High Early		Cmt.	5 sk	175 psi
			Agg.	7-1/2 sk	
		1:6	Water	100 gal.	
			Admix	1 pt/sk agg.	
			U. Wt.	50 pcf	
HE 3	High Early		Cmt.	7-1/2 sk	425 psi
			Agg.	7-1/2 sk	
		1:4	Water	98 gal.	
			Admix	1 pt/sk agg.	
			U. Wt.	60 pcf	
RS 1 (505V-C)	Regulated Set		Cmt.	3.25 sk	60 psi
			Agg.	5.76 sk	
			Water	77.5 gal.	
			Air	1 pt/sk agg.	
			U. Wt.	41 pcf	

TABLE B1 DESIGN CONCRETE MIXTURES

BATCH NO.	DATE	CEMENT lbs.	AGGREGATE[1] cu. ft.	WATER lbs.	ADMIX pints	UNIT WEIGHT lbs.	AIR[2] %
RS1	4/30/70	79 1/2	6	168	1 1/2	40.5	35
HE1	5/05/70	54.4	4	121.4	1	42	50
HE2	5/11/70	94	6	166.7	1 1/2	43	50
HE3	5/12/70	141	6	163.3	1 1/2	49	51

[1] 1 sk = 4 cu. ft.

[2] Measured with pressure meter.

TABLE B2, BATCH DATA

VERMICULITE MODEL MODULES

Module	Concrete Batch	Design f'c psi	Actual f'c psi	h[1] inch	B[1] inch	C[1] inch	a[1] inch	b[1] inch
M1	RS1	50	77	9.82	19.7	6.53	0.272	0.136
M2	HE2	175	104	9.82	19.7	6.53	0.272	0.136
M3	HE3	425	220	9.82	19.7	6.53	0.272	0.136
M4	RS1	50	77	9.82	18.85	6.53	0.136	0.136
M5	RS1	50	77	9.82	20.50	6.53	0.545	0.136
M6	RS1	50	77	9.82	6.74	6.53	0.272	0.136
M7	RS1	50	77	9.82	13.20	6.53	0.272	0.136
M8	RS1	50	77	9.82	19.7	6.74	0.272	0.272
M9	RS1	50	77	9.82	19.7	7.30	0.272	0.545

[1]See Figure 1

TABLE B3 MODEL MODULE SPECIFICATIONS

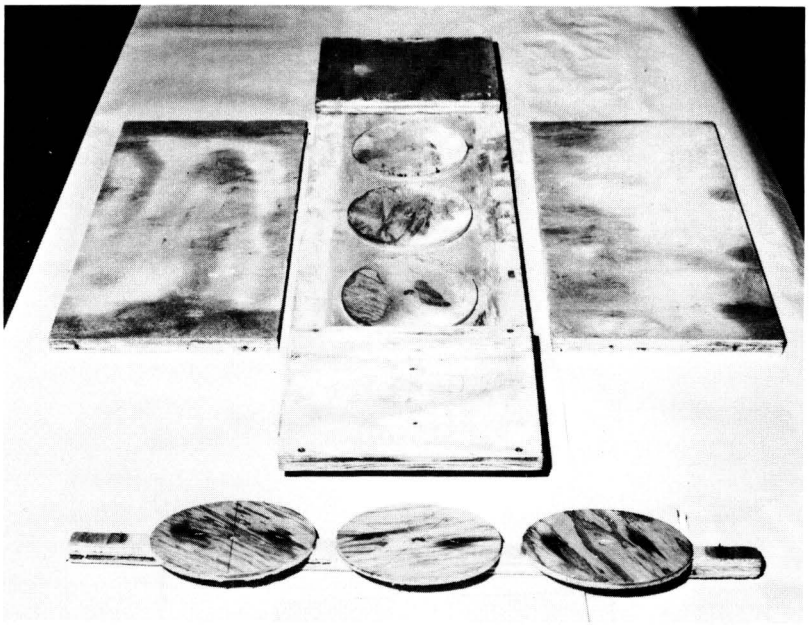

Figure B2

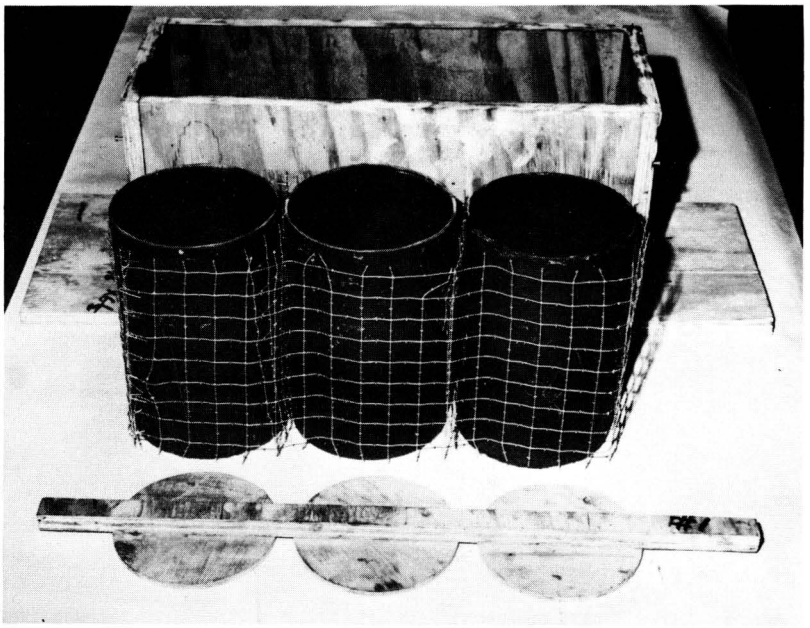

Figure B3

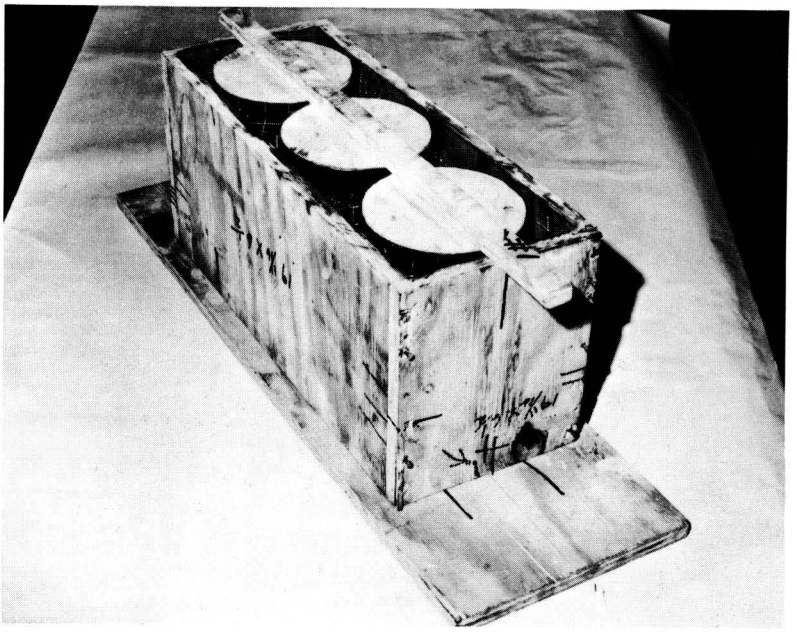

Figure B4

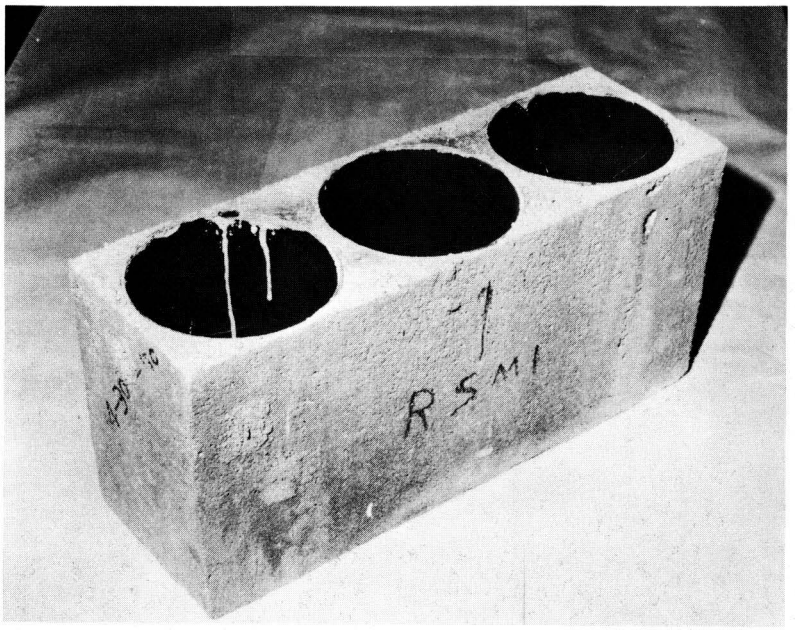

Figure B5

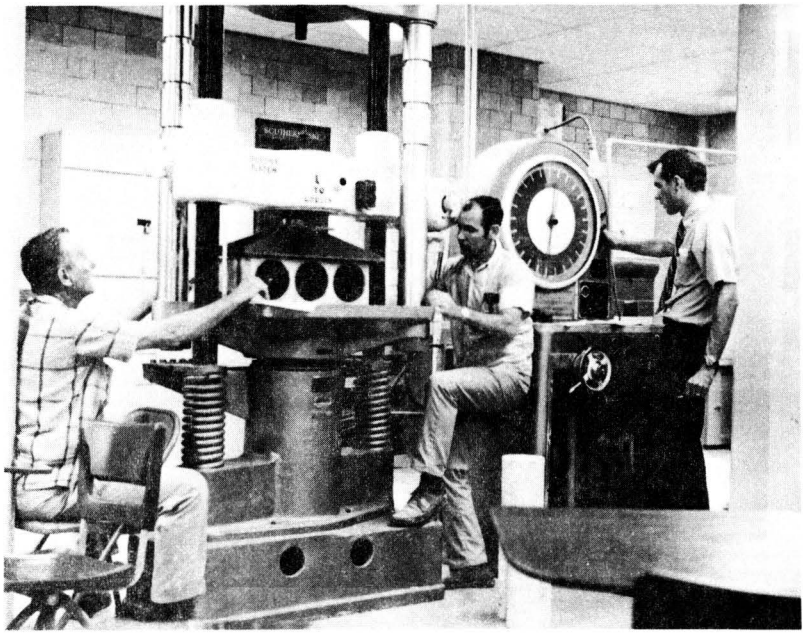

Figure B6

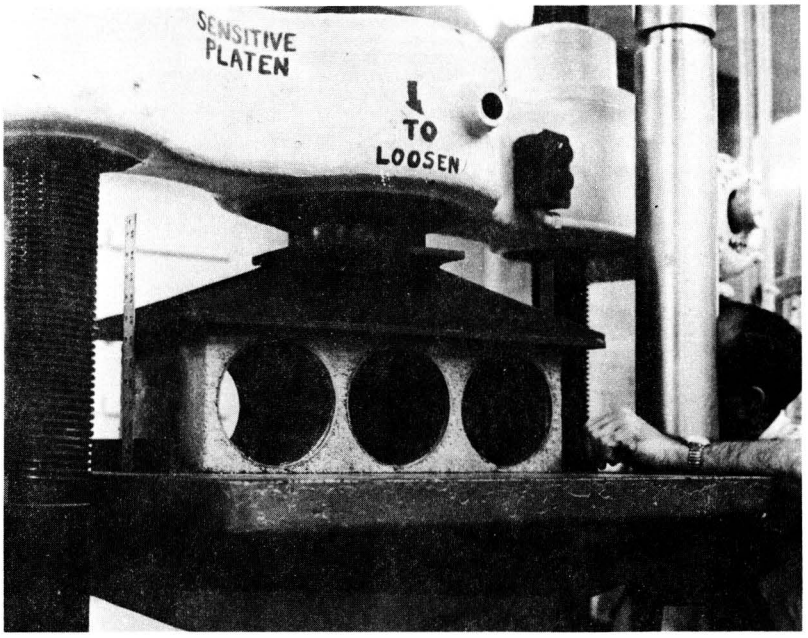

Figure B7

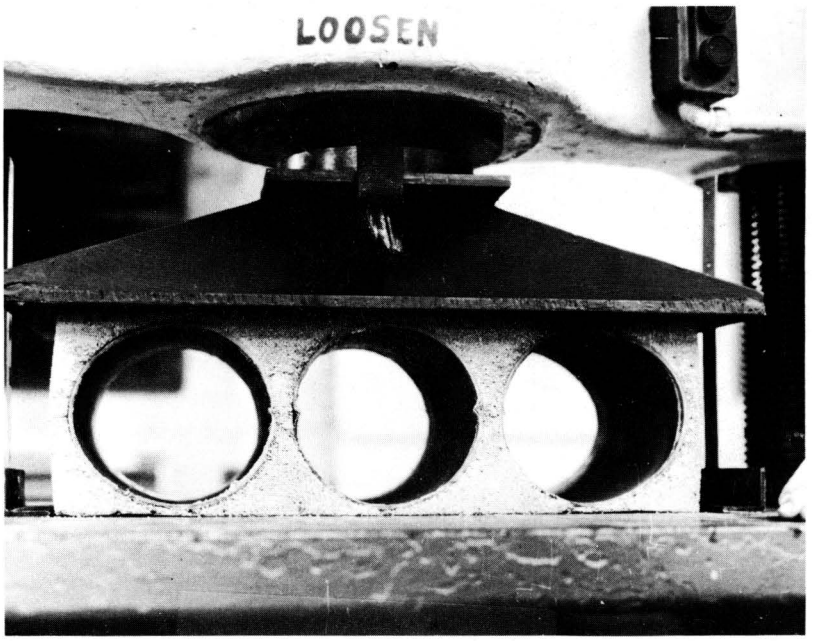

Figure B8

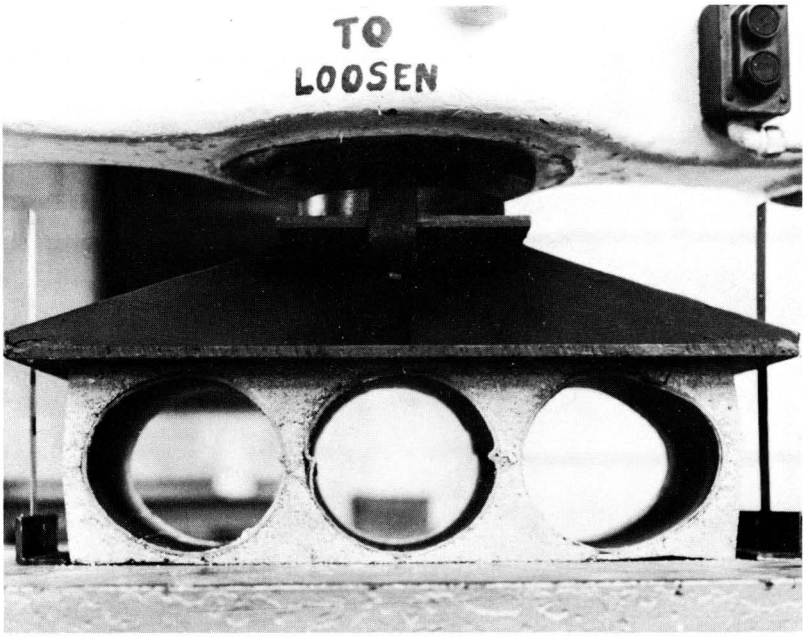

Figure B9

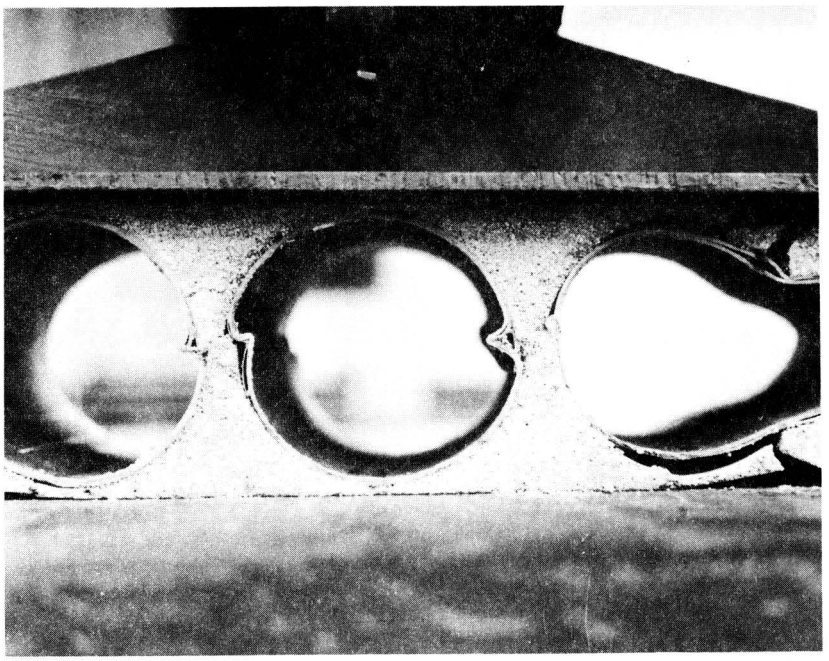

Figure B10

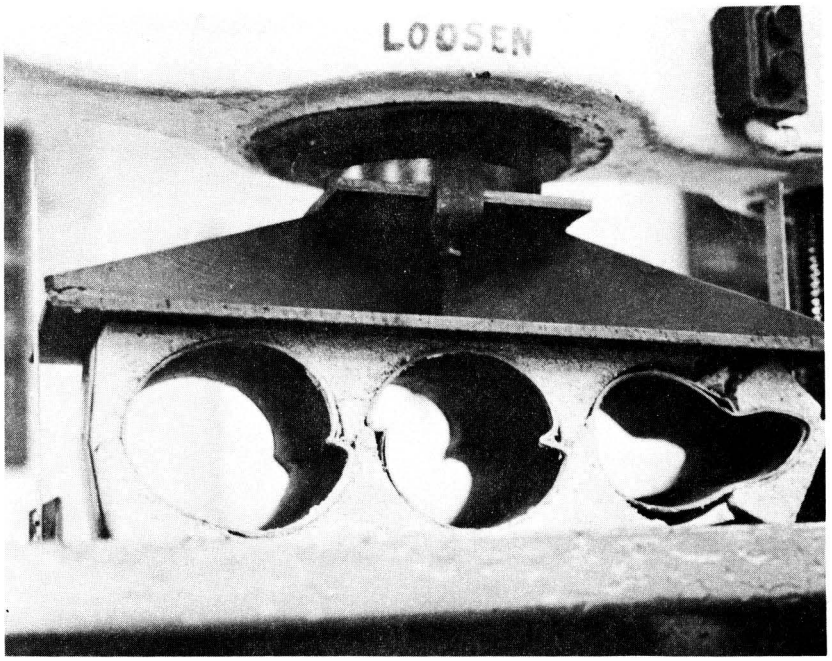

Figure B11

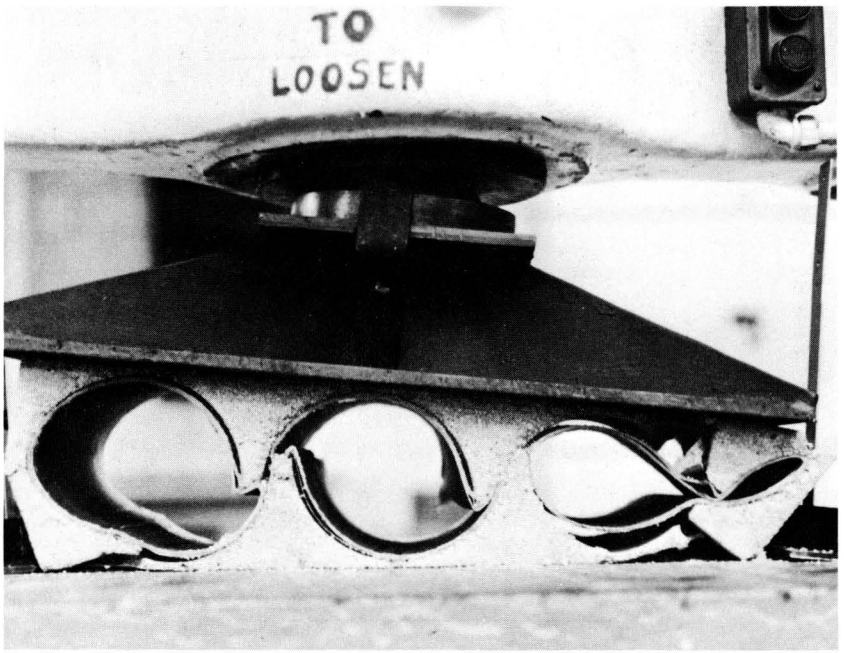

Figure B12

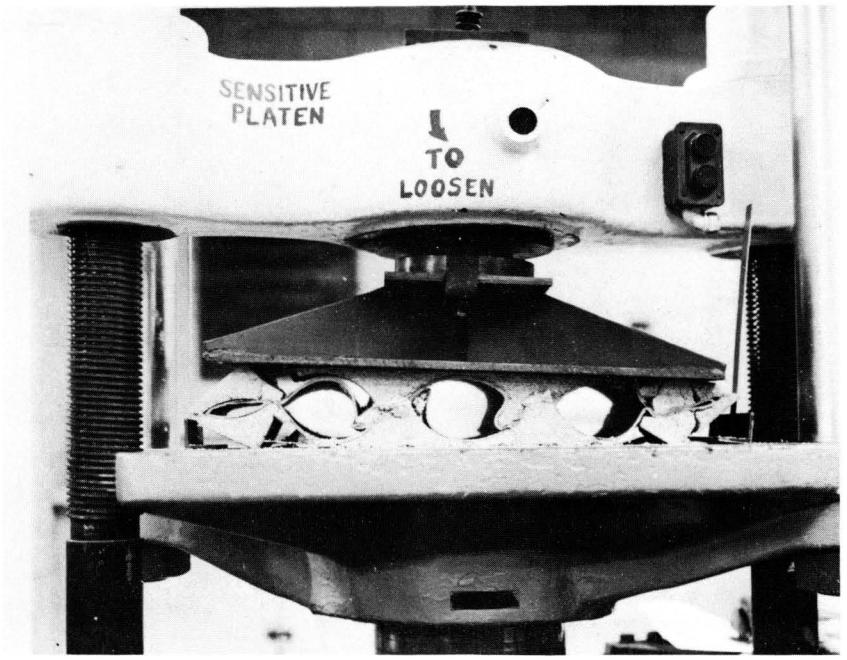

Figure B13

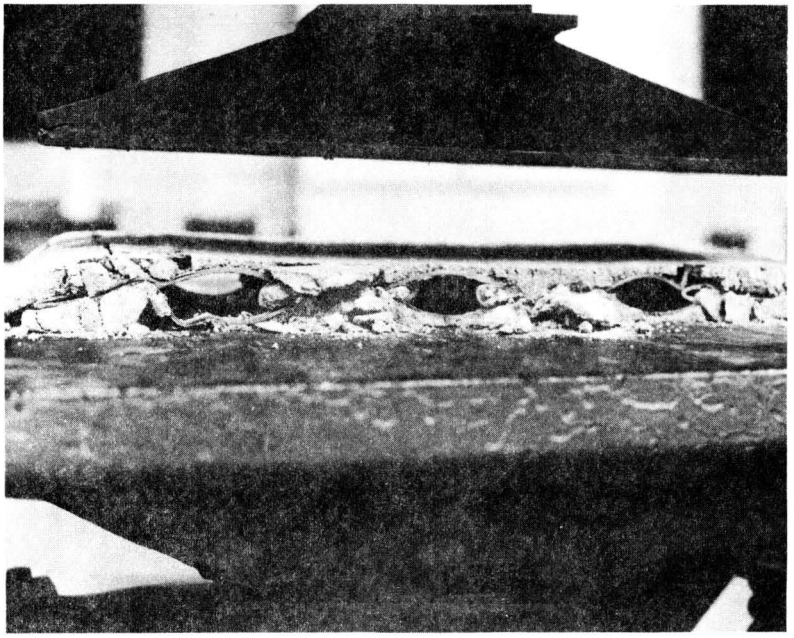

Figure B14

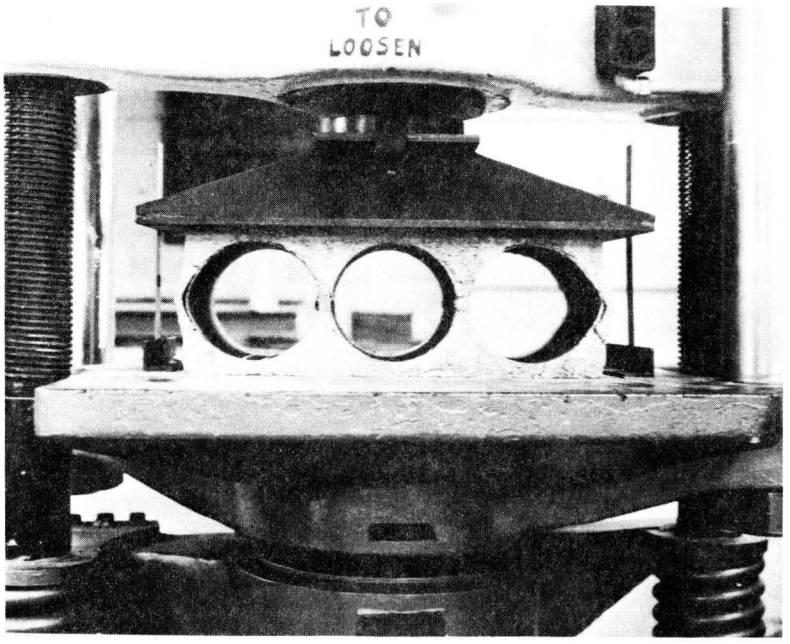

Figure B15

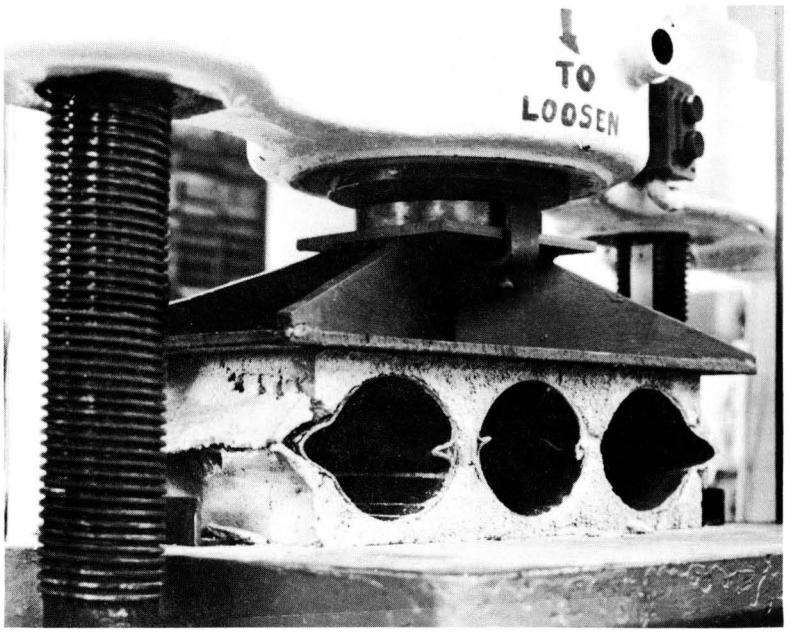

Figure B16

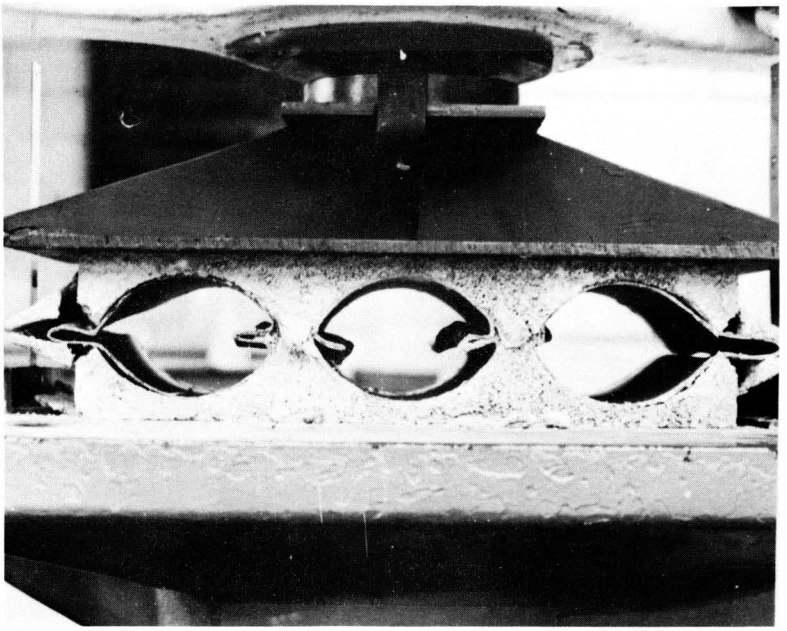

Figure B17

RESULTS

STRENGTH-TIME RELATIONSHIPS

The strength-time relationships for the four concrete mixtures are illustrated in Figure B19. As anticipated, there appears to be little gain in strength after the initial 21 days.

MODEL MODULES

Curves illustrating the relationship between crushing force and distance are shown in Figures B20 through B23. An effective crushing distance of 4.0 in. (crushing ratio = .61) was chosen for these model modules. This number represents a compromise between the point where the energy absorbing capacity of the model module was consumed and the actual crushing ratio observed for prototype cushions.

Figures B24 through B27 show the relative influence of variations in compressive strength and dimensions on the nondimensional energy parameter $E/(f'_c D^3)$. The results are most encouraging in that a rather linear relationship between the energy parameter and the other influential parameters under study is indicated. This lends additional confidence to the use of model analysis to predict prototype behavior in this particular application.

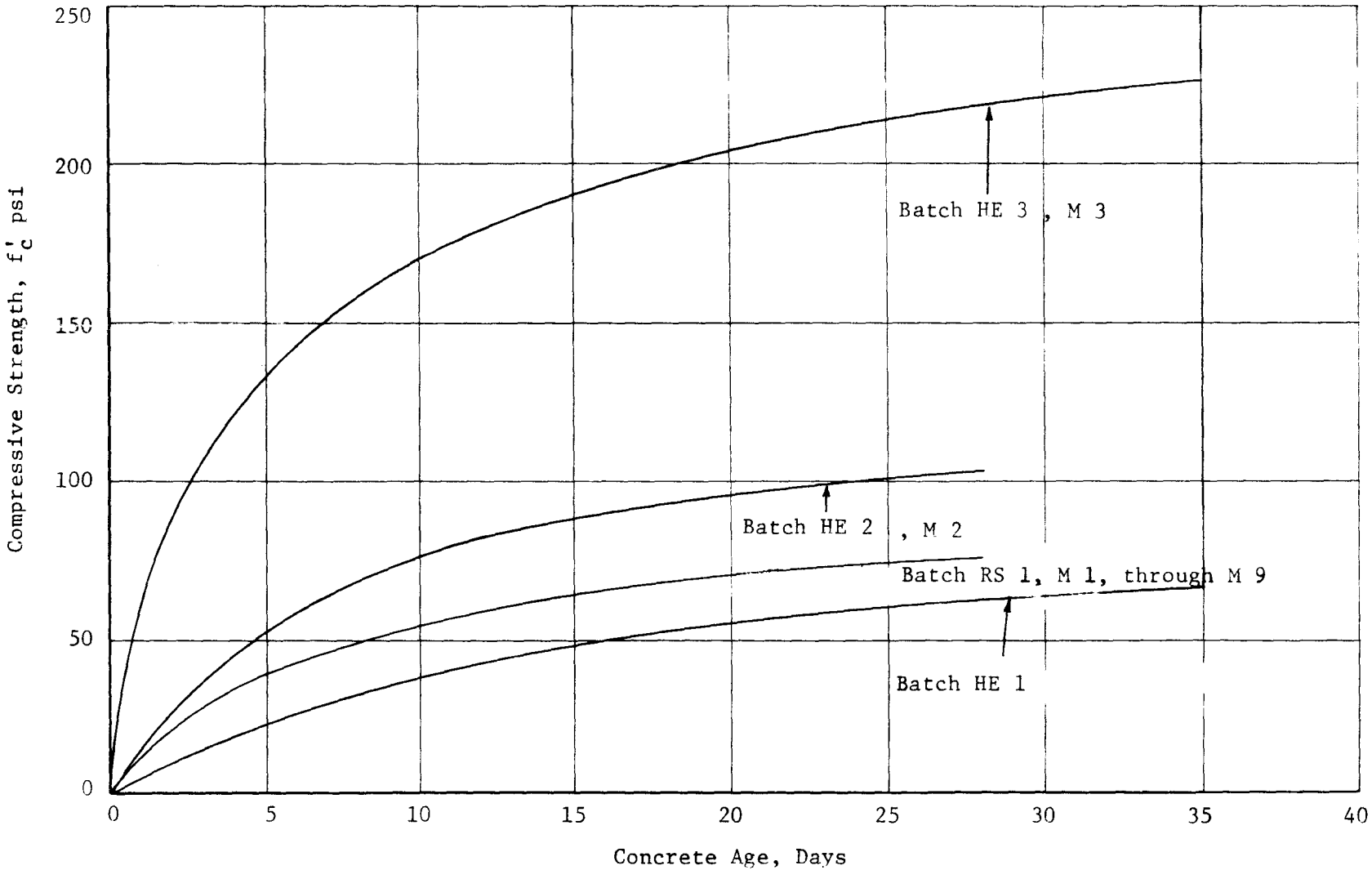

Figure B19 , Concrete Strength Development

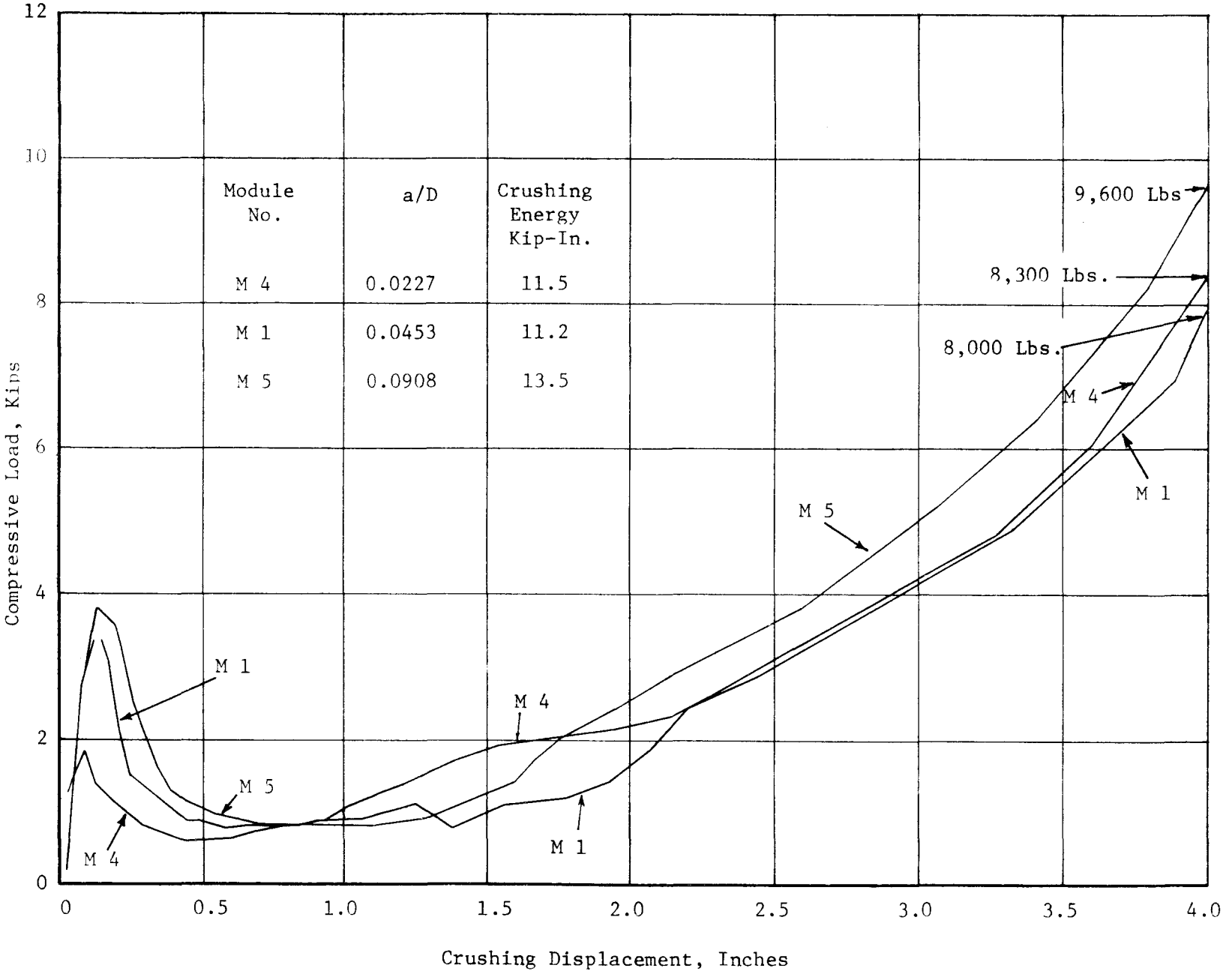

Figure B20 Model Tests For Variation In a/D Ratio

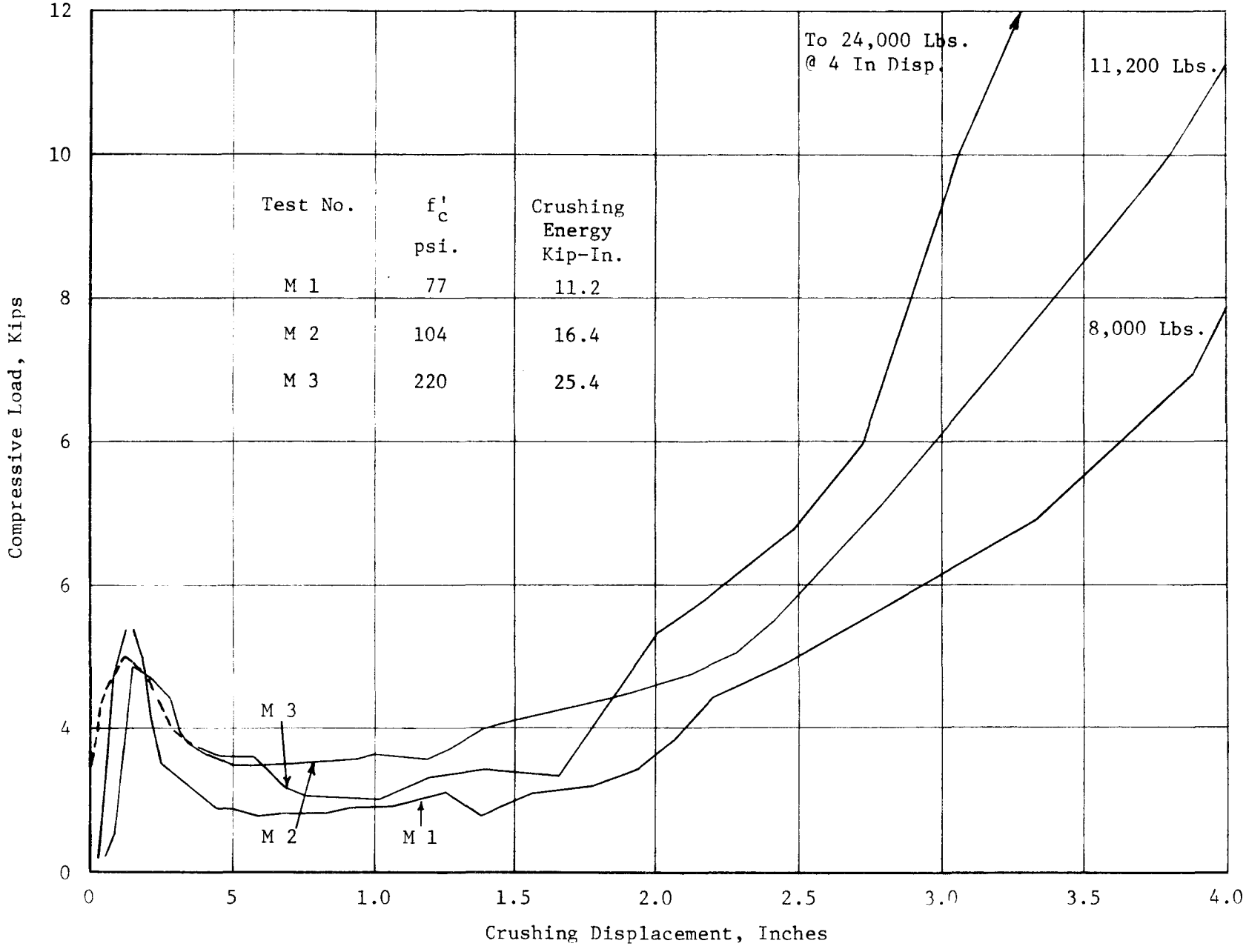

Figure B21, Module Tests For Variations In Compressive Strength

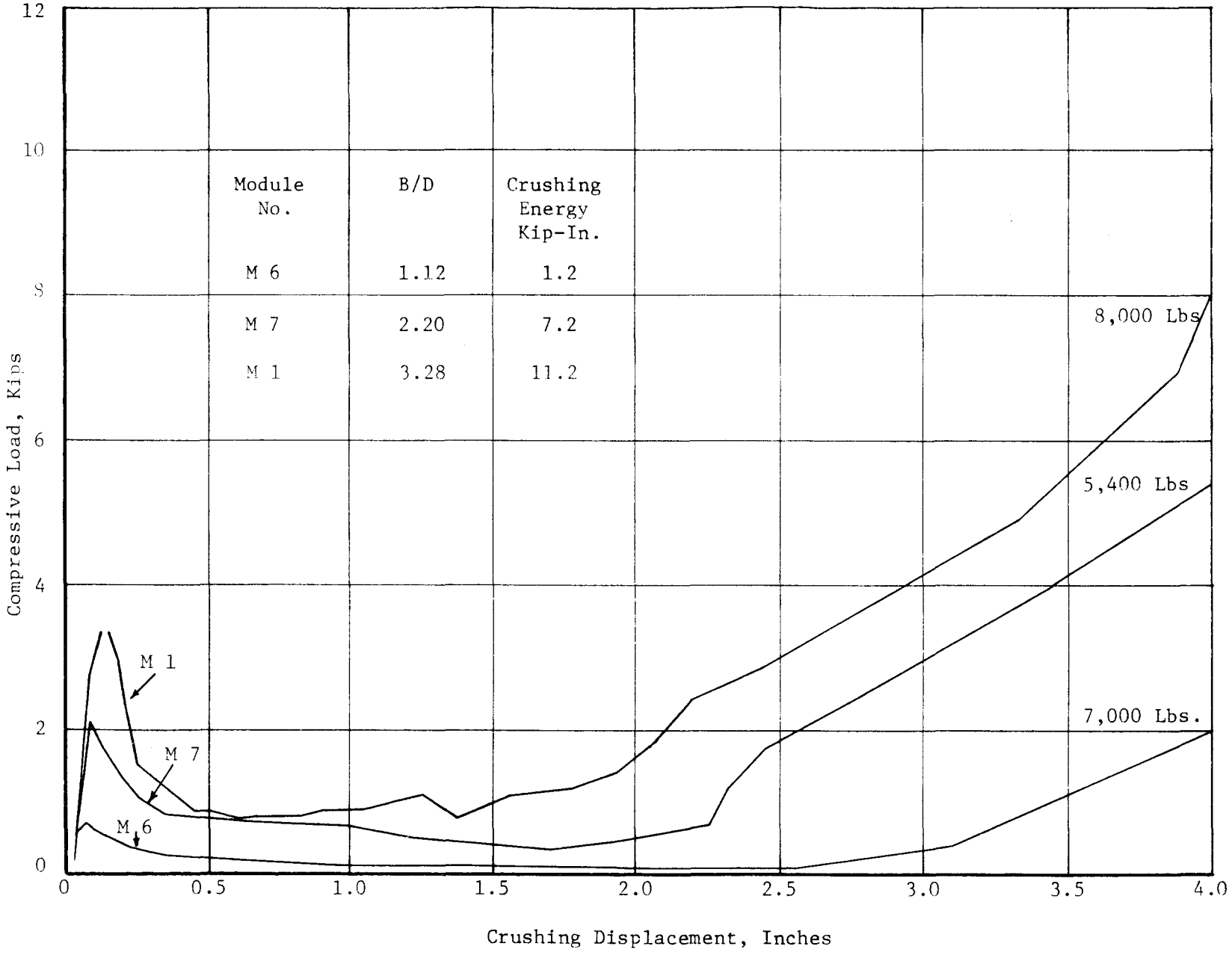

Figure B22 Model Tests For Variation In B/D Ratio

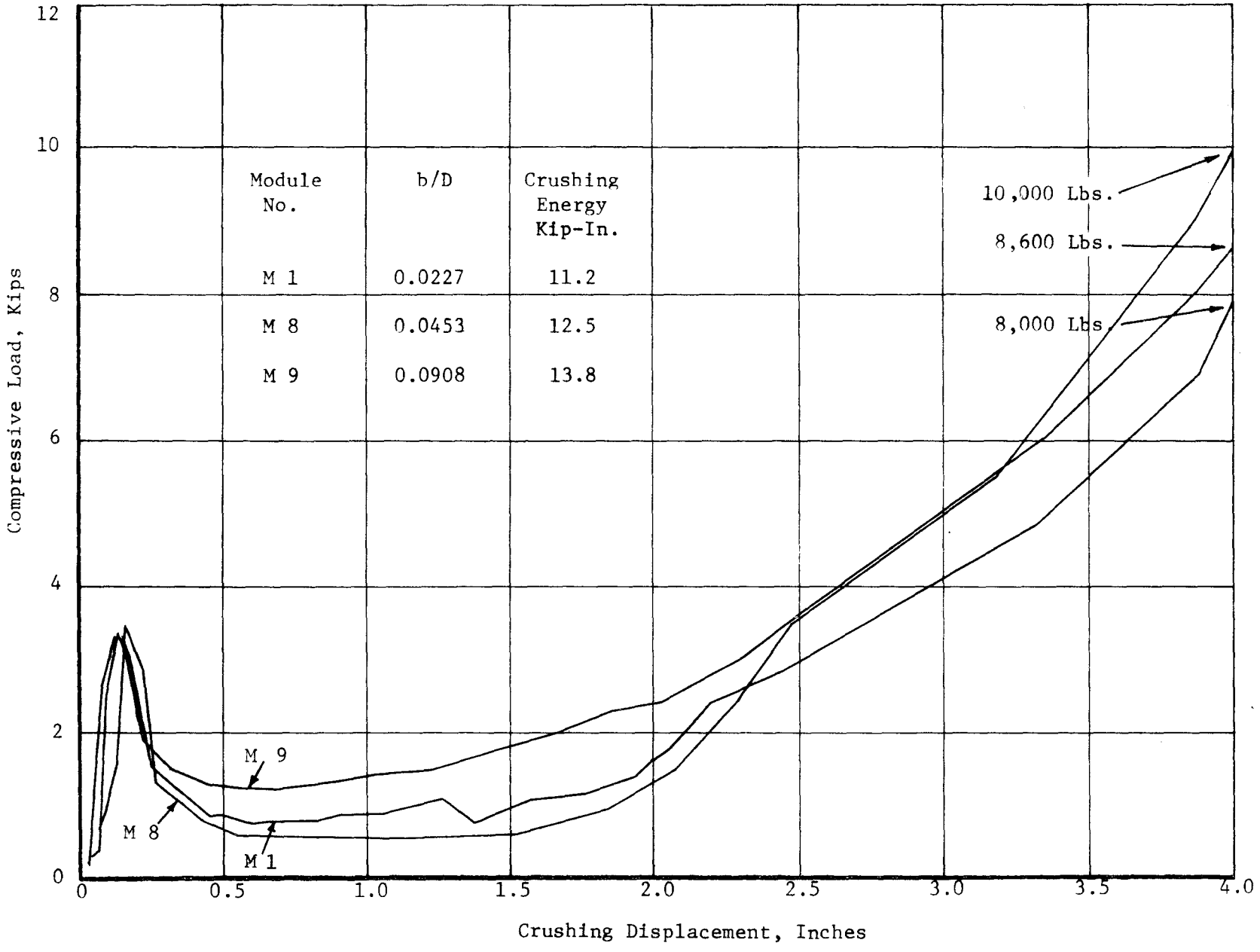

Figure B23, Model Tests For Variation Of b/D Ratio

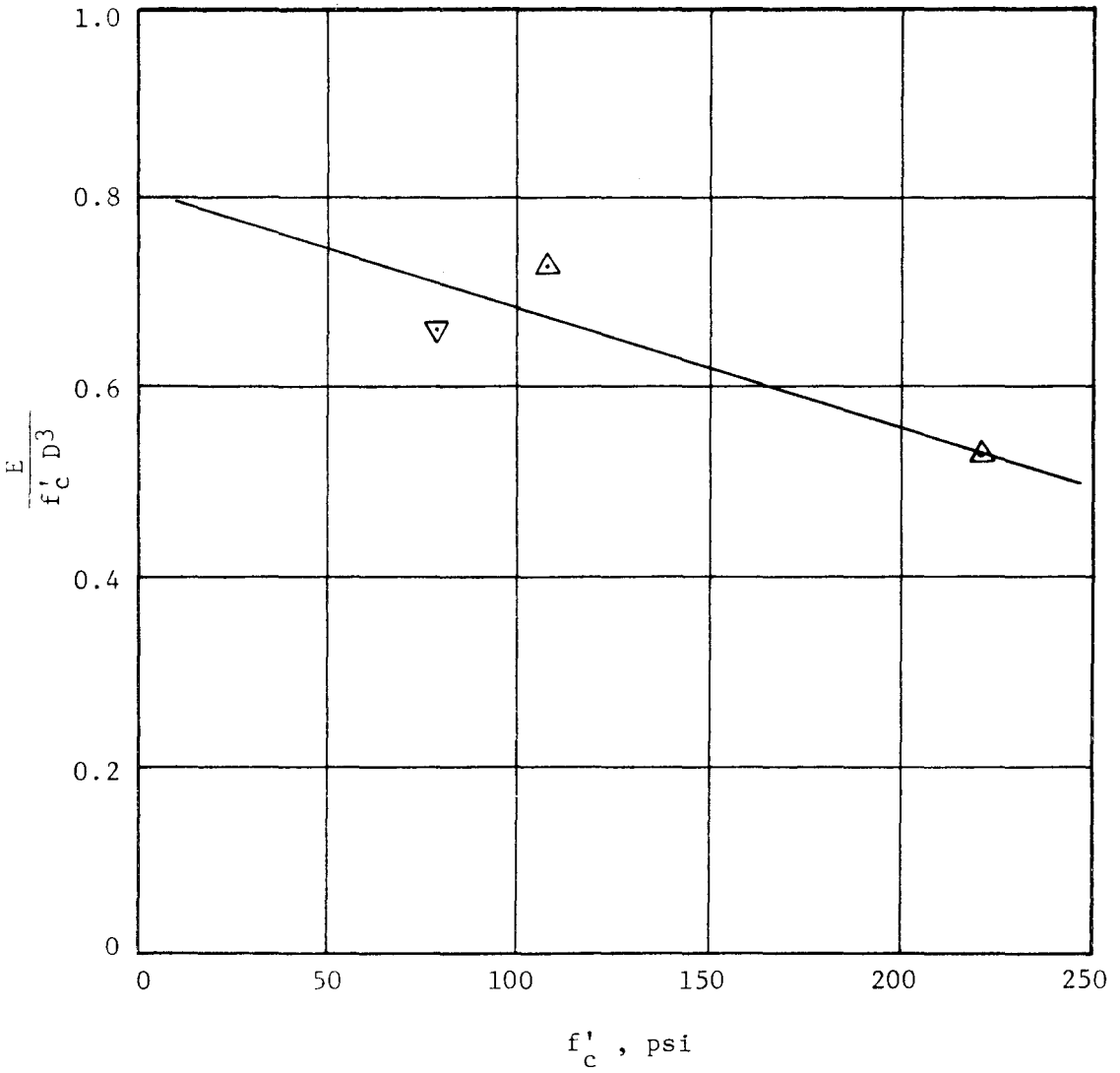

Figure B24, Influence of f'_c

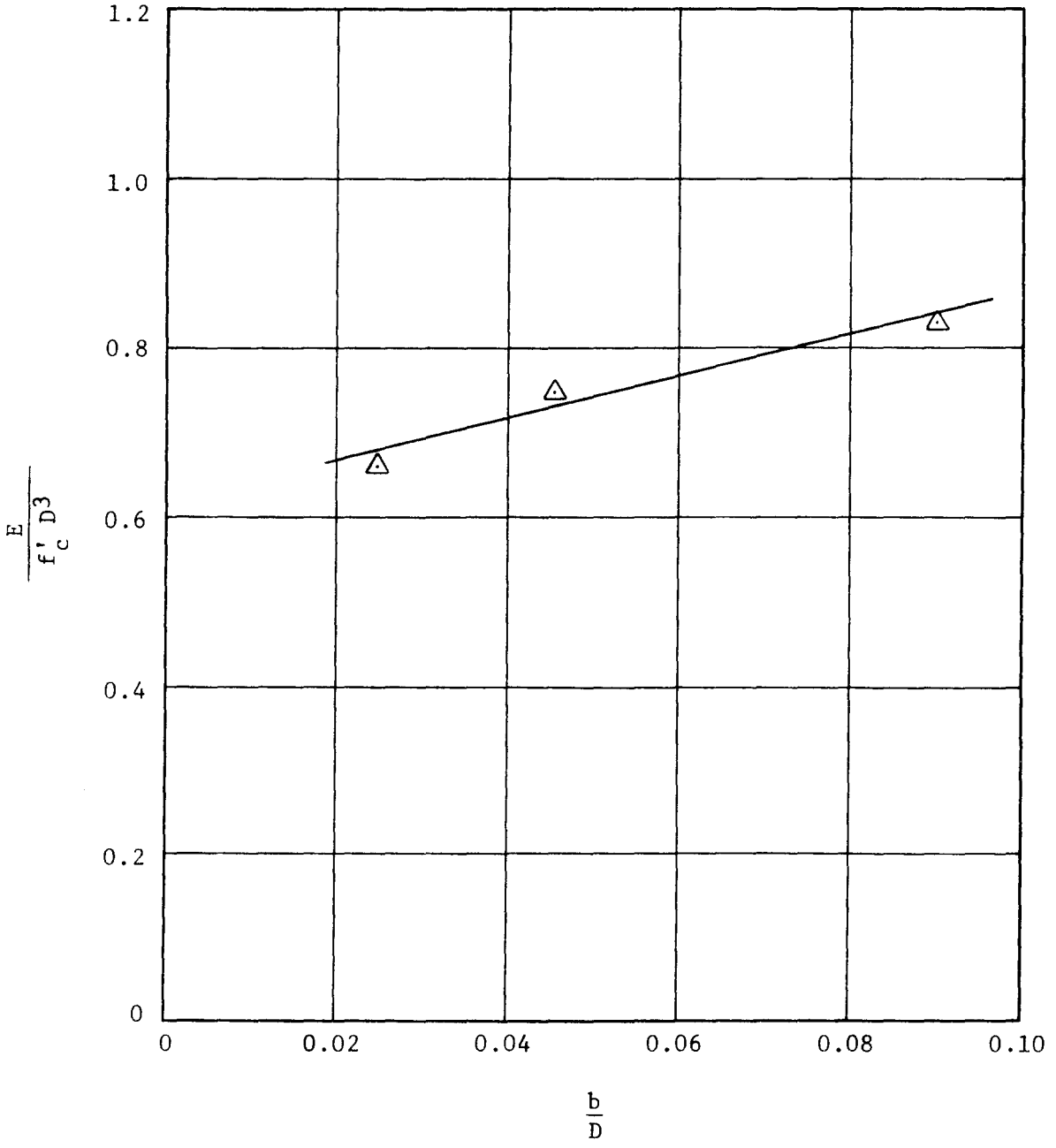

Figure B25, Influence of b/D

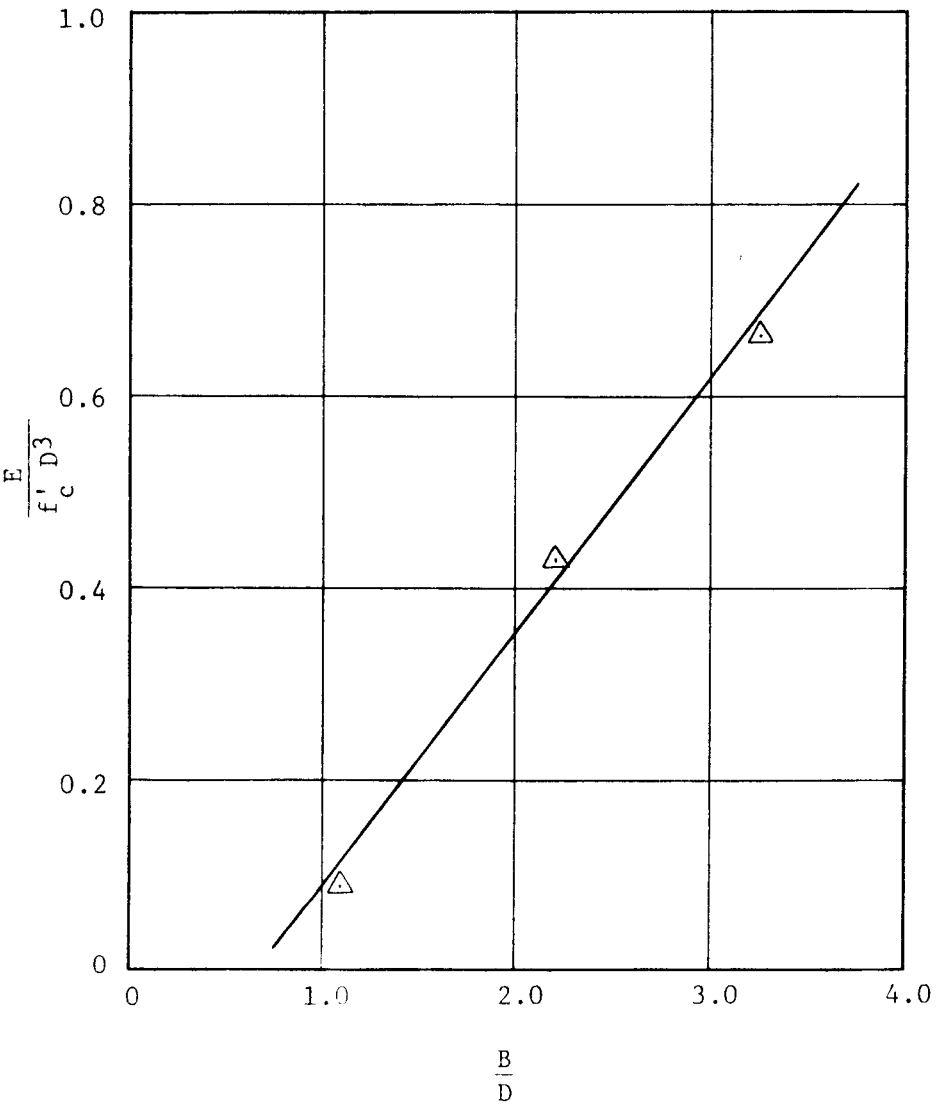

Figure B26 Infulence of B/D

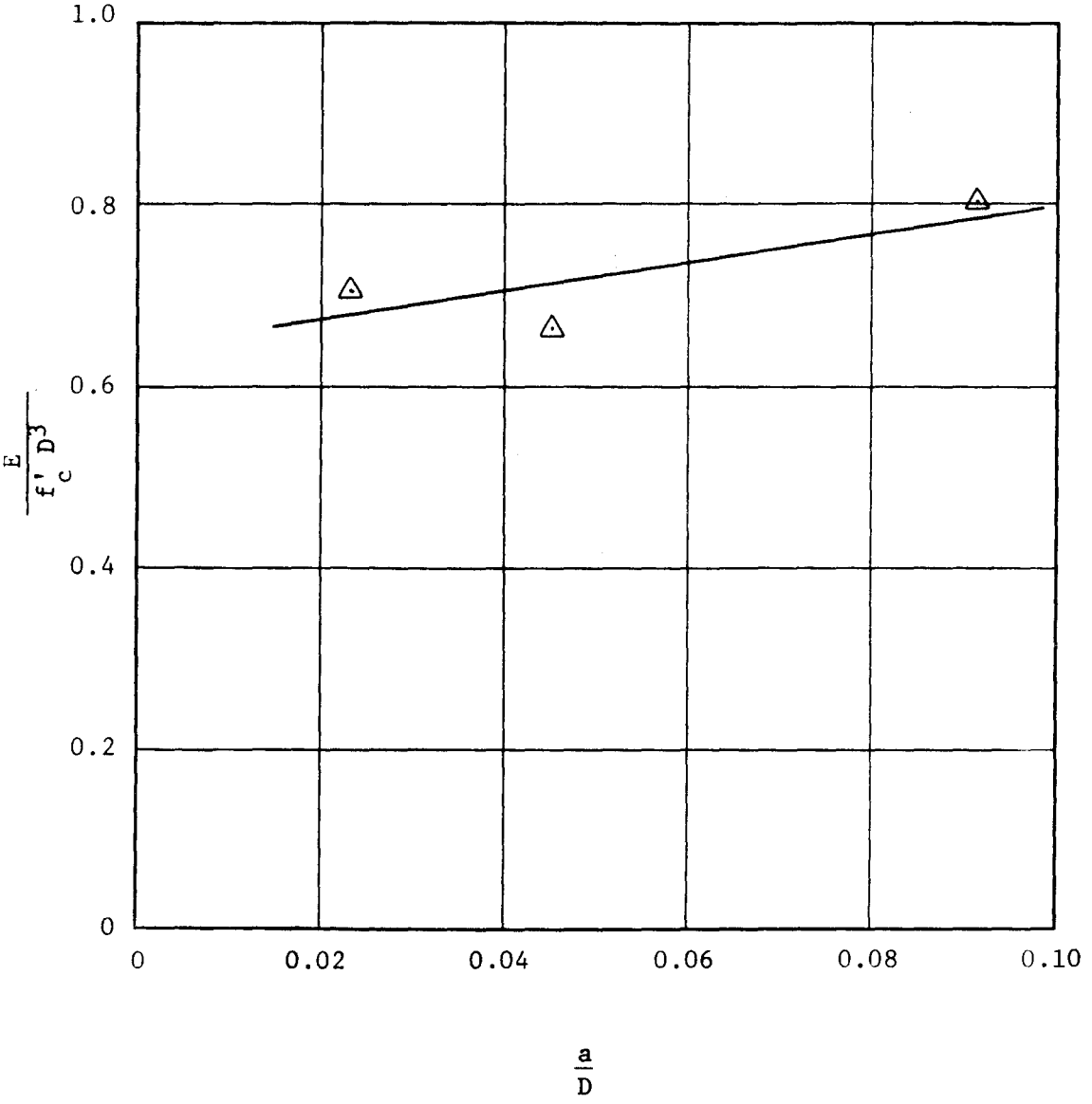

Figure B 27 Influence of a/D

PREDICTIONS WITH MODEL ANALYSIS

The test results from this model study can be used to predict the energy absorbed in the vehicle crash tests if the relationship between the energy absorbed in the dynamic and static conditions can be determined. To do this a comparison will be made between the energy predicted from the model study for the cushions tested in 505V-C and 505V-F and the actual kinetic energy absorbed during these tests. In Figures B28 through B31, the model test data in kip-in. is plotted as a function of the parameters f'_c, B/D, a/D, and b/D. If all model test values are multiplied by the cube of the scale factor and divided by 12, the result will be predicted prototype energy values in kip-ft. These new predicted values are also plotted on these Figures.

It is assumed that in test V-C, the energy absorption capacity of the cushion was exactly used up and that the capacity of this cushion is equal to the kinetic energy of the vehicle immediately before impact (namely 619 kip-ft). The crushing ratio of the modules in this cushion was experimentally determined by dividing the distance the vehicle penetrated the cushion by the original length of the cushion; 21.4 ft./24 ft. = .89. This value is assumed to be the crushing ratio for prototype modules. The predicted energy, on the basis of static model tests, is determined and adjusted for differences in compressive strengths using Figures B28 through B31. For an M7 type module, the

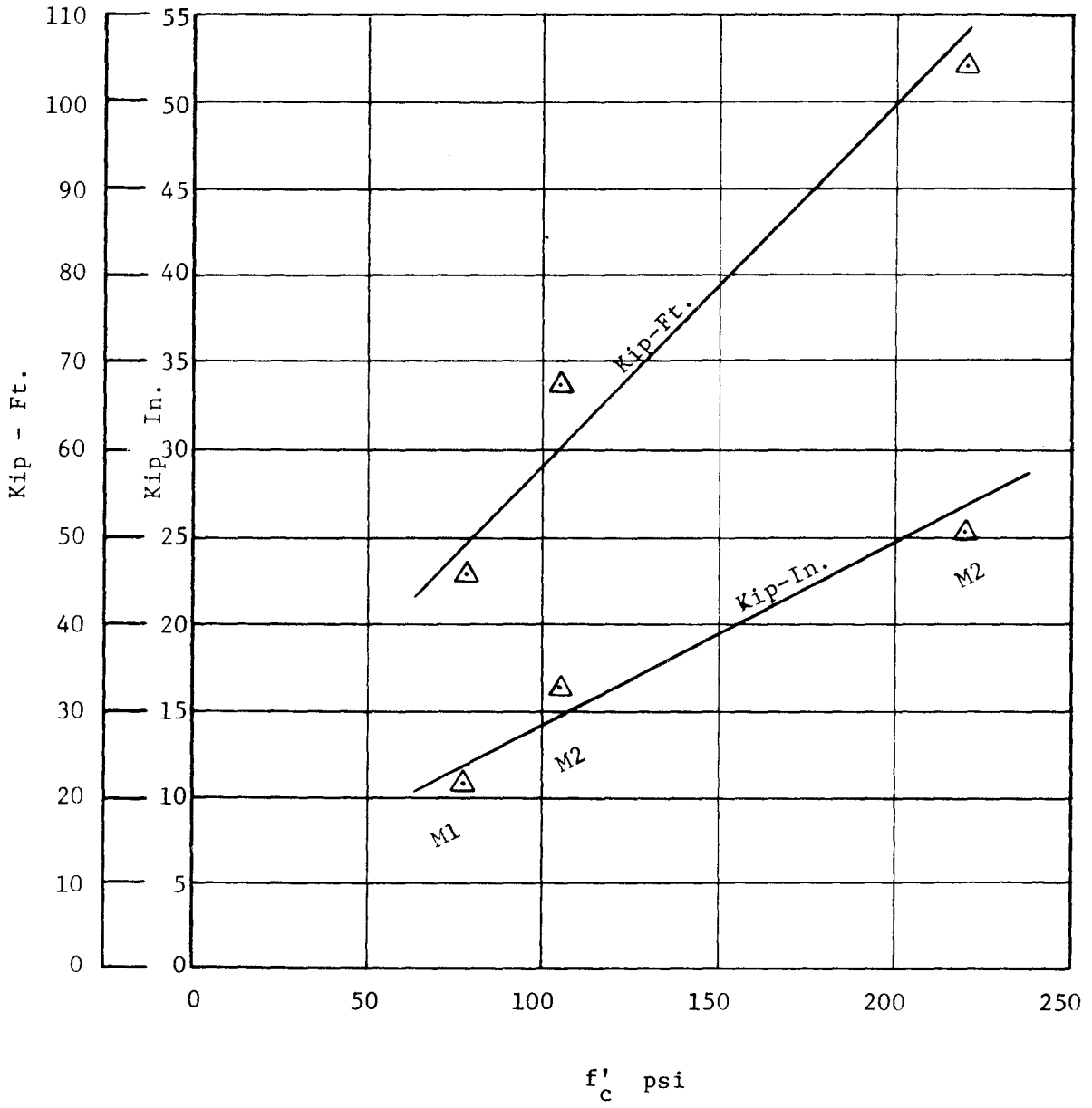
110
100
90
80
70
60
50
40
30
20
10
0
55
50
45
40
35
30
25
20
15
10
5
0
Kip - Ft.
Kip In.
Kip-Ft.
Kip-In.
M1
M2
M2
0
50
100
150
200
250
f'c psi

Figure B28

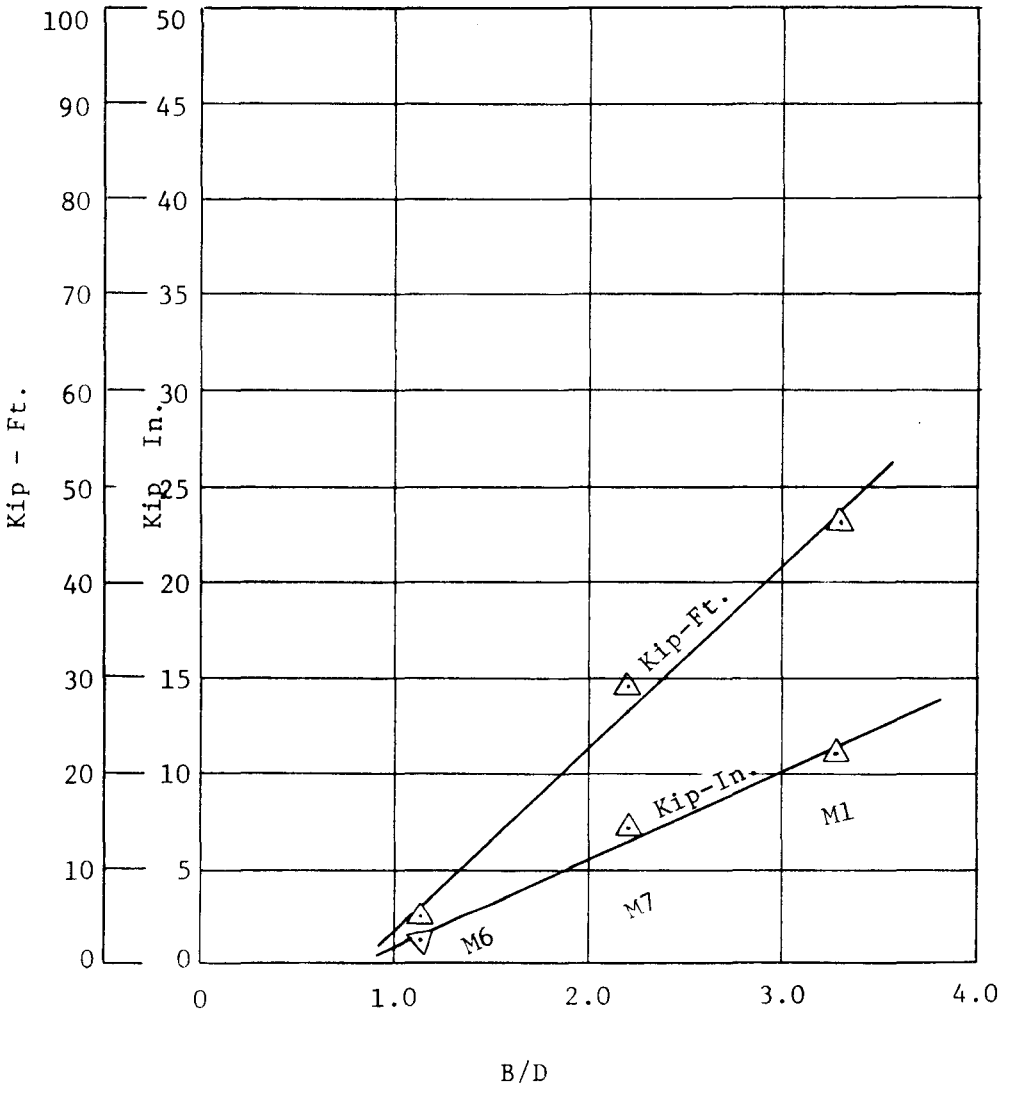
100
90
80
70
60
50
40
30
20
10
0
Kip - Ft.
50
45
40
35
30
25
20
15
10
5
0
Kip In.
0
1.0
2.0
3.0
4.0
B/D
Kip-Ft.
Kip-In.
M6
M7
M1

Figure B29

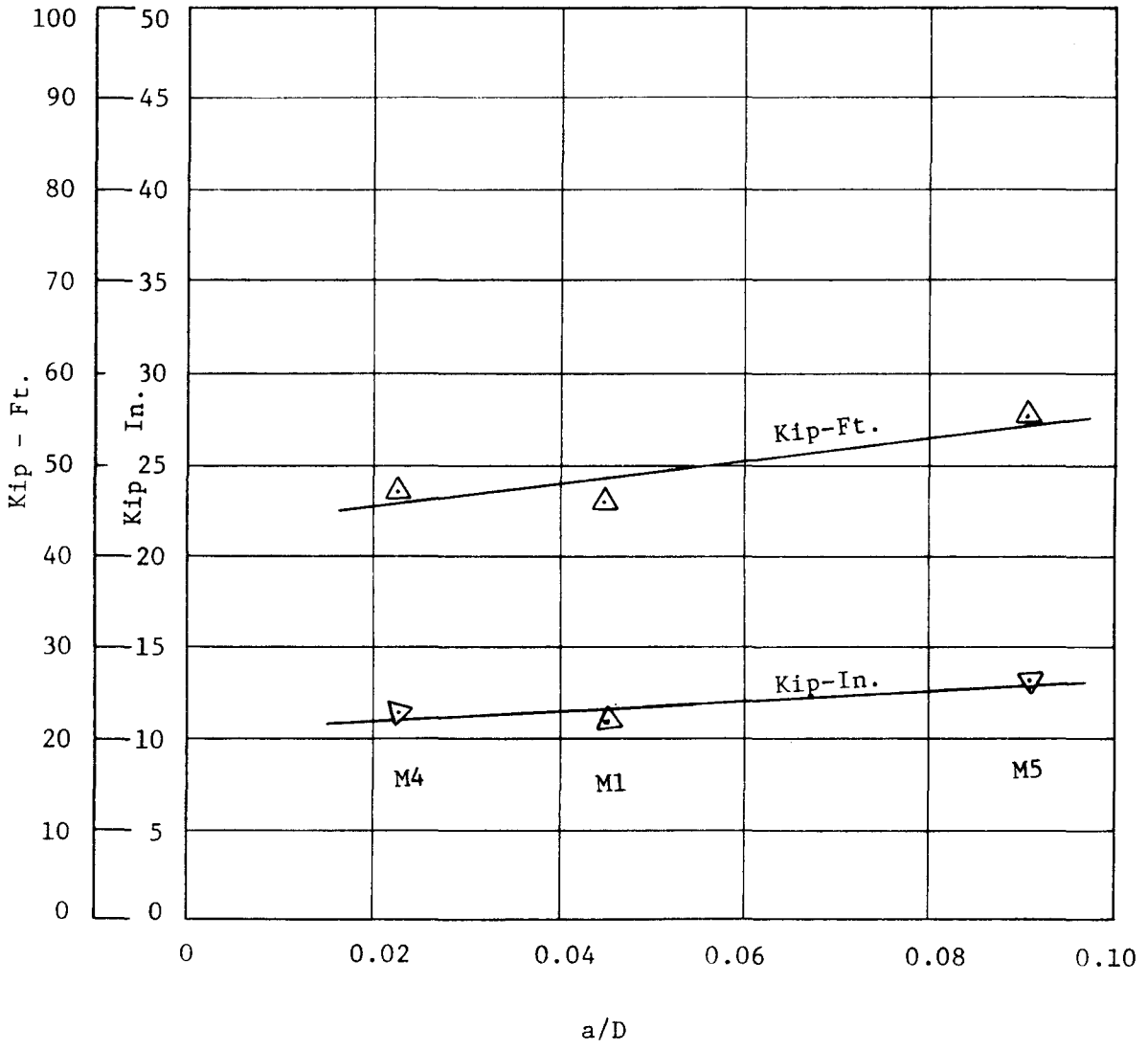
Kip - Ft.
Kip In.
100
90
80
70
60
50
40
30
20
10
0
50
45
40
35
30
25
20
15
10
5
0
0
0.02
0.04
0.06
0.08
0.10
a/D
Kip-Ft.
Kip-In.
M4
M1
M5

Figure B30

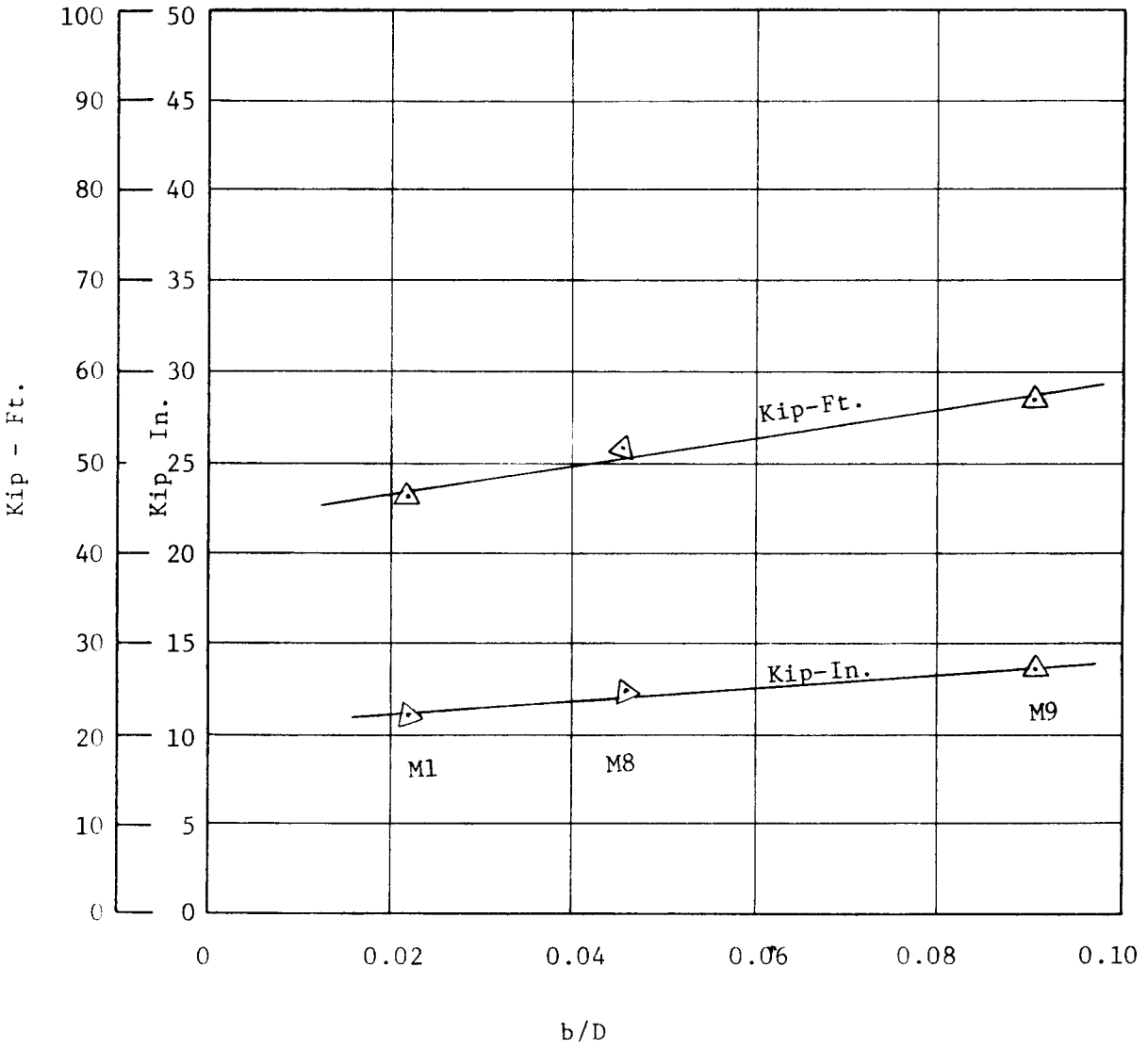
Kip - Ft.
Kip - In.
100
90
80
70
60
50
40
30
20
10
0
50
45
40
35
30
25
20
15
10
5
0
0
0.02
0.04
0.06
0.08
0.10
b/D
Kip-Ft.
Kip-In.
M1
M8
M9

Figure B31

TABLE B4

PREDICTED ENERGY ABSORPTION CAPACITY
FOR 505V-C VERMICULITE CUSHION

505V-C MODULE	CORRESPONDING MODEL MODULE	PREDICTED ENERGY kip-ft.	CUMULATIVE PREDICTED ENERGY
A	2/3 of M7	15.1	15.1
		15.1	30.2
		15.1	45.3
B	M7	22.6	67.9
		22.6	90.5
		22.6	113.1
C	M4	38.5	151.6
		38.5	190.1
		38.5	228.6
D	M1	40.1	268.7
		40.1	308.8
		40.1	348.9

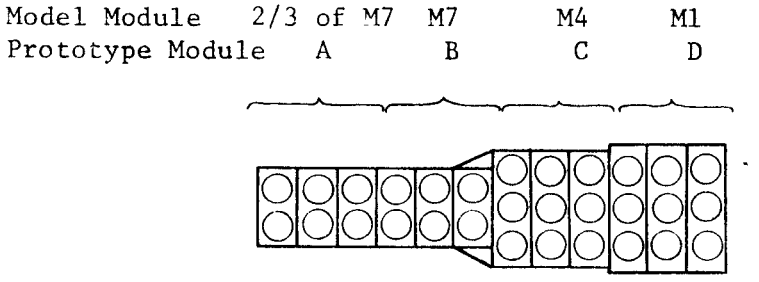

Compressive strength of prototype = 57 psi

TABLE B5

PREDICTED ENERGY ABSORPTION CAPACITY
FOR 505V-F VERMICULITE CUSHION

505V-F MODULE	CORRESPONDING MODEL MODULE	PREDICTED ENERGY kip-ft.	CUMULATIVE PREDICTED ENERGY
A	M7	23.7	23.7
		23.7	47.4
		23.7	71.1
		23.7	94.8
		23.7	118.5
B	M4	40.4	158.9
		40.4	199.3
		40.4	239.7
		40.4	280.1
		40.4	320.5
C	M1	42.0	362.5

Model Module M7 M4 M1
Prototype Module A B C

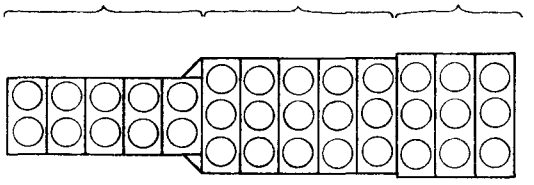

Compressive strength of prototype = 64 psi

energy is 27 kip-ft. from Figure B29. This value is based on the compressive strength of the model modules of 77 psi. To adjust for the prototype compressive strength of 57 psi, Figure B28 is used and the adjustment is: (41/49) (27) = 22.6 kip-ft. Energy values predicted in this manner for the 505V-C cushion are tabulated in Table B4 and for the 505V-F cushion in Table B5.

In test 505 F, the total capacity of the cushion was not consumed. The total penetration into the cushion was 12.2 ft. and some modules were only partially crushed. However, in order to simplify the procedure for predicting the behavior of this cushion, it is assumed that each module was completely crushed (crushing ratio = 0.89) in successive steps beginning at the front of the cushion and proceeding toward the rigid wall until a total crushing distance of 12.2 ft. is reached. This will result in an assumed complete crushing of 12.2/.89 = 13.7 ft. or 6.9 (say 7) modules. The cushion used in this test consisted of 5 modules of M7 type; 5 modules of M4 type and 3 modules of M1 type with the last module filled with vermiculite. The predicted energy absorption of this cushion would then consist of that of five type M7 modules plus two M4 type modules or 199.3 kip-ft.

TABLE B6

COMPARISON OF VEHICLE KINETIC ENERGY
AND PREDICTED STATIC ENERGY ABSORPTION

Test	Kinetic Energy of the vehicle at contact KE=1/2 MV^2 kip-ft.	Predicted Energy Absorption E_p kip-ft.	Ratio KE/E_p
505V-C	619	348.9	1.77
505V-F	277	199.3	1.39
		Average	1.58

DESIGN OF LIGHTWEIGHT CELLULAR CRASH CUSHION USING MODEL PREDICTION RELATIONSHIPS

The problem is to design a lightweight cellular concrete crash cushion which will provide an acceptable deceleration level for a 4500-lb. vehicle traveling 65 mph.

The vehicle kinetic energy is calculated by the following equation:

$$KE = \frac{1}{2} \frac{W}{g} V^2$$

Where

W is the design vehicle weight, 4500 lbs.
g is the acceleration of gravity, 32.2 ft/sec^2
V is the design vehicle velocity, 65 mph. = 95.2 fps.

Thus $KE = \frac{1}{2} \frac{4500}{32.2} (95.2)^2 = 635$ kip-ft

The required stopping distance is determined by the desired average deceleration level (chosen $G_{avg} = 7$) and is calculated as follows:

$$L = \frac{V^2}{2gG_{avg}}$$

$$L = \frac{(95.2)^2}{2(32.2)(7)} = 20.2 \text{ ft.}$$

The problem is then to select a combination of modules that will absorb 635 kip-ft of energy when crushed for a distance of 20 ft. or more. For M4 type modules with a compressive strength of 60 psi, the energy absorption capacity is 39.5 kip-ft. per module. This energy absorption capacity is increased by the average dynamic to static ratio from Table B6 of 1.58; 39.5(1.58) = 62.5 kip-ft. If these modules are used

throughout the cushion, the number of modules required to absorb the energy is:

$$\frac{635}{62.5} = 10.2, \text{ say } 11 \text{ modules}$$

A cushion constructed of 11 modules will be nominally 22 ft. long. For a crushing ratio of 0.89, the crush distance of this tentative cushion will be only 19.6 ft., which is less than the required distance. The crushing distance for a given energy absorption capacity can be increased by substitution of modules with a lower energy absorption capacity. This can be accomplished by partial substitution of M7 type modules with an energy absorption capacity of 27 kip-ft/module when 77 psi concrete is used. The adjustment in energy absorption capacity for a M7 module with 60 psi concrete is obtained from Figure B28 and is 27 kip-ft 42/49 = 22.6 kip-ft. Application of the dynamic to static ratio will yield 22.6(1.58) = 35.7 kip-ft. If five of the M4 type modules are removed from the tentative cushion and replaced with M7 type, the number of M7 modules required is as follows:

Energy required	635 kip-ft.
Six M4 modules	375 kip-ft.
Difference	260 kip-ft.

No. of M7 modules 260/35.7 = 7.3 modules, say 8 modules

The revised cushion design now consists of six M4 and eight M7 type modules which will result in a cushion 28 ft. long. The crushing distance for this cushion is 0.89(28) = 24.9 ft.

A second revision will now be made in an attempt to improve the cushion configuration. Three of the M4 modules are replaced with three

M1 modules. The energy absorption capacity of an M1 module, calculated as before, is 66.3 kip-ft. The design now consists of:

3 M1 modules @ 66.3 kip-ft. = 198.9 kip-ft.

3 M4 modules @ 62.5 kip ft. = 187.5 kip-ft.

7 M7 modules @ 35.7 kip-ft. = 250.0 kip-ft.

Total 636.4 kip-ft.

The crushing distance for this cushion is 0.89(26) = 23 ft.

APPENDIX C

DURABILITY TESTS

OF

VERMICULITE CONCRETE

One of the questions concerning practical application of vermiculite crash cushions is whether this material can withstand exposure to natural environment, particularily in colder regions. The results of a study conducted to obtain some indication of the freezing and thawing durability of vermiculite concretes are reported on the following pages.

EXPERIMENTAL PROGRAM

The properties of the concrete batches tested are listed in Table C1. Three inch by three inch by sixteen inch specimens were cast and sawed in half to result in three inch by three inch by eight inch specimens for testing. Table C2 gives the type of treatment and type of freezing and thawing cycles to which the specimens were subjected. All specimens were moist cured for three days and then cured at 50% relative humidity for at least 25 days before testing.

Household, chest-type freezers were used for the freezing tests. The specimens were out of the freezer about 18 hours and in the freezer about 6 hours during each cycle. The specimens were weighed after each cycle and deterioration was evaluated visually. Deterioration of the specimens was recorded with photographs.

TABLE C1

BATCH DATA

Batch No.	Cement Type	Cement sks/cy	Aggregate cft/cy	Water gal/cy	Wet Unit wt. lbs.	Air %	Compressive Strength, psi
RS1	Regulated Set	3.14	22.3	75.6	40.5	35	77
HE1	High Early Strength	3.27	22.6	83.0	42.0	50	64
HE2	High Early Strength	4.03	24.2	81.5	43.0	50	104
HE3	High Early Strength	5.82	23.2	76.6	49.0	51	220

TABLE C2

SUMMARY OF FREEZING AND THAWING RESULTS

SPECIMEN	TYPE OF TREATMENT	FREEZING & THAWING CYCLES TO FAILURE*	
		Type	Average No.
RS1 BATCH			
16, 16A, 17	None	F & T in water	6
17A, 18, 18A	None	F in air & T in water	11
19, 19A, 20	Two coats of Daracon brushed on	F & T in water	6
20A, 21, 21A	Sprayed one coat of resin**	F & T in water	8
22, 22A	Soaked in linseed oil 24 hours	F & T in water	44
23	Soaked in linseed oil 24 hours	F & T in water	4
23A	Flexible epoxy coating #2	F & T in water	19
24, 24A, 25	Flexible epoxy coating #1	F & T in water	13
HE1 BATCH			
19, 19A, 20	Soaked in Daracon 10 min.	F & T in water	24
20A, 21, 21A	Sprayed two coats of resin**	F & T in water	17
HE2 BATCH			
19, 19A, 20	Soaked in Daracon 10 min.	F & T in water	23
20A, 21, 21A	Sprayed two coats of resin**	F & T in water	32
HE3 BATCH			
19, 19A, 20	Soaked in Daracon 10 min.	F & T in water	35
20A, 21, 21A	Sprayed two coats of resin**	F & T in water	36

*Failure was considered to occur in one of two ways: (1) attrition of the surface to a significant depth (nominally 1/4 inch) and (2) structural cracking of the specimen resulting in separation of the specimen into parts or separation of the protective coating along with a layer of vermiculite from the remainder of the specimen. Failure in all cases was arbitrarily defined by visual inspection.

**A polyester resin normally used in fiberglas reinforced plastic.

RESULTS

Figures C1 through C29 are photographs of the specimens illustrating their condition at the listed number of cycles. The uncoated specimens suffered progressive attrition of the surface without "structural" cracking. The most effective treatment investigated was obtained by soaking the specimens in linseed oil for 24 hours. The two flexible epoxy coating treatments were applied by Perlite Industries Inc. of Midland, Texas.

Specimen RS 23, one of the group soaked in linseed oil for 24 hours prior to freezing and thawing, failed after only four cycles. A single crack formed in the longitudinal direction of the specimen and it separated into two pieces as illustrated in Figure C7. The reason for early failure of this specimen is questioned. The failure was not a classical freeze-thaw type failure and no deterioration other than the single crack was experienced.

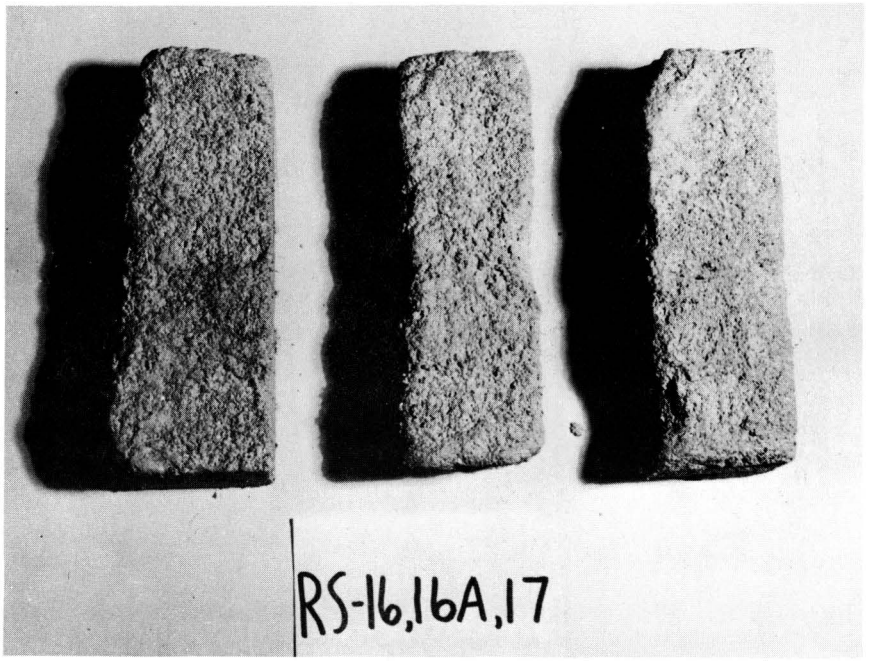

Figure C1 Conditions of specimens RS-16, 16A, 17 after six cycles of freezing and thawing.

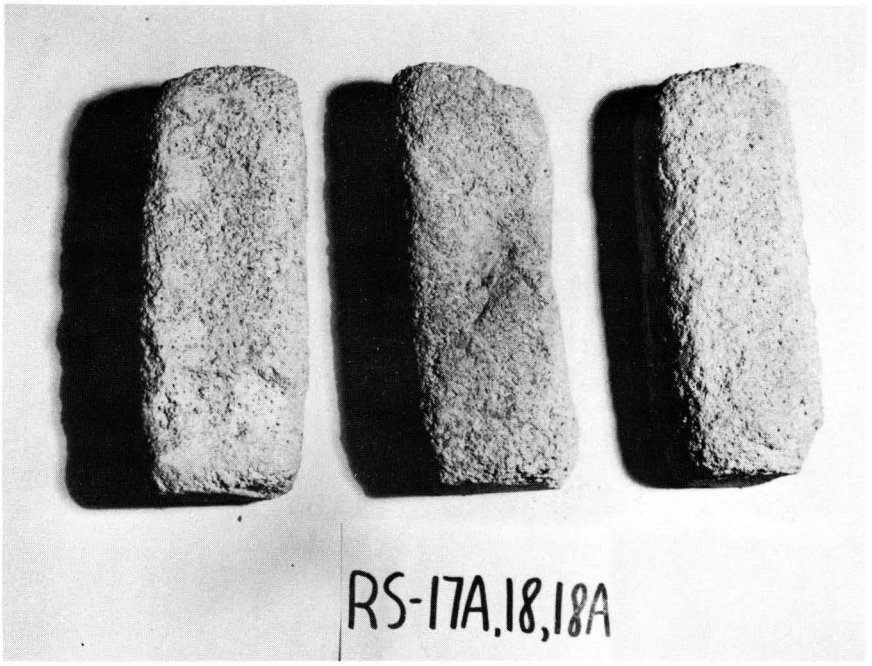

Figure C2 Conditions of specimens RS-17A, 18, 18A after 11 cycles of freezing and thawing.

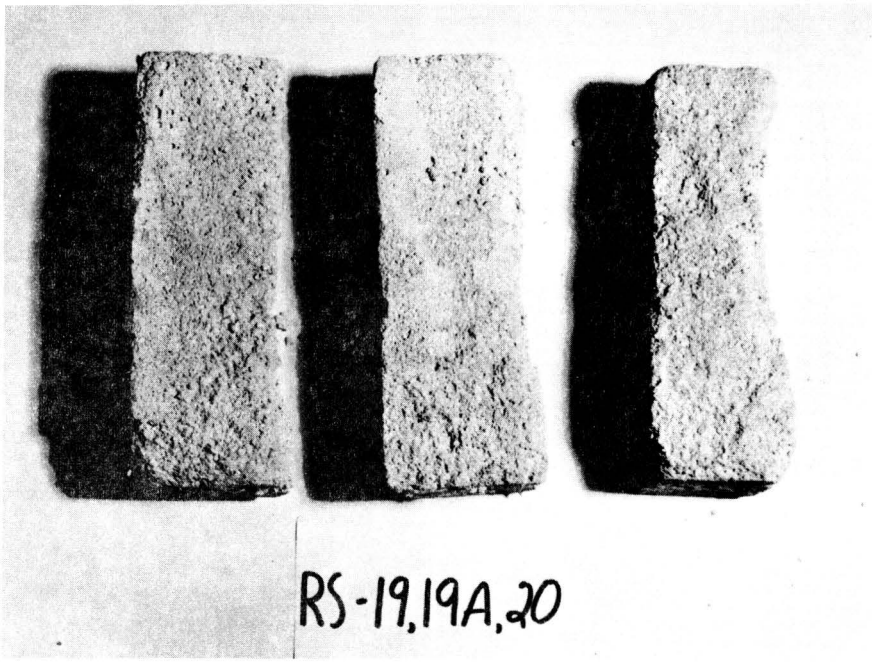

Figure C3 Conditions of specimens RS-19, 19A, 20 after six cycles of freezing and thawing.

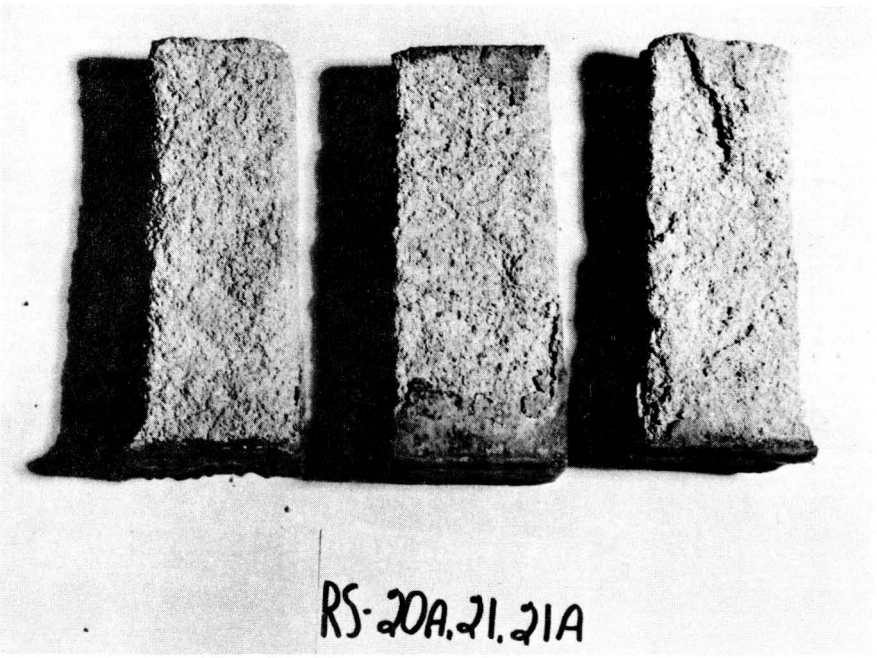

Figure C4 Conditions of specimens RS-20A, 21, 21A after eight cycles of freezing and thawing.

Figure C5 Condition of specimen RS-22 after 44 cycles of freezing and thawing.

Figure C6 Condition of specimen RS-22A after 44 cycles of freezing and thawing.

Figure C7 Conditions of specimens RS-22, 22A after 27 cycles, and RS-23 after 4 cycles of freezing and thawing.

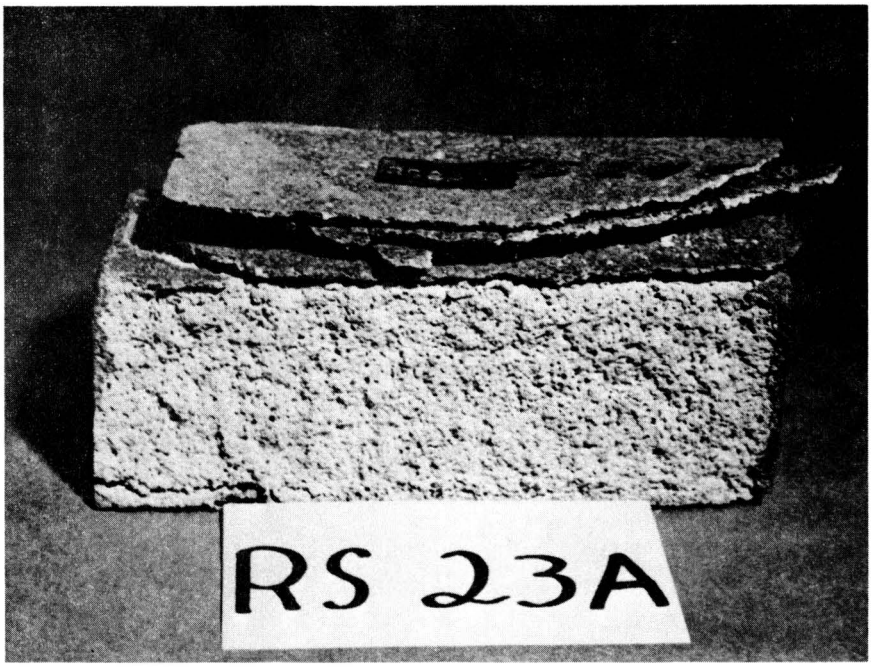

Figure C8 Condition of specimen RS-23A after 19 cycles of freezing and thawing.

Figure C9 Condition of specimen RS-24 after 14 cycles of freezing and thawing.

Figure C10 Condition of specimen RS-24A after 16 cycles of freezing and thawing.

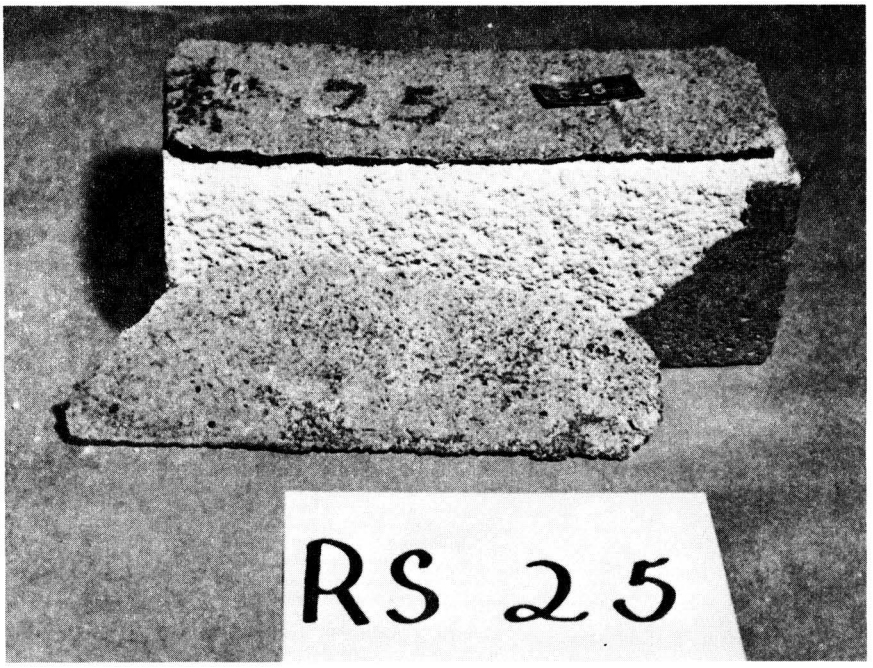

Figure C11 Condition of specimen RS-25 after 8 cycles of freezing and thawing.

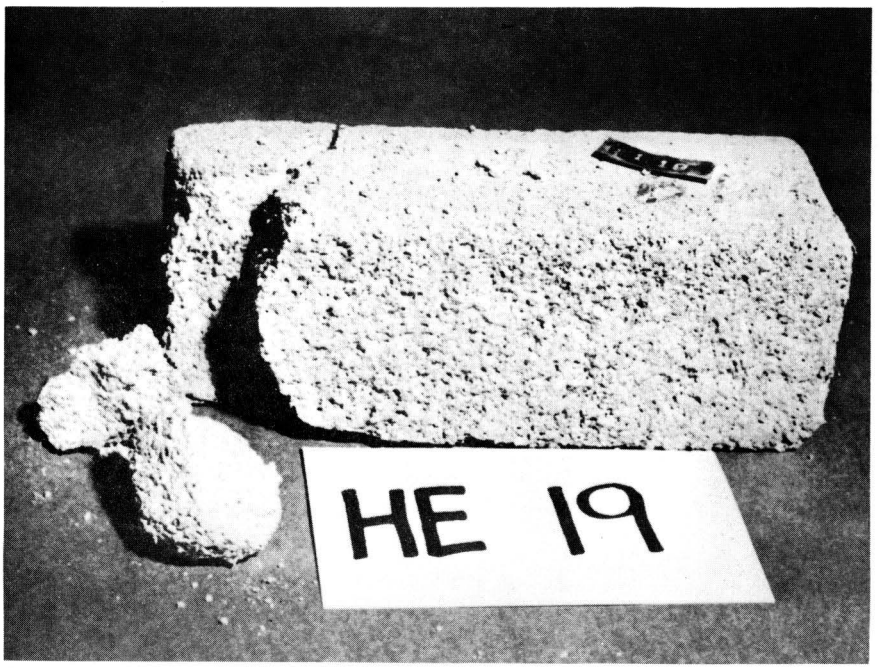

Figure C12 Condition of specimen HE1-19 after 24 cycles of freezing and thawing.

Figure C13 Condition of specimen HE1-19A after 24 cycles of freezing and thawing.

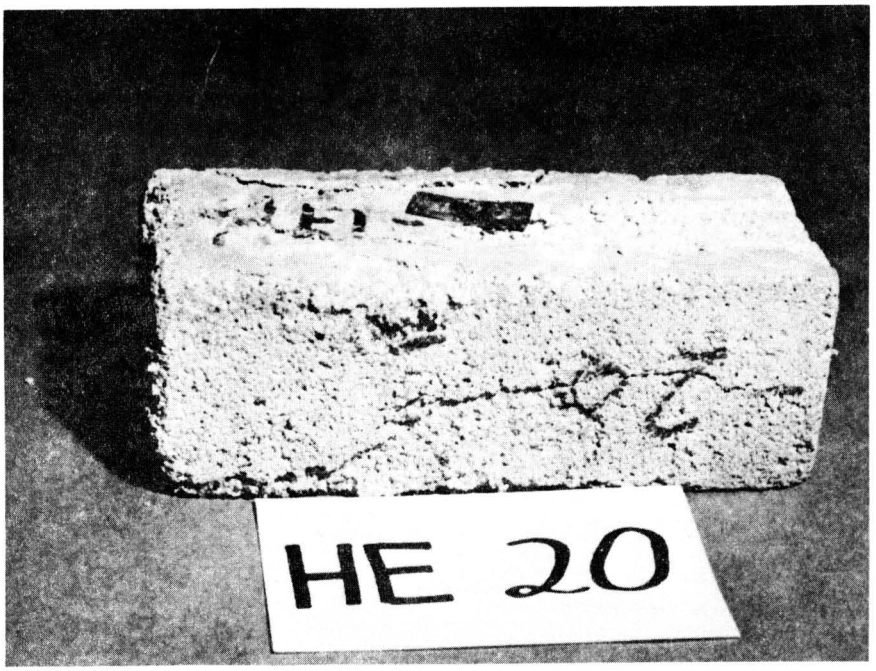

Figure C14 Condition of specimen HE1-20 after 23 cycles of freezing and thawing.

Figure C15 Condition of specimen HE1-20A after 16 cycles of freezing and thawing.

Figure C16 Condition of specimen HE1-21 after 19 cycles of freezing and thawing.

Figure C17 Condition of specimen HE1-21A after 16 cycles of freezing and thawing.

Figure C18 Condition of specimen HE2-19 after 23 cycles of freezing and thawing.

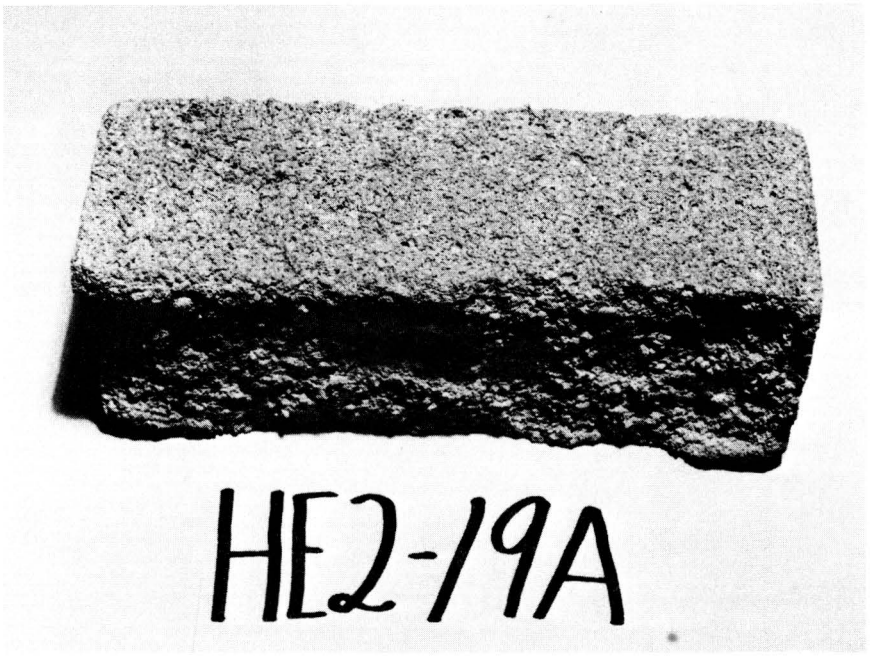

Figure C19 Condition of specimen HE2-19A after 23 cycles of freezing and thawing.

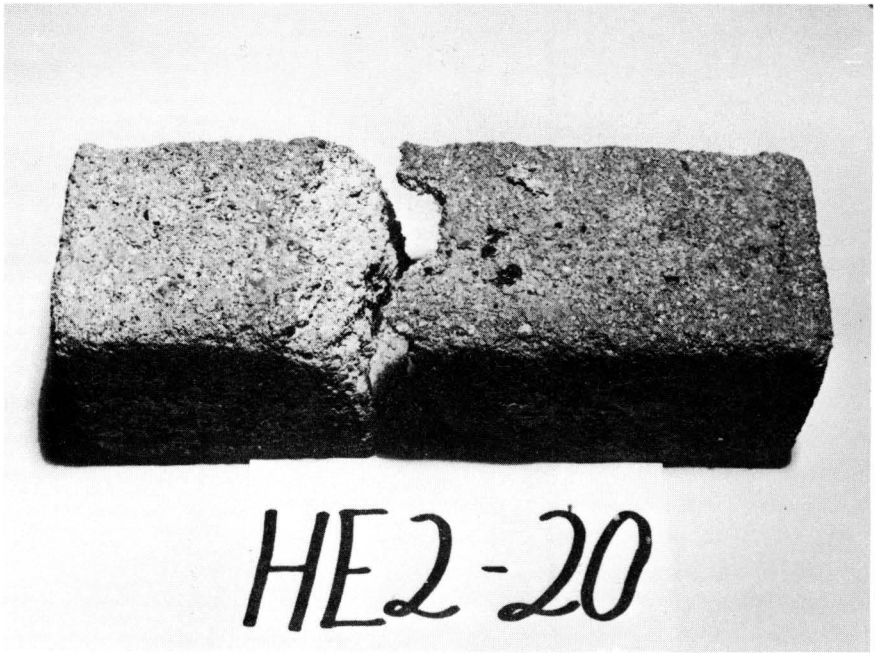

Figure C20 Condition of specimen HE2-20 after 25 cycles of freezing and thawing.

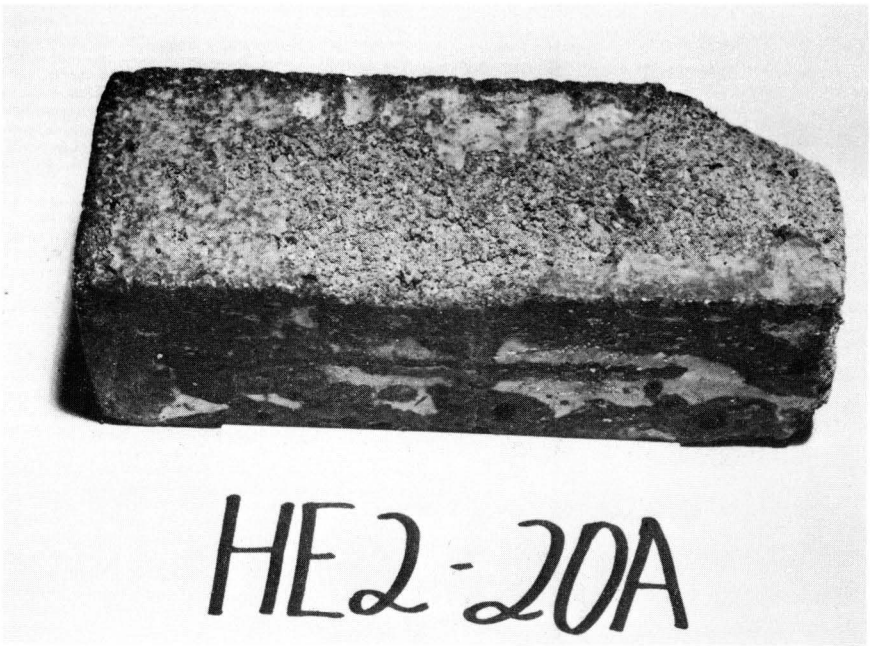

Figure C21 Condition of specimen HE2-20A after 36 cycles of freezing and thawing.

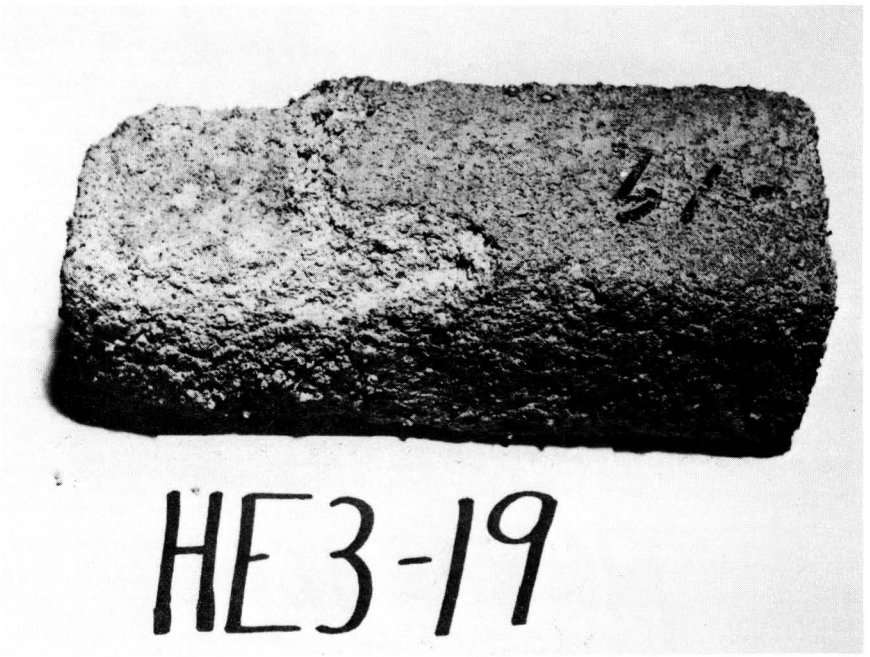

Figure C24 Condition of specimen HE3-19 after 37 cycles of freezing and thawing.

Figure C25 Condition of specimen HE3-19A after 37 cycles of freezing and thawing.

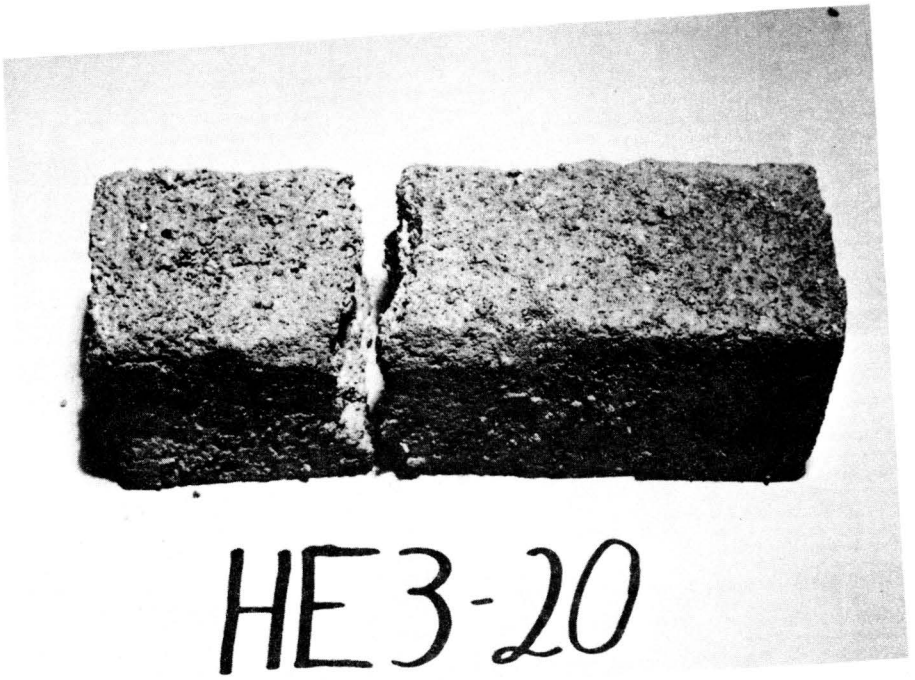

Figure C26 Condition of specimen HE3-20 after 32 cycles of freezing and thawing.

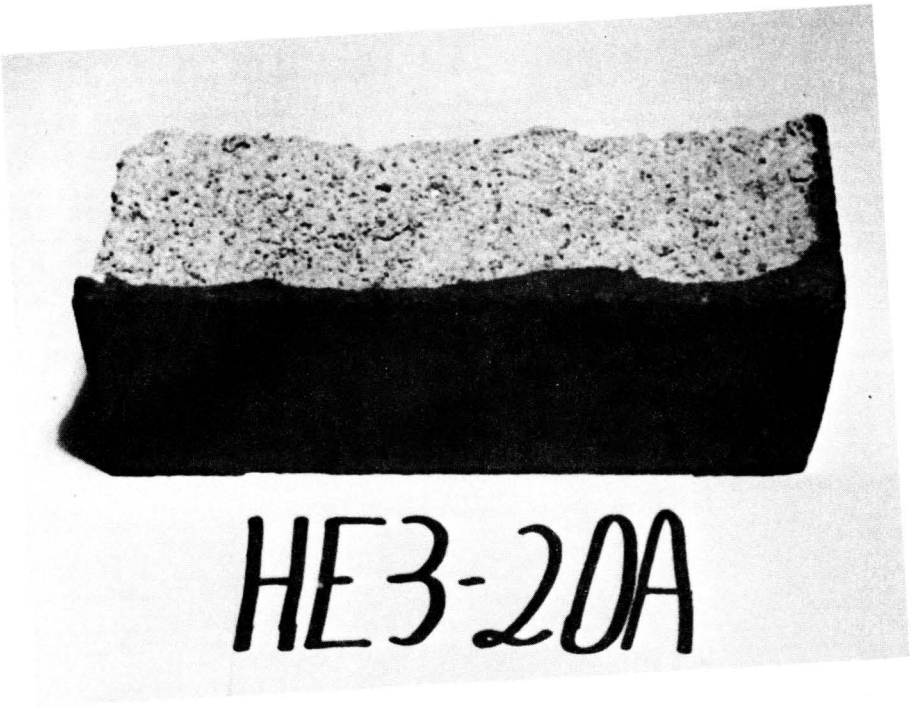

Figure C27 Condition of specimen HE3-20A after 36 cycles of freezing and thawing.

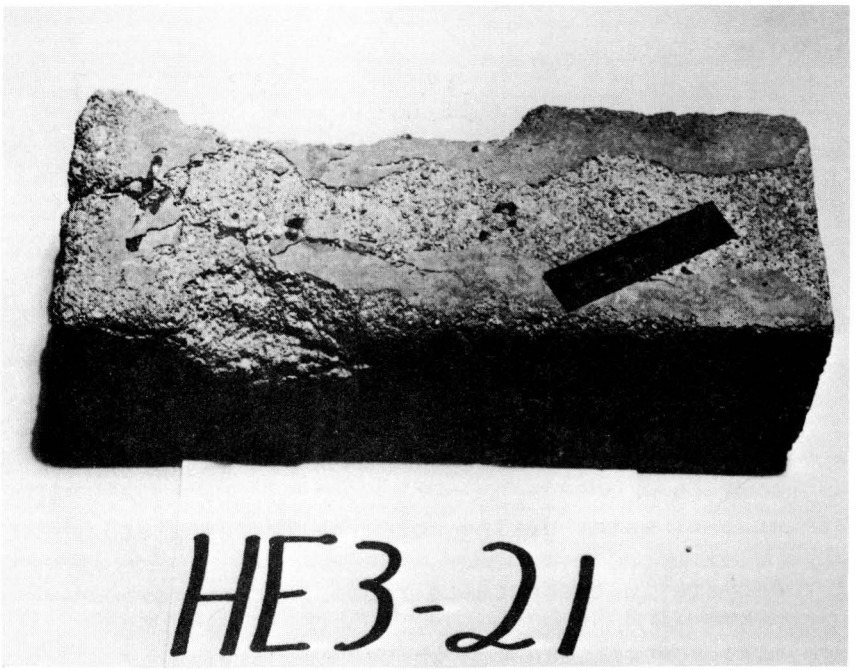

Figure C28 Condition of specimen HE3-21 after 36 cycles of freezing and thawing.

Figure C29 Condition of specimen HE3-21A after 38 cycles of freezing and thawing.

CONCLUSION

The accurate prediction of the durability of a material in a freezing and thawing environment on the basis of laboratory tests has historically been a very difficult or almost impossible task. However some indications of the expected behavior can be obtained from such tests.

The presence of water during both the freezing and the thawing portion of the cycle in these tests represents an exposure condition that is much more severe than one where some drying is allowed. In actual field installations of crash cushions, free drainage occurs and extended periods of exposure to water do not occur. This is beneficial in that the concrete will experience drying periods and the continuous, cumulative saturation of the concrete will be disrupted.

The tests indicate that vermiculite concrete can withstand a significant number of cycles of freezing and thawing even when continousuly exposed to water. All of the protective coatings used were successful, to varying degrees, in inhibiting absorption of water by the concrete and thereby improved the durability. An additional consideration is that deterioration due to freezing and thawing manifests itself by attrition of the surface which can be monitored by visual inspection.